CONSTRUCTION OF BORON DOPED DIAMOND (BDD)/ CYTOCHROME C BIOSENSOR FOR DETERMINATION OF TOXIC COMPOUNDS

By

Xolile Godfrey Fuku

A thesis submitted in fulfilment of the requirements for the degree of Magister Scientiae in the Department of Chemistry, University of Western Cape.

TITTLE PAGE

Supervisors**:**

Prof. Priscilla G.L Baker

Prof. Emmanuel I. Iwuoha

DATE:……May 2011

KEY WORDS

Cytochrome c (cyt c)

Boron doped diamond (BDD)

Prussian blue (PB)

Arsenic trioxide (As)

Incubation

Drop coating

Intoxication

Toxicity

Electron-transport chain

Asphyxiates

Cyclic voltammetry (CV)

Square wave voltammetry (SWV)

Electrochemical impedance spectroscopy (EIS)

Fourier Transform Infrared Spectroscopy (FTIR)

UV/vis spectroscopy

Subtractive Normalization Fourier Transform Infrared Spectroscopy (SNFTIR)

ABSTRACT

Cytochrome *c* is an important redox heme protein found in the membrane of mitochondria, where it transfers electrons between cytochrome *c* reductase (complex III) and cytochrome c oxidase (complex IV). Disruption of the electron transport chain results in tissue and organ failure which will ultimately result in cell death since energy in the form of ATP will not be produced. Cyanide and arsenic compounds, important inhibitors of the protein, are potent and rapid-acting asphyxiants causing tissue hypoxia, which is a deprivation of oxygen. Several methods have been developed for detection of cyanide and arsenic compounds including include titrimetry, colorimetry spectrophotometry, ion selective electrodes (ISEs), chromatography, spectrophotofluorometry and indirect atomic absorption spectrometry. However, all these methods are subject to interference problems.

In this work, an electrochemical method based on a cyt c biosensor has been developed, for the detection of selected arsenic and cyanide compounds. Boron Doped Diamond (BDD) electrode was used as a transducer, onto which cyt c was immobilised and used for direct determination of Prussian blue, potassium cyanide and arsenic trioxide by inhibition mechanism. The sensitivity as calculated from cyclic voltammetry (CV) and square wave voltammetry (SWV), for each analyte in phosphate buffer (pH= 7) was found to be (1.087- 4.488 $\times 10^{-9}$ M) and the detection limits ranging from 0.0043- 9.1 μM. These values represent a big improvement over the current Environmental Protection Agency (EPA) and World Health Organisation (WHO) guidelines. The protein binding was monitored by SWV and electrochemical impedance spectroscopy (EIS) at peak potential of -300mV (vs. Ag/AgCl). EIS also provided evidence that the electrocatalytic advantage of BDD electrode was not lost upon immobilisation of cytochrome c. The interfacial

kinetics of the biosensor was modelled as equivalent electrical circuit based on electrochemical impedance spectroscopy data. UV/vis spectroscopy was used to confirm the binding of the protein in solution by monitoring the intensity of the soret bands and the Q bands. FTIR was used to characterise the protein in the immobilised state and to confirm that the protein was not denatured upon binding to the pre-treated bare BDD electrode. SNFTIR of cyt c immobilised at platinum electrode, was used to study the effect of oxidation state on the surface bond vibrations. The spherical morphology of the immobilised protein, which is typical of native cyt c, was observed using scanning electron microscopy (SEM) and confirmed the immobilisation of the cyt c without denaturisation.

DECLARATION

I declare that Development/construction of BDD/Cyt c biosensor for determination of toxic compound is my own work, **that it has not been submitted for any degree or examination in any other university, and that all sources I have used or quoted have been indicated and acknowledged by means of complete references.**

Xolile Godfrey Fuku **May 2011**

Signed…….

ACKNOWLEDGEMENTS

To my God; He is always there watching over me, He is my Sheppard, He said: Ask and it will be given to you; seek and you will find; knock and the door will be opened to you. For everyone who asks receives; the one who seeks finds; and to the one who knocks, the door will be opened. I asked and he gave me this: he gave me strength, hope, dedication and courage to finish this work.

"Tumelo honna ke thebe engkgatholla pelo

Hore honna ke lelale ke tshepe lehodimo

Dira honna diqhalane ke tshepetse howena"

Thank you my lord my God you are the great one

To my supervisors: Professor Priscilla G.L Baker and Professor Emmanuel Iwuoha and, who guided me and gave me valuable suggestions regarding the project. Thank you for your excellent supervision, support, encouragement and patience during this period. To Dr. Jahed Nazeem thank you, for your continuous support throughout this research period.

I wish to express my deep sense of gratitude to my post-doctors Dr Faiza for her guidance, showing me how to handle problems in the lab, for listening, for her encouragement and useful suggestions, which helped me in completing the project and Dr Waryo who has shared his opinions and experience through which i received the required information crucial for my project. To the National Research Foundation (NRF) for their financial support. The support of my colleagues in SensorLab, Chemistry Department: Dr Muchindu, Peter, Fanelwa, Nzioki, Vivian, Euodia, Masikini, Wale, Kerileng, Gcineka, Khotso, Busiswa, Lundi, Matinise, Chinwe,

Abdul,Nicolette, Jesmina, Natasha, Njomo, thank you for being such good colleagues and friends.

To my friends: Thabiso, Morake, Mamokoena, Molantwa, Khotso, Mduduzi, Vivian and Euodia. Thank you for your assistance and having faith in me. You are true friends.

To the Fuku family: for their love and support. To my sisters and brothers: Monica, Lucky, Patrick, Zamile (R.I.P), Thabiso, Molantwa, Teboho, and Oupanyana. To my uncles and aunts: Micheal, Kleinbooi, Noluthando, thank you for giving me hope, courage and most of all making me believe.

Finally, yet importantly, I would like to express my heartfelt thanks to my beloved parents: Nontembiso Emily Fuku and Madillo Finisia Fuku for their blessings, and wishes for the successful completion of this project. Thank you for your guidance, for pushing me so i can succeed and for believing in me. You are the best i have ever had.

DEDICATION

This project is dedicated to

The

Almighty God

And

My mom my Aunt my sister and my brother

Mrs. Nontembiso Fuku, Madillo Fuku, Monica Fuku and Lucky Fuku

Table of content

LIST OF FIGURES

LISTS OF TABLES

LISTS OF SCHEMES

LIST OF ABBRIVIATIONS

CV	Cyclic voltammetry
Cyt c	Cytochrome c
EIS	Electrochemical impedance spectroscopy
BDD	Boron doped diamond
SWV	Square wave voltammetry
FTIR	Fourier transform infrared spectroscopy
PB	Prussian blue
SEM	Scanning electron microscopy
VU/vis	Ultraviolet-visible spectroscopy
ATP	Adenosine triphosphate
NADH	Nicotinamide adenine dinucleotide
$FADH_2$	Flavin Adenine Dinucleotide
Cys^{14}	Cystine 14
$Cyst^{17}$	Cystine 17
APAF-1	Adaptor subunit-apoptotic protease activating factor 1
ADP	Adenosine diphosphate

Pi	Inorganic phosphate
ETC	Electron transport chain
CWA	Chemical warfare agent
SNFTIR	Subtractive normalised Fourier transform infrared spectroscopy
EPA	Environmental protection agency
WHO	World Health Organisation

Chapter 1

1.1 Background and Introduction

Oxygen plays an important role in all living systems. The very air we breathe constitutes oxygen in combination with other gases. In nature there are number of different electron donors namely organic matter in organotrophs, inorganic matter in lithotrophs. There are also a number of different electron acceptors, both organic and inorganic. When available, oxygen is used as the terminal electron acceptor in the mitochondria for electron transfer processes because it generates the greatest Gibbs free energy change and produces the most energy. [1].

Asphyxiants are substances that cause tissue hypoxia i.e. deprivation of oxygen to parts of the body and may be classified as either simple or chemical asphyxiants. Simple asphyxiants (e.g. methane and nitrogen) physically displace oxygen in air that is breathed in resulting in oxygen deficiency, whereas chemical asphyxiants interfere with oxygen transport at cellular level [2-4]. Chemical asphyxiants are used as chemical warfare agents (CWA). Chemical warfare agents are toxic chemicals contained in a delivering system such as bomb or shell. Common chemical asphyxiants which are used as chemical warfare agents include cyanogen chloride, hydrogen cyanide and arsenic. These chemicals are produced as part of or by products of common industrial preparations. Cyanogen chloride (ClCN) is used in industry for synthesis of herbicides and ore refining; HCN is a precursor to many chemicals ranging from polymers to plastics and arsenic hydrides are used as doping agents in microelectronics and in production of lead storage batteries [5].

We are surrounded by toxic chemicals such as cyanides, arsenic and pesticides, in everyday life. The workplace and the surroundings are an important source of exposure. Roofers, construction workers, farm workers, hospital workers, cleaners etc. are routinely exposed to these chemicals. Chemical asphyxiants or toxic chemicals are toxic to all forms of life [6-7]. Arsenic, mercury compounds, pesticides, lead acetate and cyanides are examples which chemical asphyxiants of HCN and As_2O_3 are probably the best known. Such chemicals are toxic to animals, humans, plants and microorganisms. They function by inhibition of oxidative phosphorylation. They affect biochemical processes shared by most living organisms, such as production and utilization of energy and cellular respiration. Cellular respiration is the process of oxidizing molecules, like glucose into adenosine triphosphate (ATP) and release of waste products such as carbon dioxide and water along with energy. The reactions involved in respiration are catabolic reactions that involve the redox reaction i.e. oxidation of one molecule and the reduction of another molecule [8-9]. The living cell is the site of tremendous biochemical activity called metabolism. This is the process of chemical and physical change which goes on continually in living organisms, build-up of new tissues, replacement of old tissues, conversion of food to energy, disposal of waste materials, reproduction and all the activities that we characterize as "life". The energy which is produced by cellular respiration/oxygen is released and trapped in the form of ATP. The trapped energy is used by all the energy-consuming activities of the cell. Cellular respiration process occurs in two phases: glycolysis, the breakdown of glucose to pyruvic acid and the complete oxidation of pyruvic acid to carbon dioxide and water [9]. The overall reaction resulting in ATP synthesis as a result of electrochemical (proton) potential is shown below

$$2NADH + 2H^+ + 6ADP + 6P_{inorganic} \rightarrow 2NAD^+ + 2H_2O + 6ATP$$

The remaining processes of cellular respiration take place in the mitochondria**.** Mitochondria are membrane-enclosed organelles distributed through the cytosol of most eukaryotic cells. Their number within the cell ranges from a few hundred to thousands, in very active cells. Their main function is the conversion of the potential energy of food molecules into ATP**.** Mitochondria carries out energy-yielding oxidative reactions that produce the maximum amount of ATP necessary to support cellular functions [10]. Interruption of this mitochondrial function in vivo leads to death. Indeed, a major advance in the last 20 years has been the recognition of many mitochondria-related diseases that result from severely compromised energy generation. Animal cells derive energy from mitochondria through oxidative phosphorylation, a process called the electron transport chain (ETC) in which electrons are passed along a series of carrier molecules to produce ATP. These electrons are generated from NADH (reduced nicotinamide adenine dinucleotide) and succinates, which are produced by oxidation of nutrients such as glucose, and are ultimately transferred to molecular oxygen [11]. ETC consists of four respiratory enzyme complexes in the mitochondrial inner membrane. The passage of electrons through these complexes releases energy, which is then stored in the form of a proton gradient across the membrane, and ultimately used by ATP synthase.

In the mitochondria there is an inner membrane and this membrane contains 5 complexes of integral membrane proteins i.e. NADH dehydrogenase (Complex I), succinate dehydrogenase (Complex II), cytochrome c reductase (Complex III; also known as the cytochrome b-c_1 complex), cytochrome c oxidase (Complex IV) and ATP synthase (complex IV) [12]. These integral membrane proteins constitute an electron transfer chain and this is where cytochrome c

plays a vital role in shuttling or transportation of electrons between the third and the fourth complex [13-14].

Cytochrome c is a protein found in almost all living organisms [15]. Cyt c is a common evolutionary origin as a result of its existence in many different kinds of living organisms, from bacteria to man [15]. It is a heme-containing redox active protein used in electron transfer pathways (respiratory chain of mitochondria) and is found loosely associated with the inner membrane of the mitochondrion which is an essential component of the electron transport chain. It also transfers electrons between Complexes III and IV [16-17]. If this transportation or its function of shuttling electrons has been disrupted, tissues and organs that mainly depend on aerobic respiration such as central nervous system, muscles, lungs, heart etc. are affected and this will lead to death since ATP will not be produced. Toxic compounds like arsenic and cyanides can be harmful to humans and all living organisms. These compounds may affect the function of the protein cyt c in the body and hence, poisoning by arsenic and cyanide compounds can both have an acute effect- a condition produced after short-term use of a toxic agent and chronic effect- a condition produced after long-term use of a toxic agent, depending on the level of exposure [18]. Cyanides are used widely and extensively in the manufacture of synthetic fabrics and plastics, in electroplating baths and metal mining operations, as pesticidal agents and intermediates in agricultural chemical production, and in predator control devices. Elevated cyanide levels i.e.10^{-3}, are encountered in more than 1,000 species of food plants and forage crops [19-20] and this probably represents the greatest source of cyanide exposure and toxicosis to man and to animals. Elevated cyanides levels ($\times 10^{-3}$ µg/l) can cause variety of diseases like cytotoxic hypoxia in the presence of normal oxyhemoglobin which is formed under normal

conditions during physiological respiration when oxygen binds to the heme component of the protein -hemoglobin- in red blood cells and oxygen travels through the blood stream to the cells where it is utilized in glycolysis and in the production of ATP by the process of oxidative phosphorylation [20]. Arsenic can also cause variety of diseases at elevated levels in the blood such as convulsions, cardiovascular problems, inflammation of the liver and kidneys and blood coagulation disorders. They are used in a wide range of applications such as precursor to forestry products, colourless glass production and electronics and as a wood preservative.

There are different techniques which were established for detection/determination of these toxins in both environmental water and wastewater (APHA, 1998; U.S. EPA, 1983). These methods are mainly based on titrimetric spectrophotometry , colorimetric spectrophotometry, cyanide ion selective electrodes (ISEs) chromatography, spectrophotofluorometry and indirect atomic absorption spectrometry [20]. However, all these methods subject to interference problems. These interference effects are conveniently divided into blank or additive interferences e.g. spectral interference and analyte or multiplicative interferences i.e. physical and chemical interferences [21]. In this work we wish to construct a BDD/Cytochrome c biosensor that is sensitive enough to determine not only cyanides and arsenic compounds but all toxic compounds e.g. Mercury compounds, lead compounds etc. that are harmful to the environment. Investigation of Cyt c horse heart interaction by electrochemical methods and spectroscopic methods i.e. cyclic voltammetry, square wave voltammetry, Fourier Transform Infrared Spectroscopy, UV/vis spectroscopy, Electrochemical Impedance Spectroscopy, Subtractive Normalize Fourier Transform Infrared Spectroscopy were carried out. The mechanism was also investigated and selectivity of Cyt c binding was determined.

1.2 Problem Statement

As a result of human and technological developments, a wide range of man-made chemicals and by-products formed in industrial or combustion processes have been, and still are released in the environment. Some of these substances such as arsenic and cyanide compounds are well-recognized contaminants known to affect the environment and the health of human beings. These toxic chemicals cause disruption in the function of proteins or enzymes in our bodies. Processes like the transfer of electrons in the inner membrane of mitochondria will be affected by these toxic chemicals. Detection and identification of toxic compounds in the environment, surroundings and air are of vital importance. Early detection and identification of these toxins is important. Common techniques are used for the detection of these compounds. These methods are mainly based on atmospheric pressure and chemical ionisation coupled with flame photometric detection. Other devices such as gas detection tubes and ion mobility spectrophotometers have been applied to onsite detection in gas phase [20]. Common techniques used for the detection of these compounds suffer from many drawbacks such as they are time consuming, and require large sample volumes, they are expensive, and must be undertaken by a well experienced analytical chemist in a dedicated analytical laboratory [22]. We propose to develop an early detection as well as analytical tool which is of very low cost requires minimal skill in operation, inexpensive and which produces real-time analytical results for detection of KCN, As_2O_3 and Prussian blue.

1.3 Motivation or rationale

South Africa supports as an important international goal, the peaceful and safe future for our children and generations to come. Development of new technologies for the destruction of toxic chemicals in a safe and environmentally sound manner, management with respect to handling and use of toxic chemicals and development of analytical methods and validation techniques for toxic chemicals is of utmost importance to humans/living organisms. There is a great need for research into areas of early detection of toxic chemicals. However, there are dozens of alternative technologies which can be used (gas detection tubes and ion mobility spectrophotometers etc) [5]. In this work we aim to turn the attention more closely to the use of biosensors as advanced sensing systems, with relatively low cost, ease of operation whilst maintaining high sensitivity.

1.4 Aim and Objectives

The research approach will utilize the binding event between cyanide and arsenic compounds at the cytochrome c biosensor as an analytical protocol for early detection and measurement of these compounds.

- Construction of Biosensor by direct immobilization of cytochrome c onto activated BDD platform;
- Immobilization of cyt c Horse heart on BDD electrodes by different methods of such as drop-coating and incubation;
- Characterisation of cyt c horse heart by electrochemical methods and spectroscopic methods (cyclic voltammetry, square wave voltammetry and Fourier transform infrared spectroscopy, UV/vis spectroscopy, Electrochemical Impedance Spectroscopy, Subtractive Normalization Fourier Transform Infrared Spectroscopy);
- Application of biosensor to selected compounds (arsenic trioxide, potassium cyanide, Prussian blue and potassium ferricyanide);
- Interference studies of common salts on biosensor performance.

Chapter 2

2.1 Sensors and their functions

In general, a sensor comprises an active sensing element and a signal transducer, and produces an electrical, optical, thermal or magnetic output signal. While the sensing element is responsible for the selective detection of the analyte, the transducer converts a chemical event into an appropriate signal that can be used with or without amplification to determine the analyte concentration, acidity levels (pH) etc, in a given test sample as shown by figure 1. Generally, these devices are composed of a bioactive substance as well as a physical transducer. There are different types of sensors namely calorimetric, Potentiometric, amperometric, optical and acoustic biosensors [23-24]. Below are the components of a biosensor as shown in figure 1.

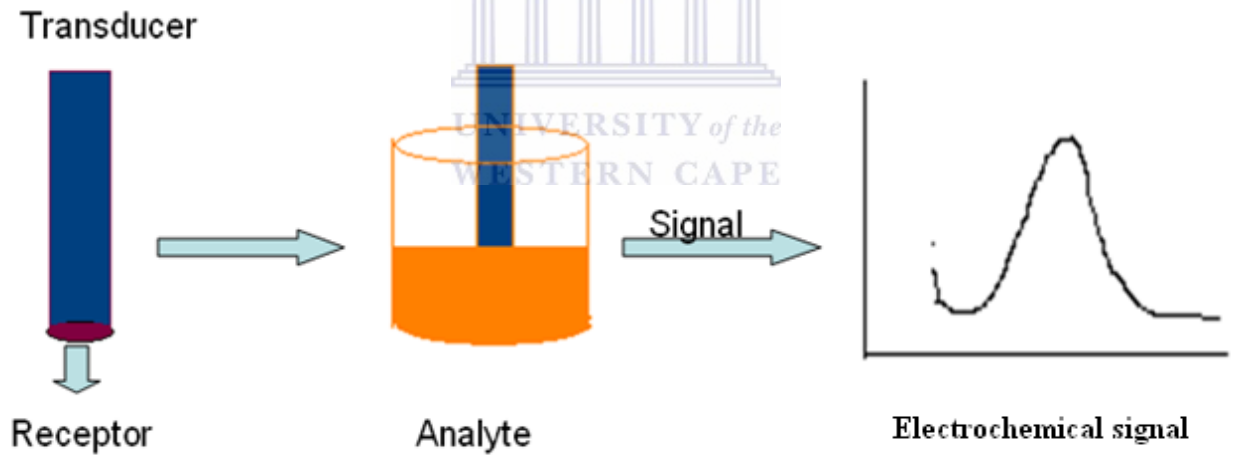

Figure 1: Schematic representation of components of a biosensor

The role of the transducer in biosensor construction is to relay the interaction of the biological active compound and the analyte into a measurable response which in most cases is an electronic signal. A suitable transuding system can be adapted in sensor construction depending on the nature of the biochemical interaction of the bioactive substance with the species of interest. Physical transducers may include thermal, piezometric, spectroscopic, surface wave technology and electrochemical transducers [25]. Electrochemical transduction is commonly based on amperometric and potentiometric transduction [26]. These methods are unique in that during the bio-interaction process, electrons are either consumed or generated producing an electrical signal, which is then detected by an electrochemical detector. An amperometric biosensor is driven by an external constant potential, during which an electrochemical reaction takes place, and the resultant current is measured [27-28]. Potentiometric biosensors are based on ion-selective or gas sensing electrodes where movement of ions into a membrane at a zero current allows for the monitoring of the cell potential. A Piezometric sensor is a type which is based on the movement of materials into or out of a surface layer where the change in mass is monitored [29-30].

In biosensors, receptors are compounds or materials that impart biosensors their selectivity characteristics [31]. In most cases these receptors undergo reactions with their respective analytes which is translated by a signal. Various receptors have been employed in sensor construction.

Plant tissues as well as tissue of mammals have been employed in the construction of biosensors resulting in sensor systems with greater selectivities as opposed to those constructed with bacterial cells. Each type of tissue slice e.g. functions the best when an appropriate analyte is present. Whole microbial cells are also widely utilized in the study of biosensors and are often

used when the desired enzyme is either unstable or difficult to purify [31]. A slight disadvantage associated with these biosensors in that they have a slow response time and require frequent calibration [32].

Biosensors first reported in the 1960s differ from the classical chemical sensors in the following two ways: (a) the sensing element consists of a biological material such as a protein (e.g., enzymes, antibodies oligo- or polynucleotides, microorganisms, or even whole biological tissues and (b) the sensor is used to monitor biological processes or for the recognition of biomolecules. For in vitro biosensing, the sample solution (such as blood serum, urine, milk etc.) is dropped onto the biosensor, and the output signal gives information on the composition of the solution. By contrast, in vivo biosensing addresses dynamic systems, aiming for instance to measure the rate of uptake or efflux of relevant species or to estimate the spatial distribution of the concentration of an analyte in a living organism [24, 33]. Biosensors can be divided into three generations depending on their level of integration. The first generation comprises of a biocatalyst that is either bound or entrapped in a membrane. The second generation of biosensors involves the adsorption of the biological components to the transducer surface thereby eliminating semi-permeable membranes. In the third generation, there is a direct binding of the biocatalyst to an electronic device that transduces and then amplifies the signal [29]. BDD/cyt c based biosensor is developed in this way.

Biosensors are used in extensive monitoring programs (e.g. detection of harmful pollutants in the environment). They are classified into various basic groups i.e. electrochemical, optical, piezoelectric and thermal sensors on the basis of the transducing element and enzymatic, non-enzymatic receptors, whole-cell and DNA biosensors on the basis of the biorecognition principle.

A key step of biosensors is the immobilization of the biological component at the transducer surface. The immobilization methods generally employed are; physical adsorption at solid surface, cross-linking between molecules, covalent binding to a surface and entrapment within a membrane, surfactant matrix and polymers methods. Advantages of biosensors over other sensors are their specificity of response, selectivity, reliability, portability, real-time analysis, simplicity of operation and rapid detection time. Biosensors used for the determination of biological oxygen demand, phenols, heavy metals, endocrine-disruptors, pesticides and also analysis of hormones, surfactants and antibodies have been reported [23, 28]. Pesticides, heavy metals and toxic compounds are well-recognized contaminants known to affect the quality of the environment. These contaminants can be detected by biosensors (Arsenic, Cyanides dioxins and Organophoshorus). These contaminants are of particular concern because of their toxicity to the environment. Most biosensors have been tested on simulated samples (distilled water) [27, 34].

An effective biosensor must possess the following features; the biocatalyst must be highly specific for the purpose of the analyte, be stable under normal storage conditions, shows good stability over a large number of assays and the reaction e.g., in the solution being used, should be independent of physical parameters i.e., stirring, pH, and temperature. It should also be free from electrical noise and also should not be prone to fouling or proteolysis. The probe should be tiny and biocompatible having no toxic or antigenic effects for monitoring in clinical situations and its response should be accurate, precise, reproducible and linear over the useful analytical range without dilution or concentration [35-36].

In this study we are developing a biosensor by immobilizing a protein e.g. cytochrome c onto a boron doped diamond electrode.

2.2 Proteins

The word PROTEIN comes from Greek language (prota) which means "of primary importance". This name was introduced by Jons Jakob Berzelius in 1838 for large organic compounds with almost equivalent empirical formulas. This name was used because the studied organic compounds were primitive but happen to be very important for animal nutrition [37].

Proteins are a class of organic compounds which are present in and vital to every living cell. Proteins are in the form of skin, hair, callus, cartilage, muscles, tendons and ligaments. Proteins hold together, protect and provide structure to the body of a multi-celled organism [38]. Proteins as e.g. enzymes, hormones, antibodies, and globulins catalyze, regulate, and protect the body chemistry [38]. Hemoglobin, myoglobin and various lipoproteins affect the transport of oxygen and other substances within an organism. Despite the variety of their physiological function and differences in physical properties-silk is a flexible fiber, horn a tough rigid solid, and the enzyme pepsin a water soluble crystal-proteins are sufficiently similar in molecular structure to warrant treating them as a single chemical family. When compared with carbohydrates and lipids, the proteins are obviously different in fundamental composition. The lipids are largely hydrocarbon in nature, generally being 75 to 85% carbon. Carbohydrates are roughly 50% oxygen, and like the lipids, usually have less than 5% nitrogen and often none at all. Proteins and peptides, on the other hand, are composed of 15 to 25% nitrogen and about an equal amount of oxygen. The distinction between proteins and peptides is their size. Peptides are in a sense small proteins, having molecular weights less than 10,000 [38-39].

The properties of proteins are determined in part by their amino acid composition. As macromolecules that contain many side chains that can be protonated or unprotonated depending

upon the pH of the medium and therefore, proteins can act as excellent buffers. The fact that the pH of blood varies only very slightly in spite of the numerous metabolic processes in which it participates, is due to buffering capacity of the blood proteins.

2.2.1 Cytochrome c and its importance

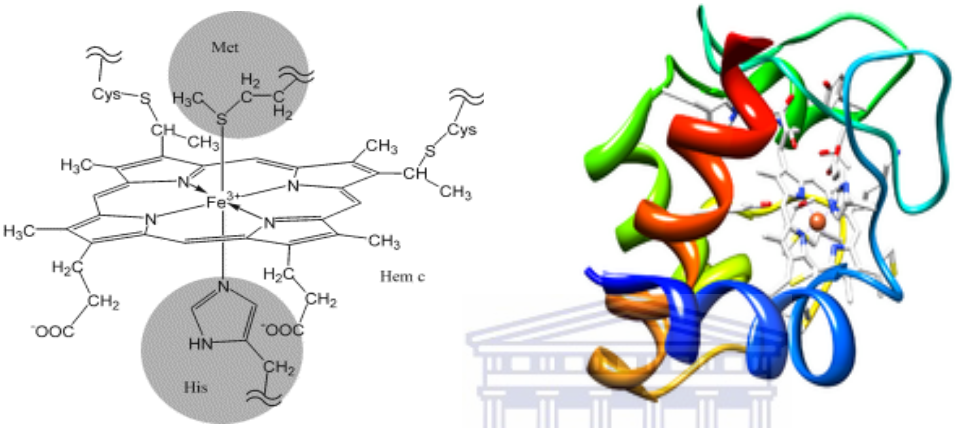

Scheme 1: Cytochrome c structure

Cytochrome c is a water-soluble mitochondrial intermembrane-space protein loosely attached to the inner mitochondrial membrane. It plays important roles in two processes: oxidative phosphorylation and oxidative respiration in mitochondrial inner membrane. In the cytosol when it is released, plays an important role as a mediator in apoptosis [18, 40]. Cytochrome c is also highly conserved ~12kDa protein, is about 104 amino acid long and consists of a peptide with a single heme group, which is covalently attached to Cys^{14} and Cys^{17} [41]. Because of its ubiquitous nature and sequence homology, cytochrome c has been used as a model protein for molecular evolution [42]. Cytochrome c is primarily known as an electron-carrying mitochondrial protein. The transition of cytochrome c from ferrous to ferric states within the cell makes it an efficient biological electron-transporter and it plays a vital role in cellular oxidations

in both plants and animals. It is generally regarded as a universal catalyst of respiration, forming an essential electron-bridge between the respirable substrates and oxygen. Its main function in cellular respiration is that in mitochondria it transports electrons between ubiquinol cytochrome *c* oxidoreductase (Complex III) and cytochrome *c* oxidase (Complex IV) [1]. Highly conserved among species, cyt c contains a covalently bound heme group and nineteen lysine residues that contribute to the relatively high isoelectric point (pI) of 9.6 [43-45].

More recently, cytochrome c has been identified as an important mediator in apoptotic pathways. The release of mitochondrial cyt c into the cytoplasm stimulates apoptosis and is commonly used as an indicator of the apoptotic process. An apoptotic process is a form of cell death in which a programmed sequence of events leads to the elimination of cells without releasing harmful substances into the surrounding area. Apoptosis plays a crucial role in developing and maintaining health by eliminating old cells, unnecessary cells, and unhealthy cells. The human body replaces perhaps a million cells a second. Too little or too much apoptosis plays a role in a great many diseases. When programmed cell death does not work right, cells that should be eliminated may hang around and become immortal, this cells maybe found in cancer and leukemia [18]. Serum cyt c levels may be an indicator of therapy-induced cell death. One of the crucial players in apoptosis is cyt c*,* which, under apoptotic conditions, is released from the intermembrane space of the mitochondria to the cytosol (Scheme 2) [46]. Once in the cytosol, cytochrome *c* combines with an adaptor subunit-apoptotic protease activating factor 1 (APAF-1) - in the presence of dATP, leading to dimerization of APAF-1 and activation of a cysteine protease-caspase 9. Caspase 9 triggers activation of other caspases, which, in turn, selectively destroy certain proteins such as DNA replicating proteins and cytoskeletal proteins resulting in cell death [47]. Release of cyt *c* from mitochondria is an early marker of apoptosis [48-49].

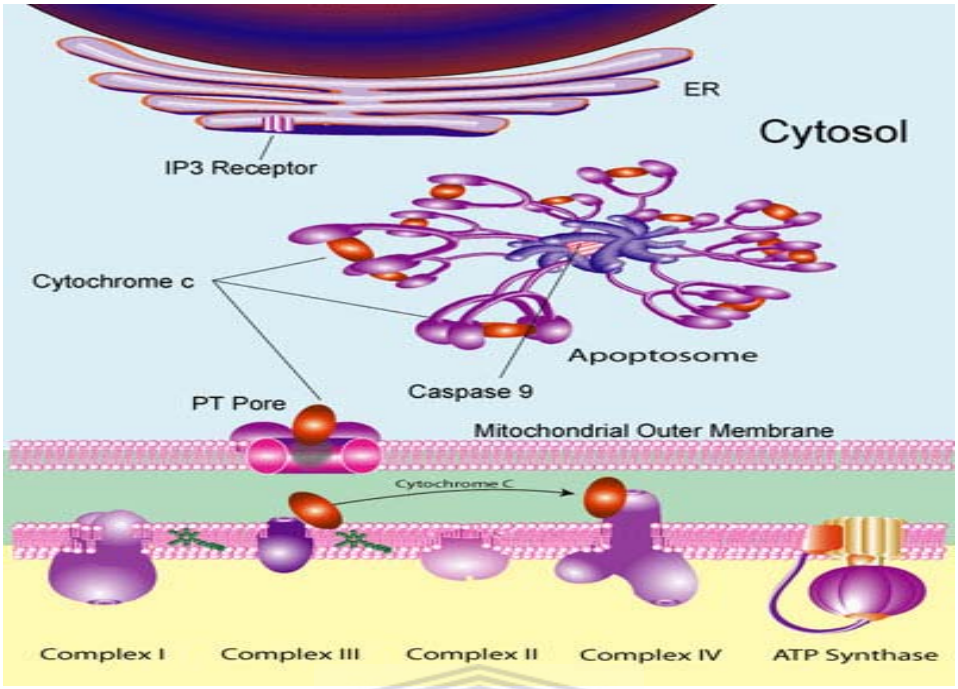

Scheme 2: Cytosol structure

2.2.3 Electron Transport Chain

The electron transport chain is a series of protein complexes embedded in the mitochondrial membrane. Electrons captured from donor molecules are transferred through these complexes. Coupled with this transfer is the pumping of hydrogen ions. This pumping generates the gradient used by the ATP synthase complex to synthesize ATP. The following complexes are found in the electron transport chain: NADH dehydrogenase, cytochrome b-c1 (cytochrome c reductase or Complex III), cytochrome oxidase, and the complex that makes ATP [50]. In addition to these complexes, two mobile carriers are also involved: ubiquinone (Q), and cytochrome c. Other key components in this process are NADH and the electrons from it, hydrogen ions, molecular oxygen, water, and ADP and Pi, which combine to form ATP [38, 51].

At the start of the electron transport chain, the electrons of NADH and $FADH_2$ are transferred to the electron transport chain onto the NADH dehydrogenase complex as shown in by scheme 3. Coupled with this transfer is the pumping of one hydrogen ion for each electron. Next, the two electrons are transferred to ubiquinone. Ubiquinone is called a mobile transfer molecule because it moves the electrons to the cytochrome b-c1 complex. Each electron is then passed from the cytochrome b-c1 complex to cytochrome c. Cytochrome c accepts each electron one at a time. One hydrogen ion is pumped through the complex (cytochrome b-c1 complex) as each electron is transferred [52-53].

The next major step occurs in the cytochrome oxidase complex (complex IV) that comprises of two hemes and two Cu atoms. This step requires four electrons. These four electrons interact with a molecular oxygen molecule. Eight hydrogen ions are formed but only four are used. The four electrons, four of the hydrogen ions, and the molecular oxygen, are used to form two water molecules. The other four hydrogen ions are pumped across the membrane,

$$4e^- + O_2 + 4H^+ \rightarrow 2H_2O$$

This series of hydrogen pumping steps creates a gradient. The potential energy in this gradient is used by ATP synthase to produce ATP from ADP and inorganic phosphate. The protein cytochrome c helps in the shuttling of the electrons between complex III and complex IV. The protein transfers one electron at a time. Cytochrome c may be regarded as a model and test system for bioelectrochemical redox reactions. The protein has a metal center of Fe^{3+}. The reduction of Fe (III) to Fe (II) can be detected voltammetrically at required potentials [53-54]. The redox behavior of cytochrome c has been reported to be strongly dependent on the

electrode material and surface preparation and may vary from fully reversible behavior to irreversible behavior, with peak potentials as high as +400 mV [55-56].

2.3 Toxicity

2.3.1 Intoxication

Intoxication is the scientific term for poisoning. It results from the interaction of a chemical "poison" with some biochemical entity or process that sustains life [6]. Like other chemical processes, intoxication is mass driven; that is, it is dependent of the degree of exposure or dose, and this dose-response relationship is perhaps the most significant feature of toxicity. The degree of subsequent harm is also controlled by the organism's ability to absorb, degrade and eliminate the toxicants, as well as its particular biochemistry and physiology. The balance of exposure to and removal of the chemical from the organism determines the toxic outcome. As the saying goes, "the dose makes the poison" [6]. These characteristics also set the stage for selective toxicity, where one species can be affected by poison while another “seemingly” is not. Selectivity is a necessary feature of most medicines and pesticides. Many weed killers, for example are almost nontoxic to mammals because they selectively kill these unwanted plants by such non-animal processes as photosynthesis. Nonetheless intoxication is common to all living organisms, from people to bacteria [57].

Classical toxicology has focused almost on adverse effects in individuals or small populations of a very limited number of readily replaceable species. However the ability of toxic chemicals to affect the structure or function of an entire ecosystem, such as species diversity or energy flow, has received scant attention until recent years [6, 57].

2.4 Factors governing intoxication

Biotransformation (Metabolism): Metabolism is the balance-wheel of intoxication. This is referred to as xenobiotic metabolism which is the set of metabolic pathways that modify the chemical structure of xenobiotics, which are compounds foreign to an organism's normal biochemistry, such as drugs and poisons. Xenobiotic metabolism is different from the intermediary metabolism that converts food into energy and living cell. In most instances, the toxic effects of a chemical are inversely proportional to its metabolic detoxication and subsequent elimination. Simply the more efficient the permanent removal of the chemical from the intoxication process, the less of it will be available at the receptor levels. One may think of intoxication as a horizontal water pipe with a pump (the absorbing membrane) at one end and a flame (the receptor) at the other. If water (the toxic chemical) is pumped in, it will eventually extinguish the flame. However, metabolism may be viewed as a side tube leading to the drain; if this tube is large enough and not blocked, the water will be diverted out of the system and little or none can reach the flame. On the other hand, metabolic transformation can convert some classes of chemicals into more toxic products. A good example is the oxidative activation of insecticidal thiophosphate esters such as parathion into their oxygen analogs e.g., oxons that inhibit enzymes, that breaks down acetylcholine, an important neurotransmitter; another is the oxidation of relatively inert polycyclic aromatic hydrocarbons such as benzo[a]pyrene to epoxides that can react with DNA and initiate tumors. Flouroacetate is activated to flourocitrate, nitrobenzenes to phenyl-hydroxylamines, and arsenate to arsenite. The substance that finally reacts with the target is called the proximate toxicant [10].

Bioavailability: Bioavailibility is defined by environmental science as the degree to which substance is free to move into or onto an organism (Hamelink et., 1994); while the pharmacologist's definition is that it is the proportion of chemical that enters the systemic circulation following oral administration where absorption is ignored. It is easy to understand the difference if we consider the following example. The physician who gives the patient a pill wants to know the concentration in the bloodstream immediately available for action, while the environmental toxicologist is concerned with the proportion of chemical available from the environment via exposure routes. For a fish swimming in polluted water, for example, the concentration of chemical ready to enter the intoxication process may be affected by such factors as adsorption onto suspended particles, the hardness of the water, the ambient temperatures, and any residues already in the food [58].

The various species, and even individuals, may react differently towards any particular chemical. Plants, animals, and microorganisms generally do not respond in the same way to any given chemical, due partly to exposure routes, partly to type of receptors, and partly to metabolic ability [10, 58].

2.6 Boron Doped Diamond

2.6.2 Advantages and significance of BDD

Boron Doped Diamond (BDD) was used for our analysis because it has many superior physical and electronic properties such as mechanical hardness, chemical inertness, optical transparency high thermal conductivity, electrical conductivity depending on the doping level, weak adsorption and biocompatibility [59]. Therefore, the use of BDD in electrochemical work is attractive. When employed in electrochemistry, boron doped diamond with a typical doping level of 10^{20} cm^{-3}, can exhibit interesting kinetic effects due to the electronic/chemical state of the surface [59]. Similarly but less dramatic effects are known for glassy carbon type materials [60]. It has been demonstrated that pretreatment with an electron beam [59], plasma [61], or by applying a positive or a negative electrode potential when immersed in aqueous electrolyte media, can result in dramatic improvement or suppression of specific redox processes. The BDD electrode is better than a glassy carbon (GC) electrode because of low and stable voltammetric background current (about a factor of 10 atoms/cm^3 less than that of GC for similar areas). Therefore, the S/B (signal to background) ratios of analytes are enhanced in the voltammetric measurements and wide working potential window in aqueous electrolyte solutions is obtained [62]. As a result, redox analytes such as iron containing compounds with more positive standard reduction potentials can be investigated in the absence of excessive background current. In addition, diamond electrodes have recently been found to show high resistance to deactivation, via fouling. These properties make diamond a promising material for electroanalytical applications. They are superior to other carbon-based materials and motivated us to employ BDD as an electrode material for electrochemical measurements. Analysis of cyanide and Arsenic

compounds are very important because they are widespread in nature, such as food, pesticides, antimicrobial drugs and in industries. The detection of these compounds using electrochemical methods of analysis is a more attractive option because the cyanide and Arsenic compounds are inexpensive, highly sensitive and have long-term reliability and reproducibility. The electrochemical detection of these compounds has been reported, using carbon, platinum, mercury and gold as working electrodes. Nevertheless, the severe detection condition can damage the electrode and cause fluctuating background currents. Some researchers have reduced this problem by modifying the electrode, or using other electrochemical detection techniques such as pulse electrochemical detection. BDD can be used to eliminate this problem without any pretreatment of the electrode because of the stable surface morphologies and the surface carbon terminated by hydrogen. Thus, the BDD surface is relatively non-polar and suffers less adsorption of polar molecules [63].

Many standard methods have been established for the determination of cyanide and arsenic compounds in both environmental water and wastewater (APHA, 1998; U.S. EPA, 1983). These methods make use of for example titrimetric, colorimetric (spectrophotometry), and cyanide ion selective electrodes (ISEs) chromatography, spectrophotofluorometry, and indirect atomic absorption spectrometry. However, all are subject to interference problems such as blank or additive interferences e.g. spectral interference and analyte or multiplicative interferences e.g. physical and chemical interferences [64]. In this work we want to construct a BDD/Cytochrome c biosensor that is sensitive enough to determine not only cyanides and arsenic compounds but all toxic compounds that are harmful to the environment.

2.6.1 Structure and occurrence of BDD

Boron doped diamond is made of polycrystalline diamond formed by Chemical Vapour Deposition (CVD) in a high temperature microwave process. In the tetrahedral diamond lattice, each carbon atom is covalently bonded (sp^3) to its neighbours forming an extremely robust crystalline structure. Some carbon atoms in the lattice are substituted with boron to provide electrical conductivity. Boron acts as an electron acceptor due to its electron deficiency in its outer shell [65]. Scheme 4 below shows a structure of diamond,

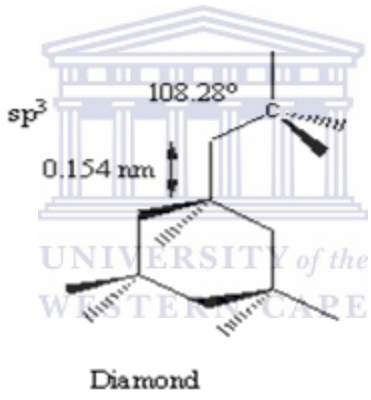

Scheme 3: Structure of diamond

Boron doping levels are in the range 10^{19} to 10^{21} atoms/cm^3 (up to 8000 ppm) to provide adequate conductivity. The BDD electrodes are available as solid wafers or as coatings on a range of suitable substrates that may include silicon, tungsten, niobium and tantalum. An example of a solid BDD electrode is shown below.

Scheme 4: Boron doped diamond (BDD)

There are many applications for Boron Doped Diamond such as, electrosynthesis, corrosion protection, electrochemical-based toxic waste remediation, detection of sodium azide in ground, anodic stripping voltammetry of heavy-metal ions in aqueous media [66]

2.6.1.2 Activation procedures for BDD

In contrast to as grown boron doped diamond electrodes, industrially grown, polished and cleaned boron-doped electrodes have initially only relatively low level of defects and electronic surface states. For most applications in electrochemistry but not all, a surface "activation'' procedure is required. A convenient and reliable process can be based on the following electrochemical procedure**:** Boron doped diamond electrodes have to be 'activated' by cycling the potential in vigorously stirred aqueous 1M HNO_3 to remove gas bubbles between -3 and +5 V vs. SCE until a stable signal is detected with 10-20 cycles with 0.1 V/s scan rate and current densities up to 2 A cm^{-2} [67-68]

2.5 Cyanides and Arsenic

People today are surrounded by, and often depend on, a wide array of toxic chemicals that require understanding and control if one is to live in a safety place [10, 69]. Cyanides and Arsenic compounds are one of those toxic chemicals.

2.5.1 Cyanides

2.5.1.1 Sources of cyanides

Cyanides are used widely and extensively in the manufacture of synthetic fabrics and plastics, in electroplating baths and metal mining operations, as pesticidal agents and intermediates in agricultural chemical production and in predator control devices. Elevated cyanide levels are normally encountered in more than 1,000 species of food plants and forage crops, and this probably represents the greatest source of cyanide exposure and toxicosis to man and to different animals [70].

Anthropogenic sources of cyanide in the environment include certain industrial processes, laboratories, fumigation operations, cyanogenic drugs, fires, cigarette smoking, and chemical warfare. Although cyanide is ubiquitous in the environment, levels tend to be elevated in the vicinity of metal processing operations, electroplaters or electroplating, gold-mining facilities, oil refineries, power plants, and solid waste combustion. Many chemical forms of cyanide are present in the environment, including free cyanide, metallocyanide complexes and synthetic organocyanides, also known as nitriles. But only free cyanide (i.e., the sum of molecular hydrogen cyanide, HCN, and the cyanide anion, CN^-) is the primary toxic agent, regardless of origin. In aqueous solution with pH 9.2 and lower, the majority of the free cyanide is in the form of molecular HCN [19, 71].

2.5.1.2 Intoxication by cyanides

Cyanides are readily absorbed through inhalation, ingestion, or skin contact and are readily distributed throughout the body via blood. Cyanide is a potent and rapid-acting asphyxiant; it induces tissue anoxia through inactivation of cytochrome oxidase, causing cytotoxic hypoxia in the presence of normal hemoglobin oxygenation. Diagnosis of acute lethal cyanide poisoning is difficult because signs and symptoms are nonspecific, and numerous factors modify its biocidal properties, such as dietary deficiencies in vitamin B12, iodine, and sulfur amino acids. Among the more consistent changes measured in acute cyanide poisoning are inhibition of brain cytochrome oxidase activity, and changes in electrical activity in heart and brain. At sub lethal doses, cyanide reacts with thiosulfate in the presence of rhodanese to produce the comparatively nontoxic thiocyanate, most of which is excreted in the urine. Rapid detoxification enables animals to ingest high sub lethal doses of cyanide over extended periods without harm [19, 71].

Cyanide compounds are useful to society in terms of their key role in synthetic and industrial processes, for certain fumigation and agricultural uses, and for some therapeutic applications [72]. Cyanides are present in effluents from iron and steel processing plants, petroleum refineries, and metal-plating plants, and constitute a hazard to aquatic ecosystems in certain waste-receiving waters [73], and to livestock [74]. Cyanide serves no useful purpose in the human body, yet it is present in our food in quantities less than 50 mg/kg , air less than 5 mg/m^3, and water less than 10 μg/l [73-74].

2.5.1.4 Reducing the risk of exposure of Cyanides to human

If your doctor finds that you have been exposed to cyanide, ask whether your children or members of the family might also have been exposed. Your doctor might need to ask your state health department to investigate. Families can reduce their exposure to cyanide by not breathing in tobacco smoke, which is the most common source of cyanide exposure for the general population. In the event of a building fire, families should evacuate the building immediately, because smoke from burning plastics contains cyanide and carbon monoxide. Breathing this smoke can lead to unconsciousness or death. Cyanide in smoke can arise from the combustion of certain plastics e.g., polyacrylamines, polyacrylics, polyurethane, etc. [75].

Compounds that release cyanide are naturally present in plants. The amounts are usually low in the edible portion but are higher in cassava (is the third-largest source of carbohydrates for meals in the world, Cassava is the most important tropical root crop. Its starchy roots are a major source of dietary energy for more than 500 million people [76]. It is classified as sweet or bitter, depending on the level of toxic cyanogenic glucosides; improper preparation of bitter cassava causes a disease called konzo). Pits and seeds of common fruits, such as apricots, apples, and peaches, may have substantial amounts of cyanide-releasing chemicals, so people should avoid eating these pits and seeds to prevent accidental cyanide poisoning. Parents should teach their children not to eat fruit pits and seeds. People should be aware that taking high levels of vitamin C may increase the danger of cyanide poisoning from fruit pits, because more cyanide is released from the pits and vitamin c contains cyanides in it. Studies have shown that the effects of cyanide are worse in humans and animals with poor nutrition. Diets containing adequate amounts of protein should improve recovery from cyanide exposure incidents [73, 75].

2.5.2 Arsenic trioxide

2.5.2.1 Source of Arsenic trioxide

It can be generated via many routine processing of arsenic compounds including the oxidation (combustion) of arsenic and arsenic-containing minerals in air. Most of the arsenic oxide is, however, obtained as a volatile by-product of the processing of other ores. For example, arsenopyrite, a common impurity in gold- and copper-containing ores, liberates arsenic trioxide upon heating in air. The processing of such minerals has led to numerous cases of poisonings [18].

Its large scale applications include its use as a precursor to forestry products like i.e. wood, lumber, livestock etc, in colorless glass production, and in electronics. Arsenic trioxide is the precursor to elemental arsenic, arsenic alloys, and arsenide semiconductors. Organoarsenic compounds, e.g. feed additives like Roxarsone and pharmaceuticals like Neosalvarsan, are also derived from arsenic trioxide [77]. More arsenic-based compounds sodium arsenite and sodium cacodylate are derived from the arsenic trioxide.

A variety of applications exploit arsenic's toxicity, including the use of the oxide as a wood preservative. Copper arsenates, which are derived from arsenic trioxide, are used on a large scale as a wood preservative in the US and Malaysia. This practice remains controversial. In combination with copper (II) acetate arsenic trioxide gives the vibrant pigment known as paris green used both in paints and as a rodenticide [78].

2.5.2.2 Intoxication of Arsenic trioxide

Arsenic trioxide is readily absorbed by the digestive system: toxic effects are also well known upon inhalation or upon skin contact. Elimination is rapid at first having a half-life of 1–2 days, by methylation to monomethylarsenic acid and dimethylarsenic acid, and excretion in the urine, but a certain amount (30–40% in the case of repeated exposure) is incorporated into the bones, muscles, skin, hair and nails i.e., all tissues rich in keratin and eliminated over a period of weeks or months [78].

The first symptoms of acute arsenic poisoning by ingestion are digestive problems: vomiting, abdominal pains, diarrhea often accompanied by bleeding. Sub-lethal doses can lead to convulsions, cardiovascular problems, inflammation of the liver and kidneys and coagulation of the blood disorders. These are followed by the appearance of characteristic white lines called as Mees stripes on the nails and by hair loss. Lower doses lead to liver and kidney problems and changes in the pigmentation of the skin. Even dilute solutions of arsenic trioxide are dangerous on contact with the eyes [78-79].

Chronic arsenic poisoning is known as arsenicosis. This disorder affects workers in smelters, in populations whose drinking water contains high levels of arsenic (0.3–0.4 ppm), and in patients treated for long periods with arsenic-based pharmaceuticals. Similarly, studies on workers exposed in copper foundries in the U.S., Japan and Sweden indicate a risk of lung cancer 6–10 times higher for the most exposed workers than compared with the general population. Long-term ingestion of arsenic trioxide either in drinking water or as a medical treatment for cancer and leukemia can lead to skin cancer. Reproductive problems , high incidence of miscarriage,

low birth weight, congenital deformations have also been indicated in one study of women exposed to arsenic trioxide dust as employees or neighbours of a copper foundry [80].

2.5.2.3 Reducing the risk of exposure of arsenic to humans

Some people may be concerned about the effects of direct skin contact with arsenic in the soil. Such exposures rely heavily on personal activities, and require intimate contact between an individual and the contaminated soil. Typically, soil exposures are higher for children than for adults, because of frequent direct contact with soils during play and other outdoor activities. Arsenic in soil is generally strongly bound to soil particles and not readily absorbed through the skin. There are various ways to reduce exposure to arsenic in the environment**:** (**a)** limit contact with soil, if the soil is known to have levels of arsenic above ground. **(b)** preventing children especially toddlers from activities where they might ingest soil, and **(c)** reducing consumption of garden root vegetables **(d)** if drinking from a well, especially in an area with high natural arsenic in the soil, ensure that the water arsenic level is as low as possible [46]

2.6.3 Analytical methods for cyanide and arsenic detection reviewed

There are certain inherent difficulties in the detection and determination of cyanide and arsenic especially in biological samples. Therefore microbial and enzymatic biosensors have been developed or constructed for detection of cyanide and arsenic compounds. Recently, many biosensors have been developed for environmental monitoring, such as those for the determination of ammonia, phosphate and biological oxygen demand. Biosensors are suitable for environmental monitoring because of their rapid response, high selectivity, inexpensive and convenient to use devices. A number of microbial and enzymatic biosensor systems for cyanide

determination have been developed. A microbial cyanide sensor was constructed. Many microorganisms that have the abilities to degrade cyanide have been reported. Some bacterial strains that aerobically biodegrade cyanide have been used to develop microbial cyanide sensors. Cyanide oxidase in these bacteria converts cyanide into cyanate consuming oxygen. Therefore, the oxygen consumption by the immobilized bacteria due to the oxidative cyanide degradation could be monitored with a Clark oxygen electrode. Lee and Karube have developed the first microbial sensor for the determination of cyanide in 1995. A bacterial strain, Pseudomonas fluorescens NCIMB 11764, utilizes cyanide as a sole source of nitrogen. The decrease of dissolved oxygen by cyanide degradation of immobilized bacteria was directly determined by a Clark-electrode. This microbial sensor was capable to detect potassium cyanide (KCN) in rivers in the range from 0.1 to 1 ppm. Since then Karube's group has developed several devices based on immobilized cyanide degrading bacteria such as a biosensors for detection of gaseous cyanide in solution and a reactor type system for river water. On the other hand, several cyanide biosensors have been developed based on inhibition of microbial respiration. Cyanide inhibits cytochrome oxidase in the respiratory chain of aerobic cells. Subsequently, the decrease in oxygen consumption by the microbial cells was monitored with the Clark-electrode. The yeast, Saccharomyces cerevisiae (s. cerevisiae), was used by Ikebukuro et al. 1996a, 1996b, to develop biosensors for cyanide detection [81]. Recently, a practical device for determining cyanide in fruit brandies was developed by Filipovi´c and Kovaˇcevi´c (2002) also using *s*. cerevisiae. The detection limit of this amperometric biosensor was up to 0.8 ppm (3.04×10^{-5} M). Cyanide biosensors based on cyanide degrading enzymes was also constructed, but one disadvantage of this microbial cyanide biosensors is their selectivity. Therefore, only a few biosensors based on cyanide degrading enzymes that showed better selectivities have been developed [82]. An

enzyme thermistor which is a temperature-sensing element composed of sintered semiconductor material which exhibits a large change in resistance proportional to a small change in temperature, is used for immobilizing rhodanese and injectase that are mitochondrial enzymes which has been associated with protection of aerobic respiration from cyanide poisoning, were developed by Mattiasson and Mosbach (1977) for cyanide detection in blast furnace water. Their linear ranges were obtained from 20 to 600M cyanide concentrations for injectase and from 20 to 1000 M cyanide concentrations for rhodanese. The measurement of heat evaluation during the enzymatic reactions, however, is a complicated procedure and requires an expensive thermistor unit [30]. An amperometric biosensor for cyanide determination in brass plating was developed by Groom and Luong (1991). This system consisting of rhodanese immobilized on aminopropyl glass beads to form an enzyme column and sulfite oxidase immobilized on a pre-activated nylon membrane and attached to the sensing surface of an amperometric electrode. This system exhibited a linear response from 5 to 1000M cyanide concentrations. However, the data obtained were not in agreement to those of the commercially available cyanide selective electrodes as the author's state. The above biosensors lack sensitivity for cyanide detection. Based on the rhodanese-sulfite oxidase reactions and subsequent luminal chemiluminescence reaction where luminal is a versatile chemical that exhibits chemiluminescence with a striking blue glow, when mixed with an appropriate oxidizing agent, is a highly sensitive biosensor system that was developed and applied to river water analysis. Hydrogen peroxide produced by the sulfate oxidase was reacted with luminol catalyzed by peroxidase. This highly sensitive method had a linear detection range from 0.12 to 3.8 M cyanide concentrations [83] . McNeil and co-workers developed a superoxide sensor based on cytochrome c immobilized on short-chain thiol modified gold electrode. The sensor signal was proportional to the real O_2 concentration that fits well with

the mathematical model *in vitro* studies [84]. Yang co-workers used phosphatidycholine (PC) to embed Cyt *c* and to study the electro-catalytic activity of protein towards NO, found out that the modified electrode might offer an alternative to investigate enzyme biomimetic (substances, devices, or systems that imitate nature) towards NO. Oh et al., adopted two different methods to fabricate micro-pattern of self-assembled cytochrome *c* monolayer. The bioelectrochemical activity between cytochrome *c* molecular center and electrode interface for the self-assembled cytochrome *c* monolayer was investigated through the measurement of cyclic Voltammetry [85]. Paolo et al. examined the incorporation and electrochemical behavior of cytochrome *c* at glassy carbon electrode modified with polyestersulfonated ionomer Eastman AQ 55, and they found that the modified electrode incorporating cytochrome *c*, displayed electrocatalytic properties with respect to anionic substrates, such as Fe $[(CN)_6]^{3-}$ and ascorbate. However, the draw-back was that it does not display electrochemical properties with respect to a possible cationic substrate such as FA^{2+}. The glassy carbon electrode was modified with DNA molecules by adsorption action firstly and then, Cyt *c* was immobilized to DNA modified electrode by multi-cyclic voltammetric method. The direct electrochemical behavior of cytochrome *c* on DNA modified electrode was achieved and their relative electrochemical parameters were obtained. Cyt *c*/DNA modified electrode exhibited elegant catalytic action for electrochemical reduction of NO, which would be applied as a biosensor to determine concentration of nitric oxide [56]. A novel method for fabricating Cyt c/GNPs (gold nanoparticles)/ room temperature ionic liquid (RTIL)/ multi-wall carbon nanotubes (MWNTs) modified GC electrode was developed by a layer-by-layer (LBL) self-assembly technique. The results show that the RTIL (room temperature ionic liquid) nanohybrid composite film can promote direct electron transfer between the Cyt c and the underlying electrode since it is very difficult for Cyt c to exhibit a

voltammetric response at a bare electrode because of its extremely slow electron transfer kinetics at the electrode/solution interface and its short-lived and transient response on a metal electrode surface. Based on these, a novel biosensor was constructed. The biosensor showed a stable, sensitive and fast response to H_2O_2 [86].

2.7 Electrochemical methods/ Characterisation Techniques:

A very sensitive BDD/cyt c biosensor for detection/determination of toxic compounds (potassiun cyanide, arsenic trioxide and Prussian blue) was constructed. Different techniques like cyclic voltammetry (CV), square wave voltammetry (SWV), UV/vis spectroscopy, electrochemical impedance spectroscopy (EIS), fourier transform infrared spectroscopy (FTIR), have been used for characterization and applications of cytochrome c horse heart and detection of toxins.

27.1 Electroanalytical techniques.

Electrochemistry affords some of the most sensitive and informative analytical techniques in the chemists arsenal. Electroanalytical methods such as cyclic voltammetry, stripping voltammetry, differential pulse polarography, square wave and chronoamperometry complements other analytical techniques such as chromatography and spectroscopy and are not only capable of assaying trace concentrations of an electroactive analyte, but also supply useful information concerning its physical and chemical properties. Electrochemical methods of analysis include all methods of analysis that measure current, potential and resistance and relate them to analyte concentration. Quantities such as oxidation potentials, diffusion coefficients, electron transfer rates, and electron transfer numbers are readily obtained using electroanalytical methods which are difficult to obtain using other techniques. Arguably, the most popular electroanalytical

techniques are cyclic voltammetry and square wave voltammetry. This section describes the basic components of the modern electroanalytical system, the principles of cyclic voltammetry and square wave voltammetry.

2.7.2 Basic components of an electroanalytical system

The basic components of a modern electroanalytical system for voltammetric measurements are a potentiostat, an electrochemical cell and a computer. The role of the potentiostat is to apply accurate and controlled potential and monitor the current produced. The electrochemical cell, where the electrochemical measurements are carried out, consists of a working (indicator) electrode, reference electrode, and counter (auxiliary) electrode. The working electrode is where the reaction or electron (e^-) transfers of interest take place hence usually referred to as the indicator electrode. In this three electrode system, voltage is carefully regulated between the working and the reference electrodes, while the current passes between the working and the counter electrode. It is noteworthy that at no time does current pass through the reference electrode; this is ensured by the use of a potentiostat. Figure 2 show a three electrode arrangement.

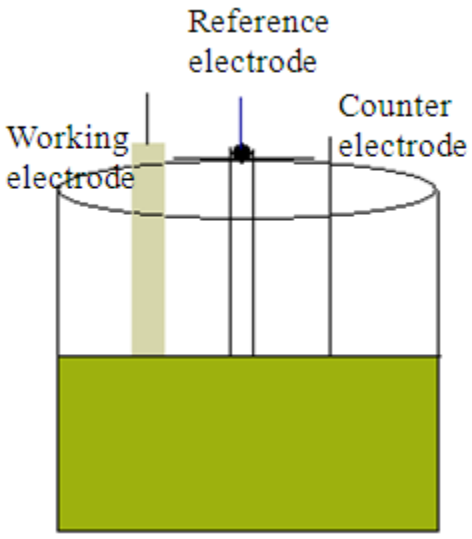

Figure 2: Representation of an electrochemical cell consisting of three electrodes.

Electrodes used were BDD working electrode, Ag/AgCl reference electrode and Pt counter electrode.

Working electrode (indicator electrode)

This is the electrode at which the electrochemical phenomena investigated takes place. The commonly used materials for working electrodes include platinum, gold or glassy carbon in my case we used boron doped diamond.

Reference electrode

This is the electrode with a constant and a known potential. Its potential is taken as the reference, against which the potentials of the other electrodes are measured. The commonly used reference electrodes for aqueous solutions are the saturated calomel electrode (SCE) and silver/silver chloride (3M Ag/AgCl).

Counter electrode (auxiliary electrode)

It acts as a sink for electrons so that current can be passed from the external circuit through the cell. Reactions occurring at the counter electrode surface are unimportant as long as it conducts current well. In most cases the counter electrode consists of a metallic foil of thin platinum wire, although gold and sometimes graphite may be used.

2.7.2.1 Cyclic voltammetry (CV)

It is a technique which is widely used in the study of oxidation/reduction reactions and the detection of reaction intermediates. It is a type of potentiodynamic electrochemical measurement. The aim of cyclic voltammetry is to provide qualitative information about electrochemical processes under various conditions. In a cyclic voltammetry experiment the working electrode potential is ramped linearly versus time like linear sweep voltammetry. Cyclic voltammetry takes the experiment a step further than linear sweep voltammetry which ends when it reaches a set potential. When cyclic voltammetry reaches a set potential, the working electrode's potential ramp is inverted. This inversion can happen multiple times during a single experiment. The current at the working electrode is plotted versus the applied voltage to give the cyclic voltammogram trace. Cyclic voltammetry is generally used to study the electrochemical properties of an analyte in solution; it is widely applicable in the study of oxidation/reduction reactions. The utility of cyclic voltammetry is highly dependent on the analyte being studied. The analyte has to be redox active within the experimental potential window. It is also highly desirable for the analyte to display a reversible wave [87]. A reversible wave is when an analyte

is reduced or oxidized on a forward scan and is then reoxidized or rereduced in a predictable way on the return scan as shown by figure 5.

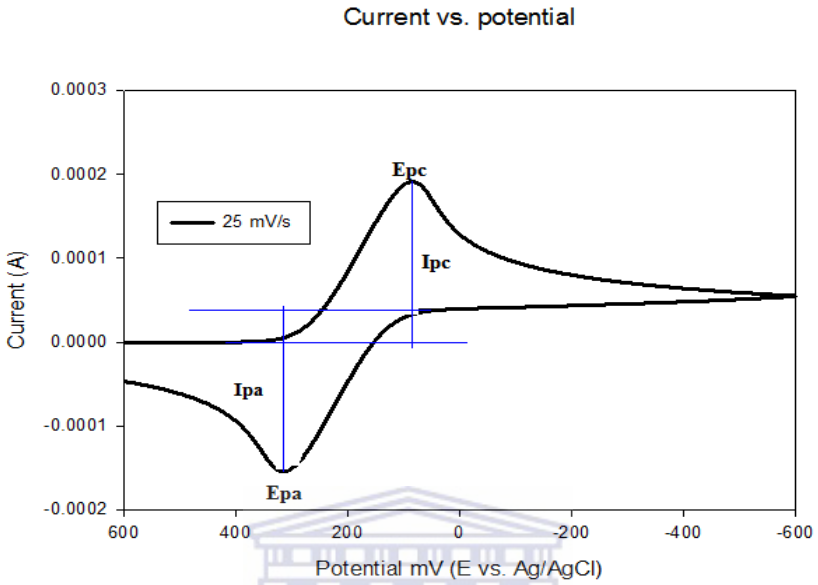

Figure 3: **A cyclic voltammogram of 5 mM ferricyanide using BDD electrode at a scan rate of 25 mV/s**

Important parameters are usually obtained from cyclic voltammogram for analysis of redox properties of an electroactive sample. These parameters include peak potentials (E_{pic}, E_{ea}) and peak currents (I_{pa}, I_{pa}) for the cathodic and anodic peaks, respectively. Consequently, important information about the sample under investigation can be obtained from the above peak parameters. This includes whether the electrochemical process displayed by the sample is reversible, irreversible or quasi–reversible. It also gives an insight into how fast the electron process is, relative to other processes such as diffusion. For instance, if the electron transfer is fast relative to the diffusion of electroactive species from the bulk solution at the surface of the

electrode, the reaction is said to be electrochemically reversible and the peak separation (ΔEp) is given below;

For reversible reaction, the concentration is related to peak current by the Randles-Sevčik equation (at 25 °C)

$$Ip = 2.69\times10^{5} n^{3/2} AD^{1/2} v^{1/2} C \quad (1)$$

For an irreversible reaction

$$Ipc = (2.99\times10^{5})\, n\, (\alpha n_a)\, ACD^{1/2}\, v^{1/2} \quad (2)$$

Where *I*p is the peak current in amperes, *v* is the rate at which the potential is swept in V s^{-1}, *A* is the electrode area (cm^2), *n* is the number of electrons transferred, *D* is the diffusion coefficient (cm^2 s^{-1}), pa is peak anodic, pc is the peak cathodic and *Co* is the concentration in mol cm^{-3}. Several voltammograms performed at different scan rates can lead to linear plots whose slopes could give further information about the redox properties of the sample in question. For, instance, when the peak current is plotted against the square root of the scan rate, the slope of the linear plot can be used to estimate the diffusion coefficient according to the Randles-Sevčik, equation shown above. When plotted, the log of peak current versus the log of scan rate gives a linear plot whose slope distinguishes between diffusion controlled peaks, adsorption peaks or even a mixture of the two. At plot of the log I_p versus log *v* there's linearity, in which a slope of 0.5 for diffusion peak and a slope of 1 for an adsorption peak is obtained. Intermediate values of the slope are sometimes observed, suggesting a "mixed" diffusion-adsorption peak in some cases, the sample to be characterized may be deposited on the surface of the electrode

(chemically modified electrodes). In such cases, one can estimate the surface concentration of the adsorbed material by the use of the Brown-Anson equation:

$$Ip = n^2F^2\Gamma Av/4RT \quad (3)$$

Where Γ represents the surface coverage concentration (mol/cm^2), *v* is the scan rate, A (cm^2) is the electrode surface area, Ip is the peak current, n is the number of electrons per reactant molecule F is the Faraday constant [23, 88-89].

2.7.2.2 Square wave voltammetry (SWV)

It is a large amplitude differential technique in which waveform composed of a symmetrical square wave: (a) is superimposed on a base staircase potential and (b) it is applied to the working electrode (Figure 4) below,

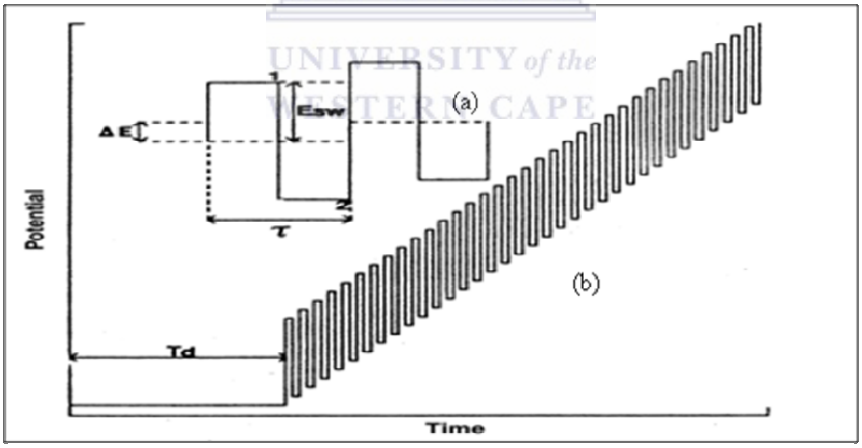

Figure 4: Square-wave waveform showing the amplitude, Esw; step height, E; square-wave period, delay time, Td; and current measurement times, 1 (forward pulse) and 2 (reverse pulse).

The current is sampled twice during the end of the forward pulse and once at the end of the reverse pulse. The difference between the two measurements is plotted versus the base staircase potential. A dimensionless plot of the theoretical forward, reverse and difference in currents for a rapid reversible redox system is shown below (Figure 5)

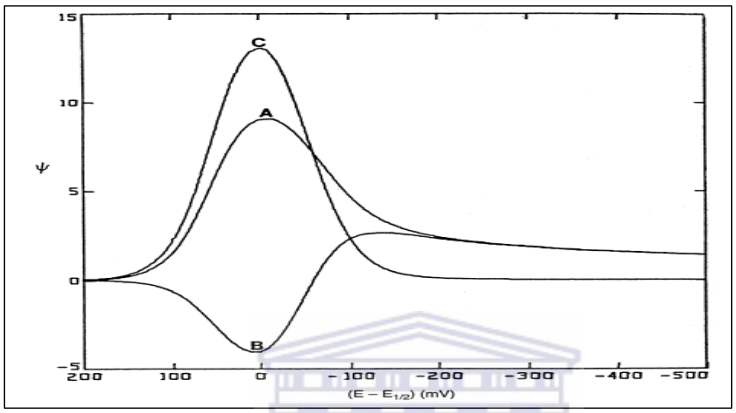

Figure 5: Square-wave voltammograms for reversible electron transfer. Curve A; forward current. Curve B: reverse current. Curve C: net current

The resulting peak-shaped voltammogram is symmetrical about the half-wave potential, the peak potential is proportional to the concentration. Its excellent sensitivity occurs from the fact that the net current is larger than either the forward or the reverse components (since it is the difference between them. The sensitivity is higher than differential pulse polarography (in which the reverse current is not used). Very low detection limits near 1×10^{-8} can be attained for reverse and irreversible cases. For reversible and irreversible cases the square-wave currents are 4-3.3 times higher than DPV or CV. The peak potential and peak current are described by the following equations:

$$E_{1/2} = E^{O} + (RT/nF)\ln(D_R/D_O)^{1/2}\ \Delta\Psi_P \quad (4)$$

$$\Delta Ipc = \pi^{1/2} tp^{1/2}\, D^{1/2}\, /nFAC_O\ \Delta\Psi_P \quad (5)$$

where n is the number of electrons, F is Faraday's Constant (96485 C/mol), A is the electrode area (cm^2), D_O is the diffusion coefficient of species O (cm^2/s), C_O is the concentration of species O (mol/cm^3), t_p is the experimental time scale (1/2 Square period - Sample window), and $\Delta\psi_p$ is a Dimensionless Peak Current parameter depends on, n number of moles, E_P peak potential and E_S static potential and R is a gas constant

Advantages of Square wave voltammetry is its speed, the effective scan rate is given by frequency (*f*) and ΔEs. Frequency of 1-100 cycles per second permit the use of extremely fast potential scan rates (e.g. *f* = 50 H_Z ΔEs = 10 mV, then the effective scan rate is 0.5 V/s) as a results the analysis time is drastically reduced, a complete voltammogram can be recorded within few seconds and kinetic studies can also benefit from the rapid scanning capability and the reversal nature of square-wave voltammetry [89-91].

2.7.3 Spectroscopic Methods

2.7.3.1 UV/vis spectroscopy

It is a reliable and accurate analytical laboratory assessment procedure for analysis of a substance. Specifically, ultraviolet and visible spectroscopy measures the absorption, transmission and emission (not at the same time) of ultraviolet and visible light wavelengths by matter. Comprise only a small portion of the wide ranging electromagnetic radiation spectrum. Although lower in frequency and therefore lower in energy than cosmic, gamma or X-rays, ultraviolet and visible light are of a higher frequency and, therefore of higher energy, than

infrared, microwave and radio waves. Spectroscopy can also be defined as a measure of the absorption, emission, or scattering of electromagnetic radiation by atoms or molecules. By such measurements, the type of the atoms or molecules present in a sample, as well as a measure of their concentration or abundance, can be made to an astonishing degree of accuracy.

When ultraviolet or visible light strike atoms or molecules they can either bounce off or cause electrons to jump between energy levels. Absorption of ultraviolet/visible light electromagnetic radiation causes an electron to move from lower energy levels to higher energy levels. Because the spectrum of an atom or molecule depends on its electron energy levels, UV-vis absorption spectra are useful for identifying unknown substances. If a material absorbs UV-visible light, then we can monitor its concentration using Beer-Lambert relationship;

$$Abs = \varepsilon C_0 l \qquad (6)$$

The optical absorbance, *Abs*, is defined

$$Abs = \log_{10} (\text{T with no sample}) / (\text{T with sample}) \qquad 7$$

where *T* is the transmittance of light following its passage through the cell [89, 92].

2.7.3.2 Electrochemical Impedance Spectroscopy (EIS)

EIS is an electrochemical technique with applications in corrosion, biosensors, battery development, fuel cell development, paint characterization, sensor development, and physical electrochemistry. EIS can even be used to test the quality of food (J. Food Science., 2000). The reason for this popularity is the high information content. EIS provides a more thorough understanding of an electrochemical system than any other electrochemical technique. Its

principle aim is to measure the impedance between the current and the potential at a fixed DC potential during frequency scan with a fixed superimpose AC signal of small amplitude. The physical values are the phase (φ) shift and modulus (Z)

In cyclic voltammetry and other dynamic electroanalysis, an applied potential is either constant (potentiostatic) or changing (potentiodynamic) when ramped at a constant rate of v =dE/dt. However, in impedance, a small perturbing potential is applied across a cell or sample and changes in a cyclic sinusoidal manner and generates a current resulting from the over potential (η) caused by the small displacements of the potential from the equilibrium value. Because the potential is only perturbing, it has the advantage of minimizing the concentration change after the experiment. The induced current alternates because the voltage changes in a cyclic manner, and hence the term alternating current (AC). The term impedance is therefore a measure of the ability of a circuit to resist the flow of an alternating current (AC). It is synonymous to resistance (R) used in direct current (DC), which is defined by Ohm's law (equation) as the ratio between voltage (E) and current (I)

$$R = E/I \qquad (8)$$

EIS is an excellent, non-destructive, accurate and rapid insitu technique for examining processes occurring at the electrode surface. During a controlled-potential EIS experiment, the electrochemical cell is held at equilibrium at a fixed DC potential, and a small amplitude (5–10 mV) AC wave form is superimposed on the DC potential to generate a response from the equilibrium position. The response to the applied perturbation, which is generally sinusoidal, can differ in phase and amplitude from the Z'' (usually, the positive y-axis correspond to $-Z''$ = $Z_{imaginary}$), over a wide frequency range normally ranging from 100 kHz to 0.1 Hz. The Nyquist

plot of impedance spectra includes a semicircle portion and a linear portion (but these is not always the case), with the former at higher frequencies corresponding to the electron transfer process and the latter at lower frequencies corresponding to the diffusion process. The electron transfer resistance (R_{ct}) at the electrode surface is equal to the semicircle diameter, which can be used to describe the interface properties of the electrode

Another way of presenting impedance data is a Bode plot in which the logarithm of the absolute value of Z' (Z_{real}) and the phase angle (φ) are plotted against the logarithm of the frequency *(f)*. This can be plotted together or separately. Nyquist plots are more commonly displayed for historical reasons, the data is however often poorly resolved (particularly at high frequencies), and the explicit frequency dependence is not displayed in the plot. In contrast, bode plots directly displays the frequency dependence; in addition, the data is well resolved at all frequencies, since a logarithmic frequency scale is used. When the frequency of the AC waveform is varied over a wide range of frequency (ca about 10^{-4} and > 106 Hz), the impedance obtained for the system is a function of the operating frequency. Spectra of the resulting impedance at different frequencies do reveal the different electrochemical kinetics involved in the system. While dipolar properties are manifest at the high frequency regions, bulk and surface properties will be evident at intermediate and low frequencies respectively. The total impedance of a system is determined by the impedances of the various components of the electrochemical cell; for example, electron transfer kinetics, diffusion and passivating layers. The relative contribution of the various components typically varies with frequency; for example, electron transfer. Measuring impedance over a wide frequency range allows processes with different time scales such as electron transfer, mass transport and chemical reaction to be detected within the same experiment. Impedance data is commonly analyzed by fitting it to an equivalent circuit model.

The frequently used circuit, called the Randles equivalent circuit is composed of different elements such as resistors, capacitors, and inductors joined in series or in parallel. Figure (8 and 9) below shows the impedance diagram for the real impedance (x-axis) and imaginary impedance- (y-axis) with low frequency data being on the right side of the plot and higher frequencies are on the left.

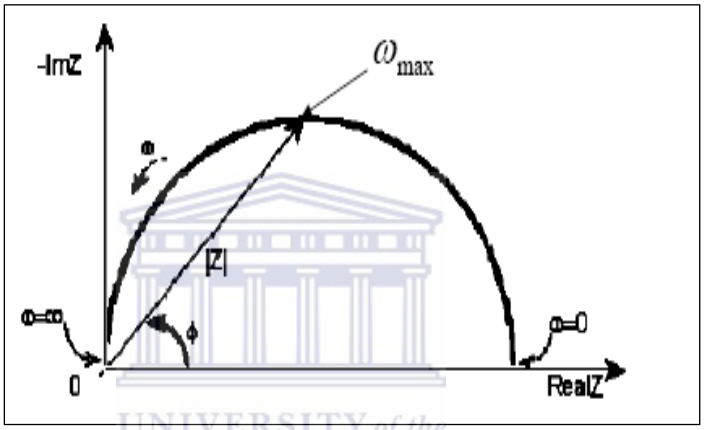

Figure 6: Nyquist Plot with Impedance Vector

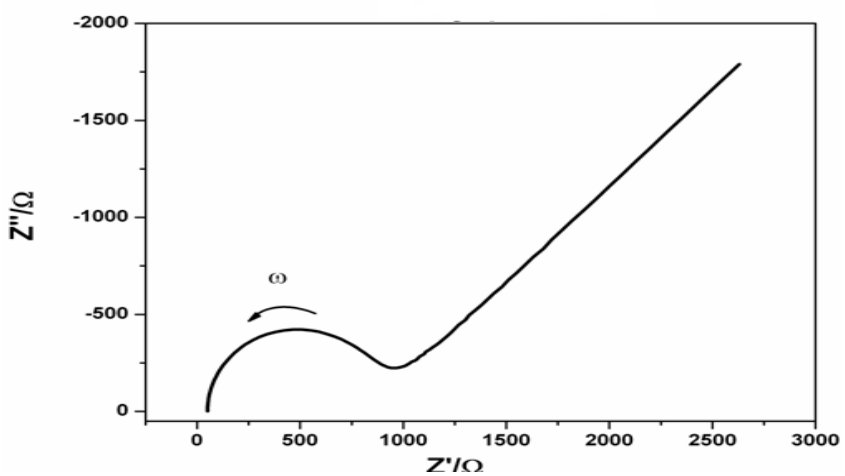

Figure 7: **A typical Nyquist plot**

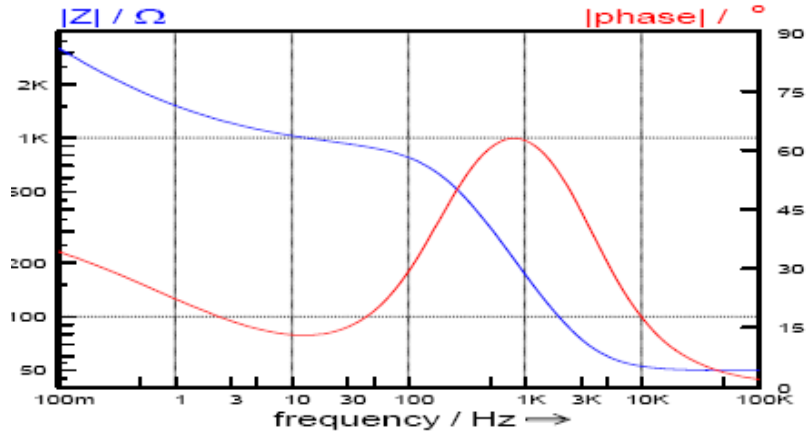

Figure 8: Typical Bode plot of Ferricyanide solution on BDD electrode showing variation of impedance and phase angle with changes in frequency

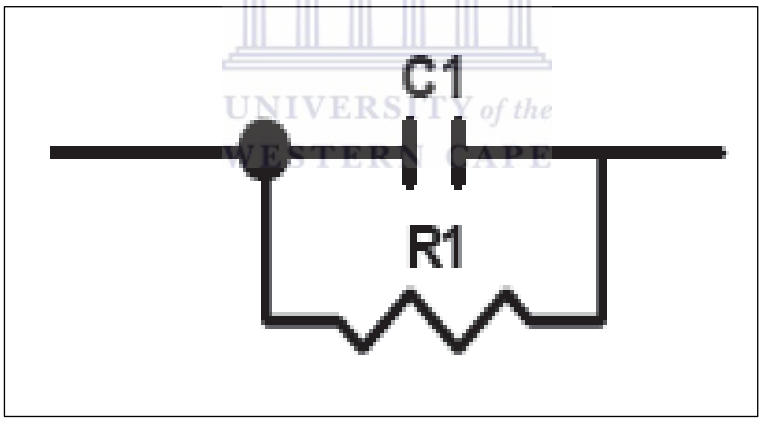

Figure 9: Equivalent circuit of a capacitor and a resistor in parallel at one time constant

Electrical circuit elements

Electrochemical Impedance plots often contain several time constants, but often only a portion of one or more of their semicircles is seen. The shape varies depending on the equivalent electrical circuits for the system. Figure 9 is a typical equivalent circuit of a capacitor and a resistor in parallel.

Any electrochemical cell can be represented in terms of an equivalent electrical circuit that comprises a combination of resistances and capacitances. There could also be contribution of inductances at very high frequencies. Contributions to the resistance of a cell are the solution resistance (R_s), the charge transfer resistance (R_{ct}), Warburg impedance (Z_w) while contribution to the capacitance could be as a capacitor (C) and constant phase element (CPE). These elements are described briefly underneath.

Solution resistance (R_s): The solution resistance is the resistance between the working electrode and the reference electrode. This is indicated as a small offset on the real impedance axis. It is measured at high frequency intercept near the origin of the Nyquist plot. The resistance of an ionic solution depends on the ionic concentration and type of ions the electrolyte is made up, temperature and the geometry of the area in which current is carried. In a bounded area with area A and length l carrying a uniform current the resistance is defined as:

$$R = \rho 1 / A \quad (9)$$

The conductivity of the solution, *p*, is more commonly used in solution resistance calculations. Its relationship with solution resistance is:

Charge transfer resistance (R_{ct}): This is the resistance associated with the charge transfer mechanisms for electrode reactions. It is the resistance to electron transfer at the electrode interface. It is deduced from the kinetically controlled electrochemical reaction at low over-

potentials. The equation for Charge transfer resistance below is deduced from Bard and Faulkner.

$$R_{ct} = RT / nFi_O \quad (10)$$

From this equation the exchange current density (*i*o) can be calculated when Rct is known. The charge transfer resistance is estimated from the diameter of the semicircular region on the real impedance axis of the Nyquist plot. When the chemical system is kinetically sluggish, the Rct will be very large and may display a limited frequency region where mass transfer is a significant factor. However, if the system is kinetically facile, then the mass transfer always plays a role and the semicircular region and R_{ct} is not well formed.

Warburg Impedance (ZW): This is the resistance associated with the diffusion of ions across the electrode/electrolyte interface. This impedance is associated with the difficulty of mass transport of electroactive species. Layers of ions at the electrode interface behave like an RC element (i.e. a resistor and a capacitor in parallel) and this produces infinite sum of RC elements called the Warburg impedance. It is characterised as a linear portion at an angle of 45° and slope of unity on the Nyquist plot and a slope of -0.5 on the Bode plot.

Capacitor (C): The capacitance (C) is the ability of an electrochemical system to store or retain charge. An electrical double layer exists on the interface between an electrode and its surrounding electrolyte. This double layer is formed as ions from the solution "stick on" the electrode surface. The potential at the terminals of this double layer (capacitor) is proportional to its charge. The impedance of a capacitor is given by the equation

$$Z_{(C)} = Z'' = 1 / j\varpi C \tag{11}$$

Therefore; Z is the imaginary value, Z" is Z real impedance, C is the capacitance and **ω** frequency

Constant phase element (CPE): A constant phase element is a non-intuitive circuit element that was invented while looking at the response of real-world systems. Often, a CPE is used in a model in place of a capacitor due to deviation of capacitance parameters from expected values. In some systems the Nyquist plot was expected to be a semicircle with the center on the x-axis. However, the observed plot may be an arc of a circle with the center being some distance below the x-axis. These depressed semicircles have been linked to a number of phenomena, depending on the nature of the system being investigated. This behaviour was traced to the non-homogeneity of the system or that there is some distribution (dispersion) of the value of some physical property of the system. The impedance of a CPE is represented by equation

$$CPE = Z = A(jw)^{-\alpha} \tag{12}$$

$$= 1/(Cjw)^{-\alpha}$$

This is similar to that of a capacitor except that the constant A = 1/C (the inverse of the capacitance) and the exponent α = 1 for a true capacitor. For a constant phase element, the exponent α is less than one. When α = 0.5, a 45° line is produced on the complex plane graph and could be used for an infinite length of Warburg element. During circuit fitting, the CPE is defined by two values, i.e., the capacitance, C, and the CPE exponent, α, which has a value between 0.5 and 1 for a non-ideal capacitor. If n equals 1, the equation is identical to that of a

capacitor and smaller values can be related to surface roughness and in-homogeneities, which lead to frequency dispersion [88, 93].

2.7.3.3 Fourier Transform Infrared Spectroscopy (FTIR),

Infrared spectroscopy reveals information about the vibrational states of a molecule. Intensity and spectral position of IR absorptions allow the identification of structural elements of molecule. Among them are typical functional groups, hydrogen bonding, but also determination of conformations or even investigation of chemical reactions. Typical vibrations of functional groups make infrared spectroscopy also an important analytical tool. In the gas phase a rotational fine structure can often be observed from which the moment of inertia of the molecule can be determined. When a spectrum is recorded using a conventional, dispersive IR spectrometer, each data point reveals the transmitted light at the respective frequency. The signal provided by the FTIR technique, however, contains information about the complete spectrum of the probe. This signal has to be transformed from the time-domain into the frequency-domain in order to reveal the spectrum. This transformation is called Fourier transformation [87].

2.5.3.4 Subtractive Normalised Fourier Transform Infrared Spectroscopy (SNFTIR).

SNFTIR was used for the analysis of the protein, which was immobilized on Platinum electrode. The techniques works hand in hand with FTIR which also helps to determine the functional groups. SNFTIR helped us to determine the formation and deformation of bonds after assignment of the peaks or the functional groups in the molecule or in our protein, as a function of applied potential.

2.5.3.5 Scanning Electron Microscopy (SEM)

A scanning electron microscope (SEM) uses an electron microscope to image samples by scanning it with a high-energy beam of electrons in a raster scan pattern. The electrons interact with the atoms that make up the sample producing signals that contain information about the sample's surface topography, composition, and other properties such as electrical conductivity. In a typical SEM, an electron beam is thermionically emitted from an electron gun fitted with a tungsten filament cathode. Tungsten is normally used in thermionic electron guns because it has the highest melting point and lowest vapour pressure of all metals, thereby allowing it to be heated for electron emission, and because of its low cost. When the primary electron beam interacts with the sample, the electrons lose energy by repeated random scattering and absorption within a teardrop-shaped volume of the specimen known as the interaction volume, which extends from less than 100nm to around 5µm into the surface. The size of the interaction volume depends on the electron's landing energy, the atomic number of the specimen and the specimen's density. The energy exchange between the electron beam and the sample, results in the reflection of high-energy electrons by elastic scattering. All samples must also be of an appropriate size to fit in the specimen chamber and are generally mounted rigidly on a specimen holder called a specimen stub. Several models of SEM can examine any part of a 6-inch (15cm) semiconductor wafer, and some can tilt an object of that size to 45°. For SEM, a specimen is normally required to be completely dry, since the specimen chamber is at high vacuum. Hard, dry materials such as wood, bone, feathers, dried insects or shells can be examined with little further treatment, but living cells and tissues and whole, soft-bodied organisms usually require chemical fixation to preserve and stabilize their structure [94-95]. The morphology of the immobilized protein was imaged using energy dispersive X-ray (EDX) spectroscopy with Hitachi X650 Detector in

secondary electron capture mode. The data was analyzed using associated EDAX Genesis 2000 software.

2.8 Research Frame-work

The experimental procedures frame work is given below as mentioned from the objectives in chapter1. In this work we want to develop a BDD/Cyt c biosensor for detection of toxic compounds (arsenic trioxide, potassium cyanide and Prussian blue)

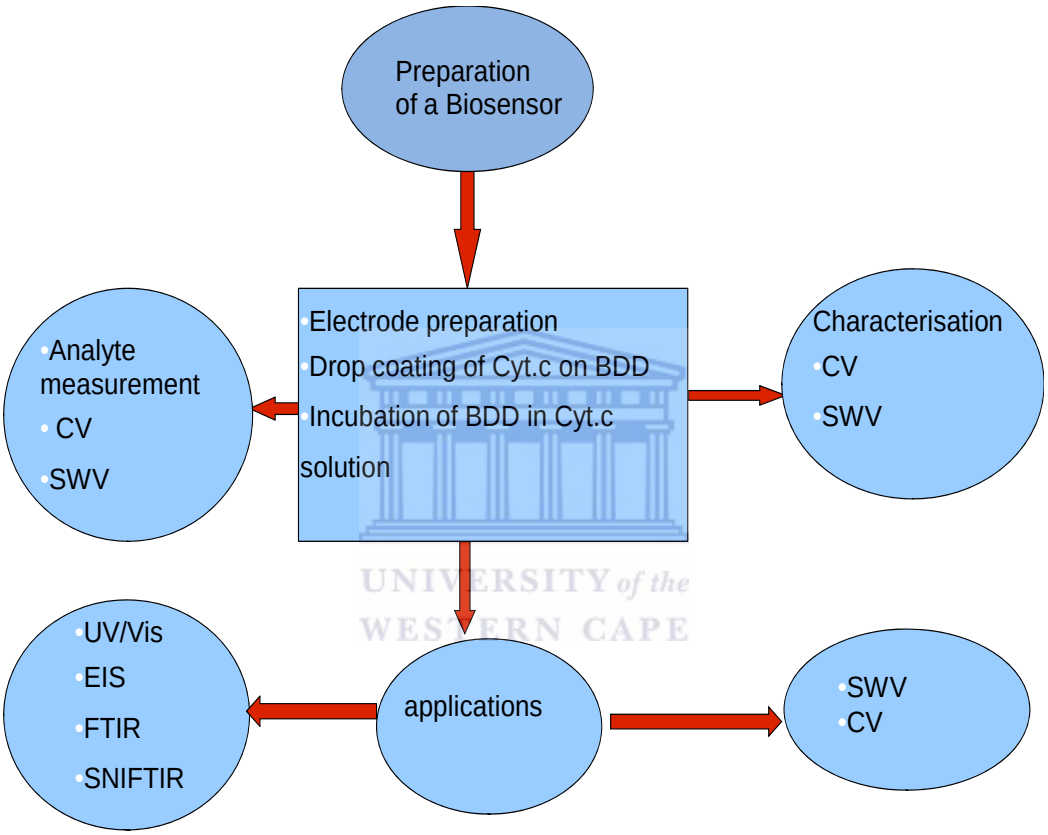

Scheme 5: Research framework

Chapter 3

Methodology

This chapter describes the general experimental procedures for the characterization of the ferricyanide and fabrication of Biosensor and its applications in the determination of toxic compounds;

3.1 Reagents and Material used

Cytochrome c horse heart (product no. 105201), arsenic trioxide (product no. 202673), Prussian blue (product no. 03899) and potassium cyanide (product no. 60178) were purchased from Sigma-Aldrich. Phosphate buffer solution (PBS), 0.1 M, pH 7.0 was prepared from anhydrous disodium hydrogen phosphate (Na_2HPO_4) and sodium dihydrogen phosphate (NaH_2PO_4). Deionized water (18.2 MΩ) purified by a milli-QTM system (Millipore) was used for aqueous solution preparations. Analytical grade argon (Afrox, South Africa) was used to degas the system. Sodium hydroxide (99.9%), Hydrochloric acid (75%), Nitric acid (65%), Potassium ferricyanide was used and was also purchased from Sigma-Aldrich. These chemicals were of analytical great. Counter electrode (platinum wire), Reference electrode (3M Ag/AgCl) and working BDD disc electrode (3mm thick, 0.07 in diameter) was used.

3.2 Instruments used:

BAS100W Bioanalytical System (Model No: 100B), Universal Pulse-EIS Voltammetry VoltaLab (Model No PGZ2402 674R052 N006, Radiometer analytical S.A, Made in France) FTIR-Spectrometer Perkin Elmer (Spectrum 100) SNIFTIR (Type MISE-PS/09/ Vertex 80v, Made in Germany) UV/vis spectroscopy Nicolette Evolution 100 Spectrometer (Thermo Electron Corporation, UK) and pH Meter.

3.3 Sample preparation

- 0.1 M PBS (Phosphate buffer solution) was prepared in 250 ml volumetric flask at pH7 this was made up to the mark using distilled water.
- Stock solution of cyt c horse heart was prepared by weighing 0.005 g (4.06×10^{-4} M) cyt c horse heart, this was dissolved in 1 ml PBS (pH 7) with final concentration of 4.06×10^{-4} M. The solution was stored in a refrigerator at 20^{o}C to prevent the protein denaturing.
- 1 M HNO_3 was prepared in 50ml volumetric flask and diluted to the mark using distilled water

Water of crystallization for Prussian blue was determined. This was done by weighing 1 g of the sample and heating it at 200^{o}C until constant masses were obtained. Table 5, 6 & 7 show the results obtained for Prussian blue.

Table 1: Weighing of watch-glass and sample

Mass of watch-glass	26.1040 g
Mass of sample (Prussian blue)	1.0014 g
Average mass of weighed	27.0826 g

Table 2: Mass of Prussian blue after heating

Number of which sample is heated	Heat 1	Heat2	Heat3	Heat4
Mass of dried sample+ watch-glass	27.0573 g	27.0336 g	27.0303 g	27.0303 g

Table 3: Mass of lost water of hydration

Mass of Prussian blue weighed (before heating)	1 g
Mass of Prussian blue weighed (after heating)	27.0303 g
Mass of lost (water of hydration)	26.0300 g

Calculated moles of Prussian blue was found to be: 0.0881 moles

Calculated moles of water was found to be : 1.4462 moles

Moles (H_2O) : 0.0881 = 16 moles

Moles (Prussian blue) :1.4462

Therefore the chemical formula was found to be: $C_6Fe_2KN_6.16H_2O$

- Stock solution of 1 mg/ml of Prussian blue was made, by dissolving 100 mg of Prussian blue in 80 ml of double distilled water, 8 ml of 1 N NaOH was added to the water and mixed well, and Prussian blue was dissolved completely. The pH of the solution was 12 at this point, which was then adjusted to 6.8 by adding 1N HCl. The stock-solution was filtered by using 0.22 µm filter and the filtrate was used as our stock-solution and the stock-solution was made-up to the mark by double distilled water in 100 ml Volummetric flask. The Stock-solution was now 1 mg/ml.

- 1mg/ml stock-solution of As_2O_3 was made, the stock-solution was made by dissolving 100mg of As_2O_3, 80 ml of double distilled water, 8 ml of 1 N NaOH was added onto the water and mixed well, and As_2O_3 was dissolved completely. The pH of the solution was

12 at this point, and was then adjusted to 6.8 by adding 1 N HCl. The stock-solution was filtered by using 0.22 µm filter and the filtrate was used as our stock-solution and the stock-solution was made-up to the mark in 100 ml volumetric flask by double distilled water. The Stock-solution was now 1 mg/ml.

- Stock-solution of 1 mg/ml KCN was made; the stock-solution was made by dissolving 1 g of KCN in 100 ml double distilled water and made to the mark. The Stock-solution was now 1 mg/ml.

3.4 Experimental procedures

3.4.1 Preparation/conditioning of Boron doped diamond electrode (BDD)

3.4.1.1 Cleaning of BDD electrode

BDD electrode was cleaned using pads and Al_2O_3 powder of different sizes (1 µm, 0.3 µm, and 0.05 µm). The electrode was rinsed with distilled water after cleaning it with Al_2O_3 powder of different microns.

3.4.1.2 Activation of BDD electrode

After the electrode was cleaned, it was activated using 1M nitric acid and it was also cleaned with the acid by running 20 cyclic scans at potentials of -1500 to 1500 mV to remove any impurities. Cyclic voltammetry at a scan rate of 50 mV/sec was used for activation of BDD electrode. The electrode was then rinsed with distilled water and dried with argon gas in preparation of drop coating of the electrode. 10 µl of (4.06×10^{-4} M) cyt c horse heart was drop coated on the electrode. The electrode was left to dry in air for 2hours, before doing any experimental work.

Incubation method was used in the preparation of the biosensor. After cleaning the electrode, the electrode was immersed in (4.06×10^{-4} M) cyt c horse heart for 4hours, for efficient attachment of cyt c.

3.5 Experimental procedures for characterisation and applications

Electrodes used: Boron Doped Diamond (BDD) electrode (working electrode), reference electrode (3M Ag/AgCl) and platinum wire (counter electrode)

3.5.1 Biosensor was prepared in two ways

Incubation method:

Boron doped diamond (3mm) electrode was incubated for 4hrs in 4.06×10^{-4} M Cyt c after cleaning and activation. This was done for proper attachment of the protein to the electrode. After incubating the electrode for four hours CVs and SWVs were run for scan rate and concentration dependent studies. This method was applied to ferricyanide detection.

Drop-coating method and application of biosensor:

10µl of 4.06×10^{-4} M cyt c solution was drop-coated on the surface of BDD (3 mm) electrode for immobilization of cyt c on the electrode. After drop coating, the electrode was dried in air for 2 hours, for the protein to be attached onto the electrode. CV and SWV analysis were carried out at scan rates (5, 10, 15, 20, 25 and 30 mV/s). Increase in current with increasing scan rates was observed, this was carried out at potentials of +600 to -600 mV. After running different scan rates spiking of analytes in PBS was done, by adding different concentrations (0 µM, 2 µM, 4 µM, 6 µM and 8 µM) of analytes (arsenic trioxide, potassium cyanide, ferricynade and Prussian blue) and a bare BDD in PBS was also run at different scan rates.

A SNFTIR platinum electrode was used as the working electrode for the immobilization of cyt c instead of BDD electrode. UV/vis spectroscopy was used to determine absorption peak for the protein and the protein with different concentrations of analyte (Prussian blue, potassium cyanide and arsenic trioxide) were added in 1 μM cyt c solution to determine/observe a change in the absorption peak of the protein. FTIR was used for characterisation of the immobilised cyt c on BDD electrode.

3.5.3 Parameters used for our techniques:

Table 4: Parameters used for CV and SWV for different scan rates

Cyclic Voltammetry Parameters			Square Wave Voltammetry Parameters	
Sensitivity	100 nA		Sensitivity	1 nA
Scan rate	5, 10, 15, 20, 25, 30 mV/s		Scan rate	1, 2, 3, 4, 5, 6 mV/s
Amplitude	50		Stepping potential	5
Initial step	600 mV		Amplitude	50
Final step	-600 mV		Frequency	5 Hz

Table 5: Parameters used for CV and SWV for different additions of Analytes

Cyclic Voltammetry Parameters			Square Wave Voltammetry Parameters	
Sensitivity	100 nA		Sensitivity	1 nA
Scan rate	25 mV/s		Scan rate	25
Amplitude	50		Stepping potential	1
Initial step	600 mV		Amplitude	50
Final step	-600 mV		Frequency	5 Hz

Table 6: Parameters used UV/vis and EIS Spectroscopy

UV/vis spectroscopy			Electrochemical Impedances spectroscopy	
Wavelength	350-700 nm		Potentials	-200 mV
Bandwidth	2.0		Stepping potential	50 And -50
Cycles	1		Frequency	1 kHZ-100 mHZ
Number of runs	14		Time	60s
			Cycles	8 bare and modified, 1 (for analytes)

Chapter 4

Results and Discussion

4.1 Characterisation of BDD electrode in PBS

An irreversible peak was observed for biosensor in 0.1 M phosphate buffer solution (PBS) pH =7 at peak potentials of -240 mV. In the presence of ferricyanide the reversible couple $Fe^{2+/}Fe^{3+}$ was observed at the biosensor with a formal potential of +198 mV and at peak potentials of -240 mV. There is a slight shift in reduction peak potential with increasing scan rates. Analyses were carried out using cyclic voltammetry and square wave voltammetry. It is well known that SWV is more sensitive than CV by magnitudes of 10^{-8} A/μM, hence it was a favourable technique to be used because of its sensitivity but nonetheless both techniques were used throughout. We investigated the electrochemistry of the bare BDD and the modified BDD (biosensor) electrode in 0.1 M PBS, in the presence and absence of 0.1 M ferricyanide.

CV of bare BDD in 0.1 M PBS (pH = 7) showed no distinguishable peaks. However the biosensors displayed an irreversible reduction peak at -240 mV in 0.1 M PBS (Figure 11). The Diffusion coefficient (D) and surface coverage (Γ) for the biosensor were calculated from plots of peak current vs. square root of scan rate for CV and peak current vs. dimensionless peak current plot for SWV, based on the slopes of the plots (Figure 12, 15 and 16).

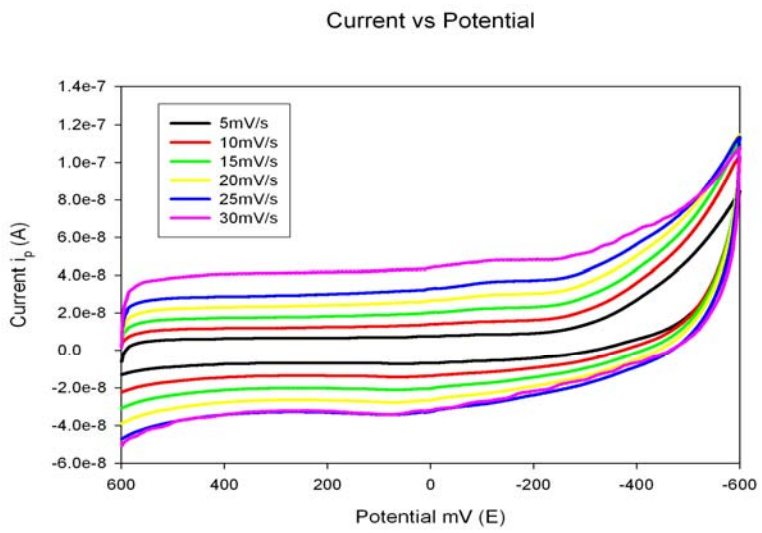

Figure 10: CV for a bare BDD in PBS pH = 7at different scan rates of (5, 10, 15, 20, 25 and 30 mV/s)

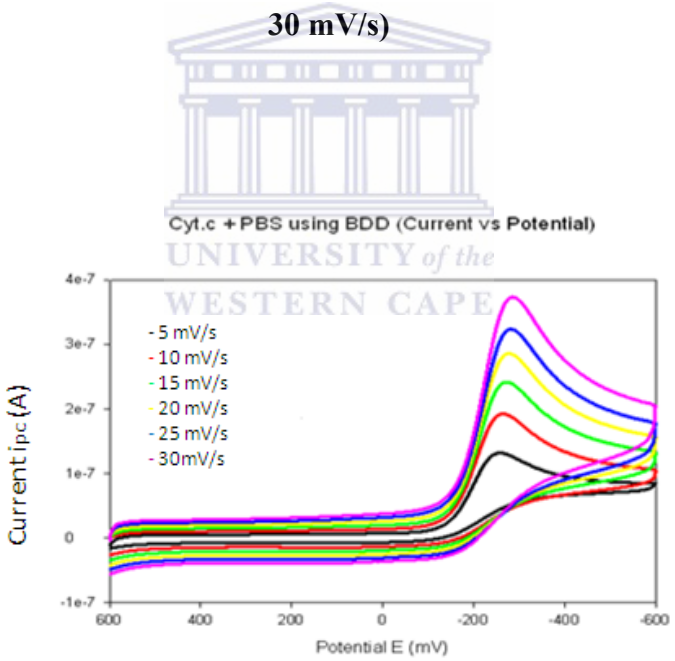

Figure 11: CV for biosensor in 0.1M PBS pH=7 at different scan rates of (5, 10, 15, 20, 25 and 30 mV/s)

Table 7: Different scan rates, currents and root scan rates for CV

Scan Rate (mV/sec)	Peak current I_{pc} (A)	$v^{1/2}$
5	1.3210×10^{-7}	2.2361
10	1.9260×10^{-7}	3.1623
15	2.4170×10^{-7}	3.8729
20	2.8570×10^{-7}	4.4721
25	3.2360×10^{-7}	5
30	3.7450×10^{-7}	5.4772

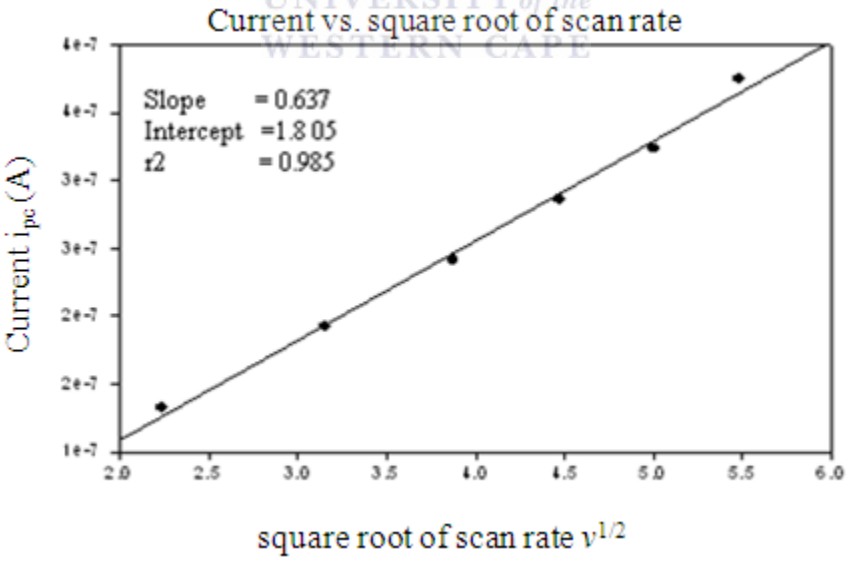

Figure 12: Cytochrome c at various root scan rates for diffusion controlled system

SWV analysis of biosensor in 0.1M PBS (pH = 7) solution at different scan rates (5, 10, 15, 20, 25 and 30 mV/s) was carried out as shown by figure 14. Dimensionless peak currents (ψ_p) values were used for our calculation. These are currents without dimensions and depend on *n* number of electrons, ΔEp and ΔEs as presented by table 8. The diffusion coeffients were calculated using the values obtained from table 8. The values obtained from table 8 were used to plot a graph of stepping potentials vs. dimensionless peak current (Figure 13 and 16). A slope (i_p/ψ_p) from a plot of peak currents vs. dimensionless peak currents (see table 8) is used to determine the dimensionless currents ψ_p values for the scan rates used for the experiments carried out which are not given in the table 8. The diffusion coefficients were calculated using these values and the following equation was used $\Delta I_p = nFAC_C Dc^{1/2} / \pi^{1/2} tp^{1/2} \Delta\psi_p$. The methodology applies to all scan rate dependance calculation for diffusion coefficients of SWV. The frequencies were kept constant (5 Hz) while the stepping potentials were varied (1, 2, 3, 4, 5 and 6)

Table 8: Dimensionless peak currents (ψ) vs. SWV operating parameters [96]

	$n\Delta E_s$/mV (ΔEp = corresponds to staircase voltammetry)		
nΔEp/mV	2	4	6
25	0.7467	0.7499	0.7533

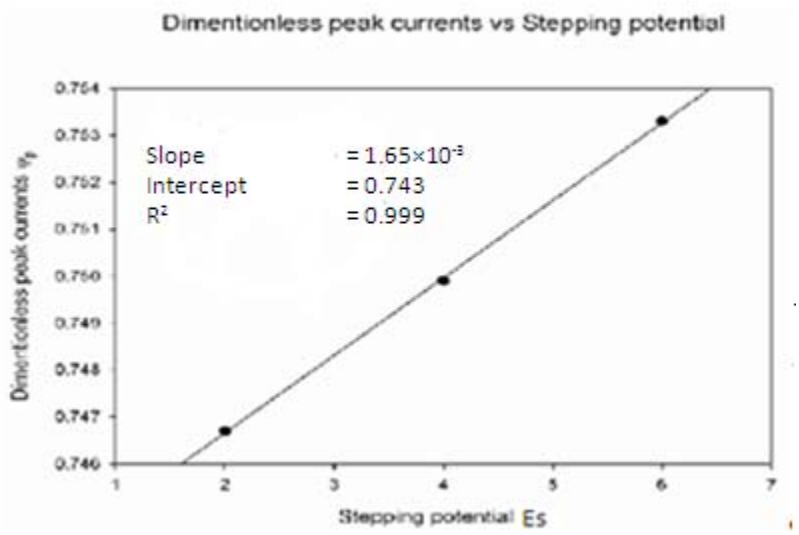

Figure 13: SWV dimensionless peak currents vs. stepping potentials (2, 4, and 6)

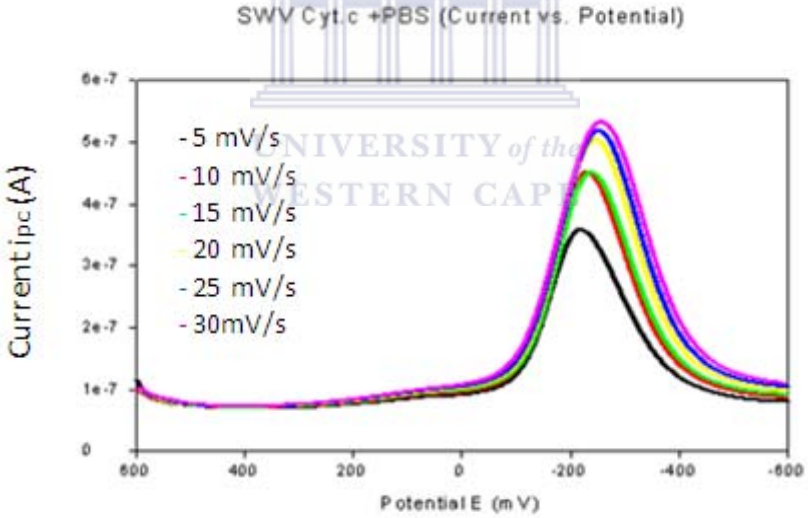

Figure 14: SWV for biosensor in 0.1M PBS pH = 7 at different scan rates of (5, 10, 15, 20, 25 and 30 mV/s)

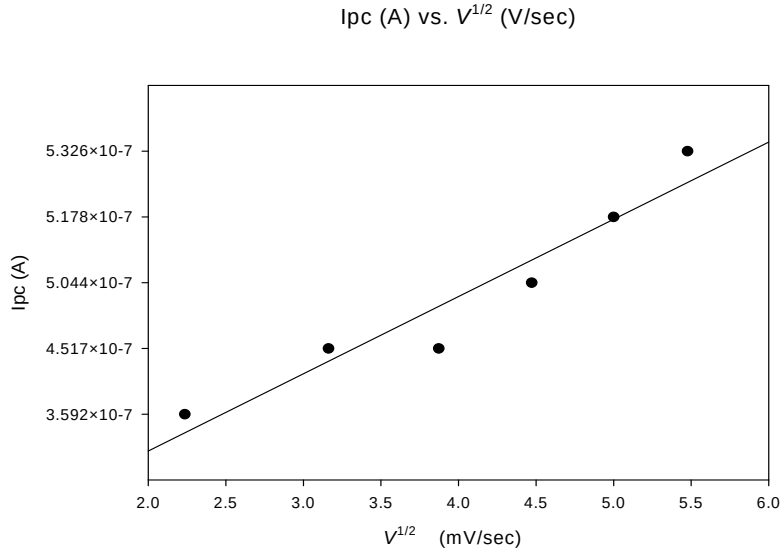

Figure 15: Peak current vs. square root scan rates for biosensor in PBS, pH = 7

Table 9: Complete table for stepping potentials E_S, dimensionless peak current, scan rates and peak currents

Stepping Potentials (E_S)	Scan rate = $E_s \times f$	Dimensionless peak current ($\Delta\psi_p$)	Change in peak current ΔI_p (A)
1	5	0.7451	3.592×10^{-7}
2	10	0.7467	4.517×10^{-7}
3	15	0.7485	4.517×10^{-7}
4	20	0.7499	5.044×10^{-7}
5	25	0.7519	5.178×10^{-7}
6	30	0.7533	5.326×10^{-7}

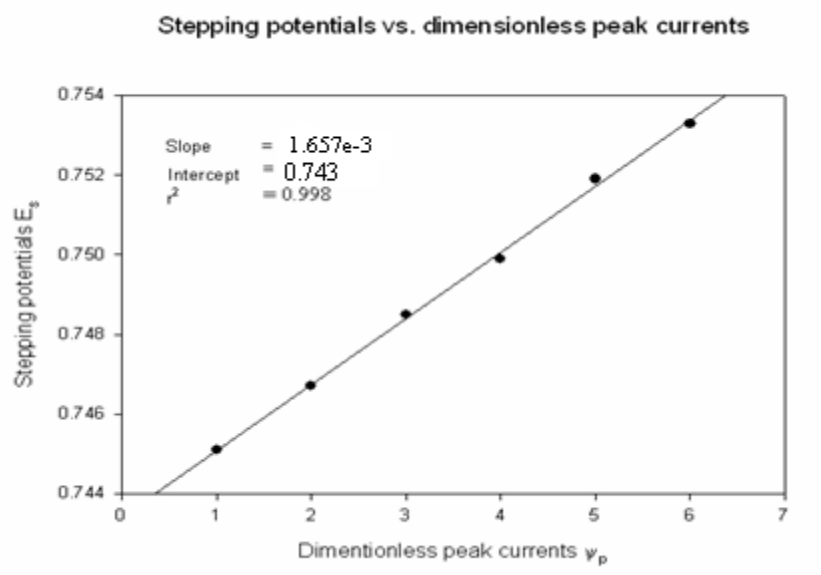

Figure 16: Plot of SWV step potential vs. dimensionless peak currents

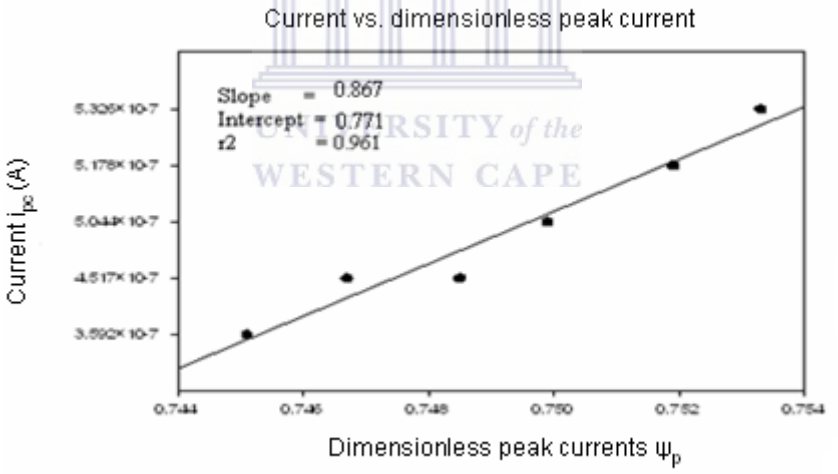

Figure 17: SWV peak currents vs. dimensionless peak currents

It is evident from the cyclic voltammetry (Figure 10) that the bare BDD electrode in PBS solution shows no notable redox electrochemistry in the potential range of -600 to +600 mV (vs. Ag/AgCl 3M NaCl). The cyt c modified BDD electrode in PBS solution shows one characteristic peak at -300mV associated with the protein cyt c as observed from Figure 11 and 14. Scan rate dependent cyclic voltammetry confirms a diffusion controlled system, evidenced by increasing peak current as a function of increasing scan rate. Values obtained are reported in table 9. The calculated diffusion coefficients for biosensor, from CV and SWV, were calculated using the following equations: for CV $I_{pc} = (2.99\times10^5)n(\alpha n_a)\ ACD^{1/2}\nu^{1/2}$, where I_{pc} is the cathodic peak current, n_a is the number of electrons involved in the charge transfer process, A is the surface area of the electrode, α is the charge transfer coefficient, C is the concentration of the solution and D is the diffusion coefficient and the diffusion coefficient was found to be 5.0927×10^{-10} cm^2/s, for SWV: $\Delta I_p = nFAC_CDc^{1/2} / \pi^{1/2}tp^{1/2}\Delta\psi_p$, were i_p is the peak current, t_p pulse width, ψ_p dimensionless peak current, F Faradaic current, n number of electrons, C concentration of the solution and D diffusion coefficient and the diffusion coefficient was calculated to be 10×10^{-10} cm^2/s. The diffusion coefficient of SWV was found to have higher value than CV, this can be due to high sensitivity of SWV (10^{-8} A/μM) or it could also be due to charging current. These parameters were calculated using a plot of current vs. square root of scan rate and peak current vs. dimensionless peak currents (Figure 12, 15, 16 and 17), some of the calibration curve (figure 15) are not very linear though they show an increase in peak current with increasing scan rate, this non-linearity can be due to an instrument error. The values obtained are of the same order of magnitude hence electrocatalytic properties of BDD electrode interface were not impeded by the immobilisation of cyt c.

The calculated surface concentration of the biomolecule at the BDD electrode surface in PBS was calculated using the Laviron's equation $I_P/v = n^2F^2A\Gamma/ 4RT$, where Ipc is the cathodic peak current, n is the number of electrons, A is the surface area of the electrode, F the Faraday's constant, v is the scan rate, R is the gas constant (8.314 J K^{-1} mol^{-1}) and Γ is the surface coverage and the surface coverage was found to be 1.7459×10^{-12} mol/cm^2 which was similar to the data obtained previously for monolayer coverage [97-98]. The k_s values were calculated using the following equation k_s (Ep) = 2.18 [D α n Fv/RT]$^{1/2}$, where k_s is the electron transfer rate constant, the sweep rate v, D is the diffusion coefficient, F the Faraday's constant, α is the charge transfer coefficient and T temperature and were calculated to be 2.719×10^{-5} cm/s for CV and for SWV was calculated to be 5.338×10^{-5} cm/s.

The determination of Cytochrome c redox peak was observed as shown by square wave voltammetry and cyclic voltammetry. The bare electrode (figure 10) showed no peak as expected of the bare electrode in the buffer solution. The irreversible peak due to the protein cytochrome c was observed at peak potential at -240 mV from both CV and SWV and this peak potential shows a slightly shifts in reduction potential with increasing scan rates. Different parameters such as diffusion coefficients, electron transfer rate constant and surface coverage were calculated from these peak potentials as observed from both CV and SWV. The diffusion coefficients were found to be of the same order of magnitude.

4.2 Biosensor response to ferricyanide and Prussian blue

Biosensor response to increasing concentration of ferricyanide, introduced into the analytical solutions as aliquots of 0.1 M of $K_3Fe_3(CN)_6$ was quantified using CV and SWV. The biosensor response was also compared to the bare BDD electrode response to the ferricyanide. Biosensor

response to increasing concentration of Prussian blue (Fe_2K $(CN)_{12}16H_2O$) was quantified in the same way. Scan rate and concentration dependence studies were carried out. Scan rate dependent CV was performed in order to calculate diffusion coefficient of the biosensor response to each analyte. The concentration studies were carried out to determine the redox chemistry of Prussian blue and ferricyanide interaction with the protein (cyt c). EIS analysis was carried out to determine the electron transfer kinetics of the Fe^{3+}/Fe^{2+}. A CV of a bare BDD in 0.1M ferricyanide was run in a potential window from +600 to -600 mV (Figure 18).

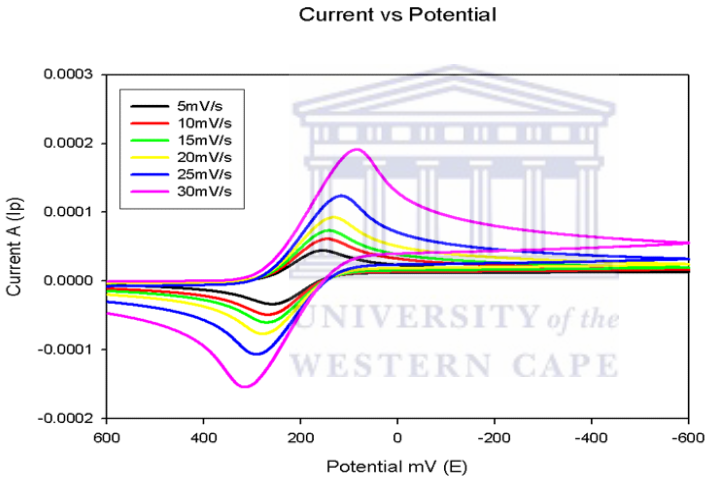

Figure 18: CV for a bare BDD in 0.1 M ferricyanide at different scan rates of 5, 10, 15, 20, 25 and 30 mV/s

4.2.1 Scan rate dependent studies for Prussian blue (Fe_2K $(CN)_{12}.16$ H_2O)

Figure 18 shows clearly the peak for Fe^{3+}/Fe^{2+} couple at formal potential of 198 mV at bare BDD electrode in ferricyanide solution. The biosensor showed two distinctive peaks as a response to the analytes which contained both Fe^{3+}/Fe^{2+} couple and CN^- ligand. We intended using these

analytes as CN^- ligands and hence the reduction peak at -240 mV was isolated at the analytical signal, in CV and SWV analysis of Prussian blue (Figure 19 and 21). Scan rate dependent cyclic voltammetry confirms a diffusion controlled system, evidenced by increasing cyt c reduction peak current at peak potentials of -240 mV, as a function of square root of scan rate (Figure 20)

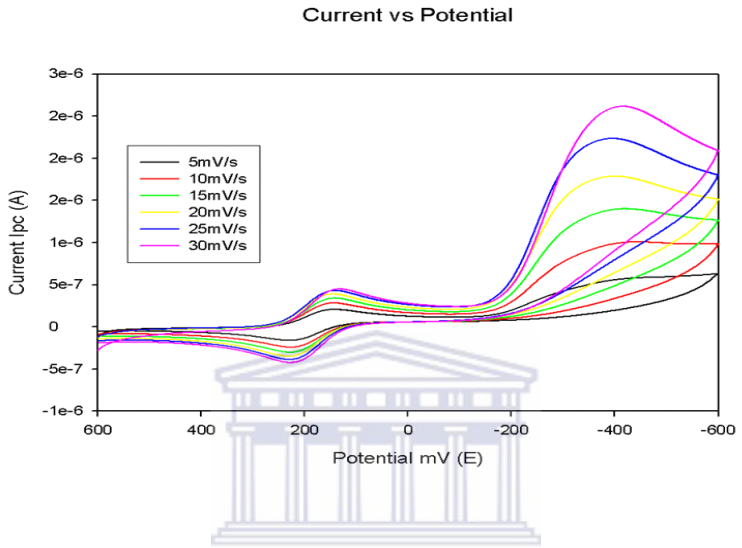

Figure 19: CV for biosensor in 1 mg/ml Prussian blue at different scan rates

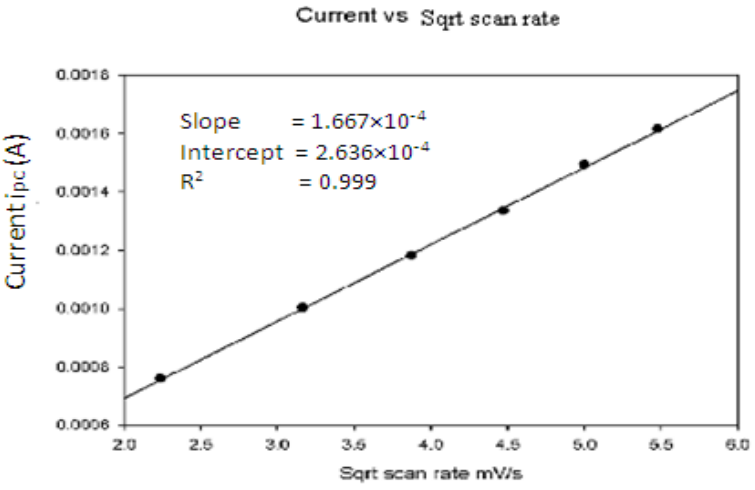

Figure 20: Peak current vs. root scan rate of biosensor in 1 mg/ml of Prussian blue solution

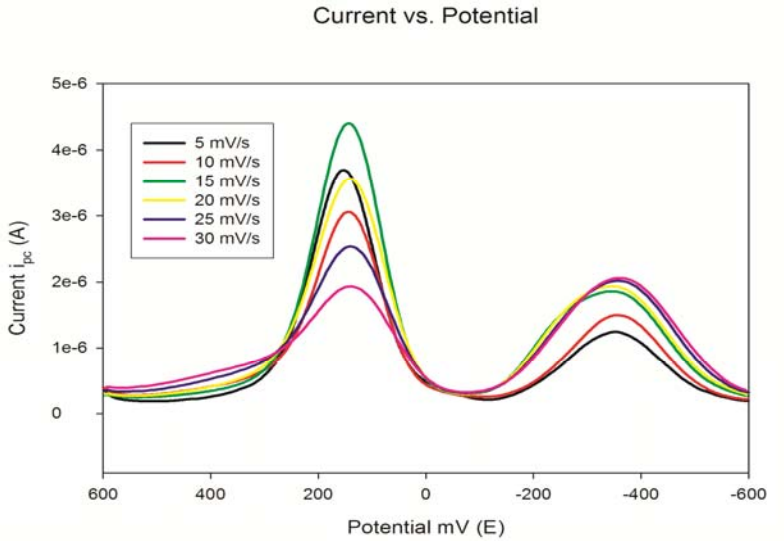

Figure 21: SWV for biosensor in 1 mg/ml Prussian blue at different scan rates (5, 10, 15, 20, 25 and 30 mV/s)

Table 10: Complete SWV results for ES (Stepping Potential), Dimensionless peak currents

Scan rate = $E_s \times f$ (mV/s)	Dimensionless peak current ($\Delta\psi_p$)	Change in peak current ΔI_p (A)
5	0.7451	2.495×10^{-7}
10	0.7467	3.590×10^{-7}
15	0.7485	4.784×10^{-7}
20	0.7499	4.676×10^{-7}
25	0.7519	4.762×10^{-7}
30	0.7533	5.070×10^{-7}

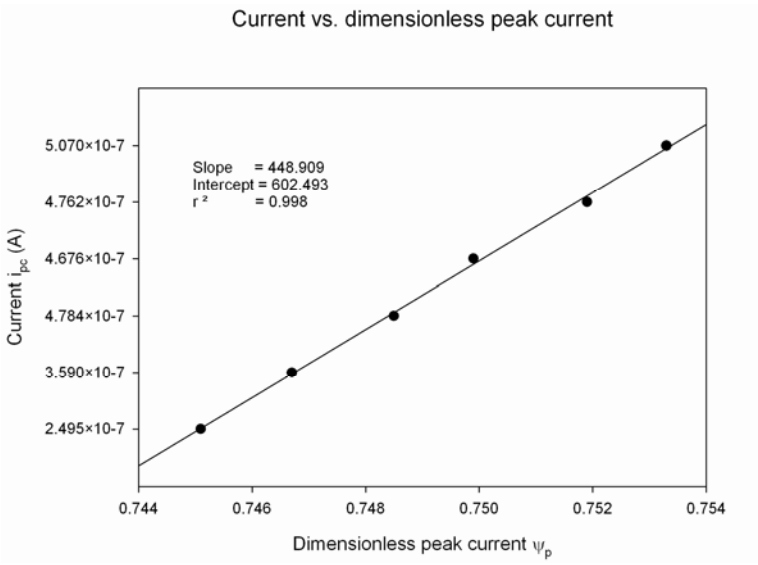

Figure 22: SWV peak currents vs. dimensionless peak currents

Figure 19 and 21 shows that the redox peak currents increase with increasing scan rate. An XY-plot of peak current as a function of square root of the scan rates ($v^{1/2}$) shows a linear increase over the range of scan rates, suggesting that the reduction process is diffusion controlled (Figure 19). The reduction peak shifts to more negative potentials, with increasing scan rates. Our system shows only one reduction peak with no evidence of reversibility. However this does not necessarily imply an irreversible electron transfer but could be due to a fast following chemical reaction [23]. Correlation coefficient R^2 for the linear plot was 0.999 and 0.998 for Prussian blue, confirming that the reduction reaction was diffusion controlled.

The diffusion coefficients of the biosensor were calculated using the irreversible equation for CV, Ipc = (2.99×10^5) n (αna) $ACD^{1/2} v^{1/2}$, was found to be 1×10^{-9} cm^3 /s for Prussian blue. This was smaller than literature value obtained by Liu et al., 5.9×10^{-7} $cm^2 s^{-1}$, using GCE/Cyt c modified with 1-pyrenebutyric acid/MWNT, in 0.1 M PBS. The surface coverage was calculated

using Laviron's equation, $Ip = n^2F^2\Gamma Av/4RT$, was found to be 2.7303×10^{-12} mol/cm^2. Geng et al., calculated a surface coverage of 2.22×10^{-9} mol/cm^2, using a nitrite biosensor based on cytochrome c. The theoretical value for monolayer coverage Chen et al., was found to have same order of magnitude as the one we obtained 1.4×10^{-12} mol/cm^2. This places our value obtained for surface coverage well within the range of surface coverage obtained for various modified surfaces employing cyt c as biosensing element. These calculations were based on the slopes of I_p/v and i_p/ψ_p (Figure 20 and 22). The diffusion coefficient calculated from SWV was obtained using equation (**5**) for Prussian blue and was calculated to be 9×10^{-9} cm^2/s, confirming that the diffusion coefficient for Prussian blue at biosensor from CV and SWV are of the same order of magnitude.

4.3 Biosensor response to increasing concentration of ferricyanide and Prussian blue

Similarly to Prussian blue CV and SWV analysis, a reversible peak for the oxidation reduction of Fe^{3+}/Fe^{2+} was observed at formal potential of +198 mV in the presence of ferricyanide. The peak current for this couple increased with every additions of analyte (ferricyanide and Prussian blue, respectively). Another irreversible peak was observed at reduction potential of -240 mV but shifted to more negative potentials, decreased with increasing concentration of the two analytes respectively. The calibration plots based on the reduction peak current vs. concentration was used to quantify the detection of CN^- using CV and SWV figure 24, 26, 28 and 30.

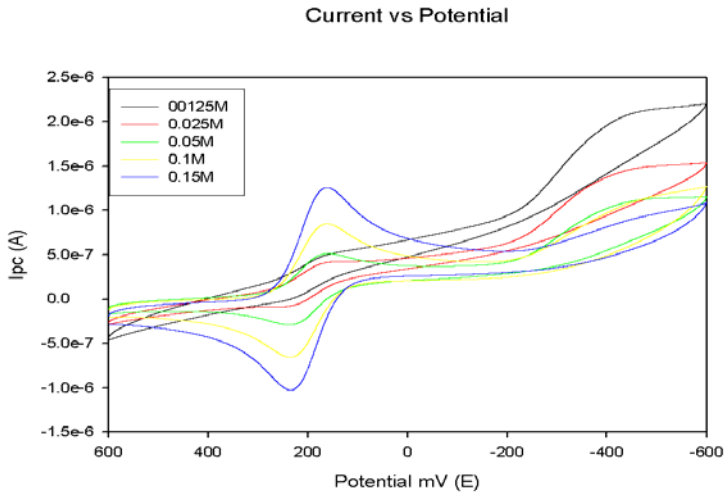

Figure 23: CV for biosensor in 0.1 M PBS (pH = 7) at 25 mV/s at different concentrations of ferricyanide

Table 11: Peak current vs. concentration obtained from CV at scan rates of 25 mV/s

Concentration (M)	Peak current Ipc (A) at -240 mV
0.0125	2.09×10^{-6}
0.025	1.47×10^{-6}
0.05	1.12×10^{-6}
0.1	1.13×10^{-6}
0.15	9.23×10^{-7}

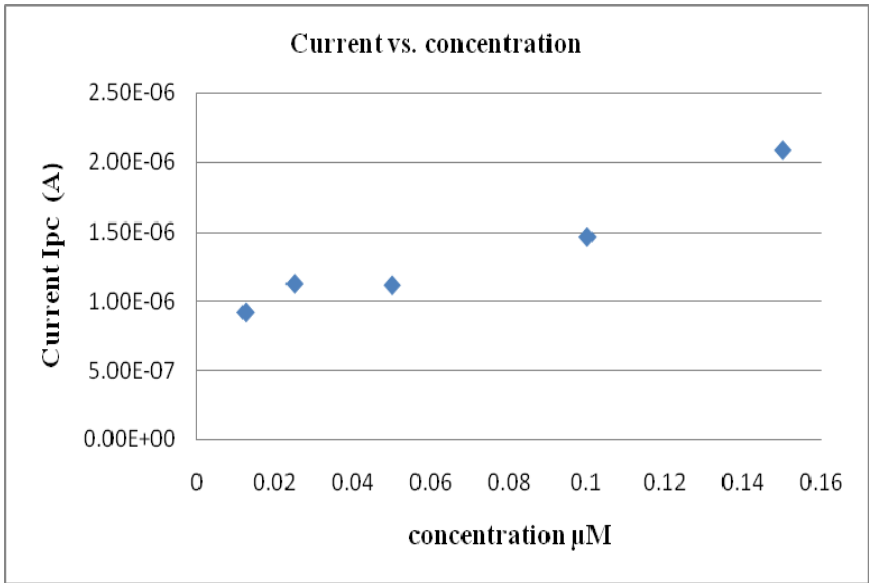

Figure 24: CV Calibration curve for biosensor in 0.1M PBS (pH = 7) at 25 mV/s at different concentrations of ferricyanide

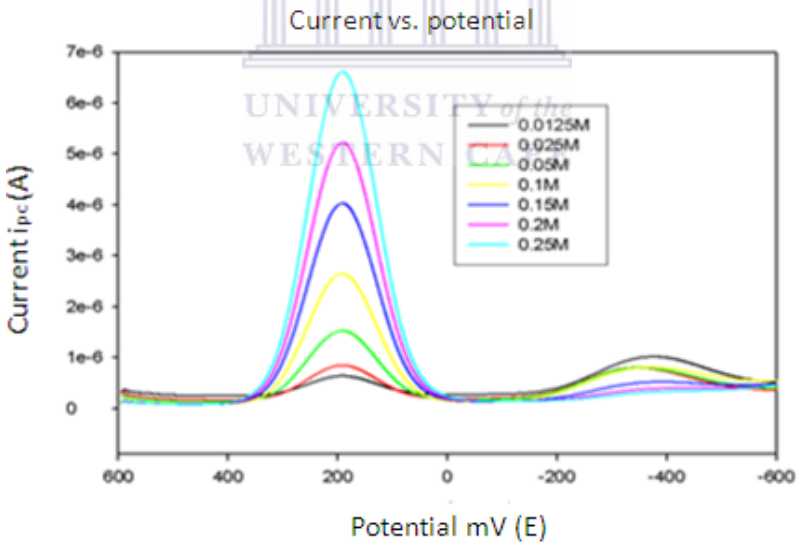

Figure 25: SWV for biosensor in 0.1M PBS pH = 7 with different additions of 0.1 M ferricyanide

Table 12: Peak current vs. concentration obtained from SWV data at scan rates of 25 mV/s

Concentration (M)	Peak current I_{pc} (A) At peak potentials of -240 mV
0.0125	8.02×10^{-7}
0.025	8.02×10^{-7}
0.05	7.93×10^{-7}
0.1	5.23×10^{-7}
0.15	3.78×10^{-7}
0.2	3.27×10^{-7}
0.25	0.25×10^{-6}

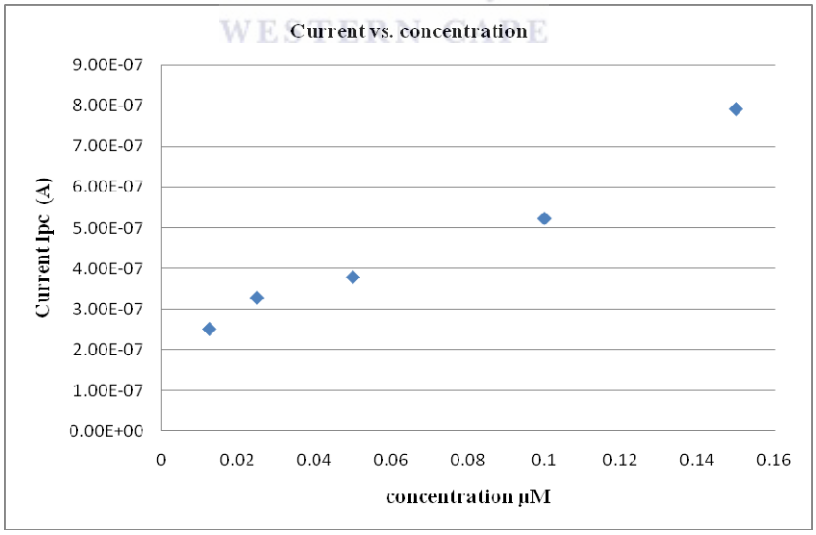

Figure 26: SWV Calibration curve for biosensor in 0.1M PBS pH = 7with different additions of 0.1 M ferricyanide

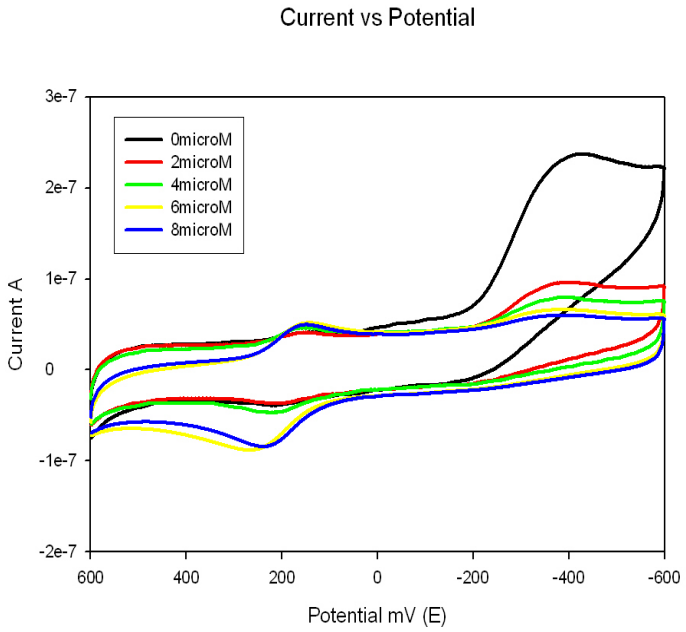

Figure 27: CV of biosensor in 0.1M PBS (pH = 7) at 25 mV/s with Prussian blue (0, 2, 4, 6, 8 and 10 µM)

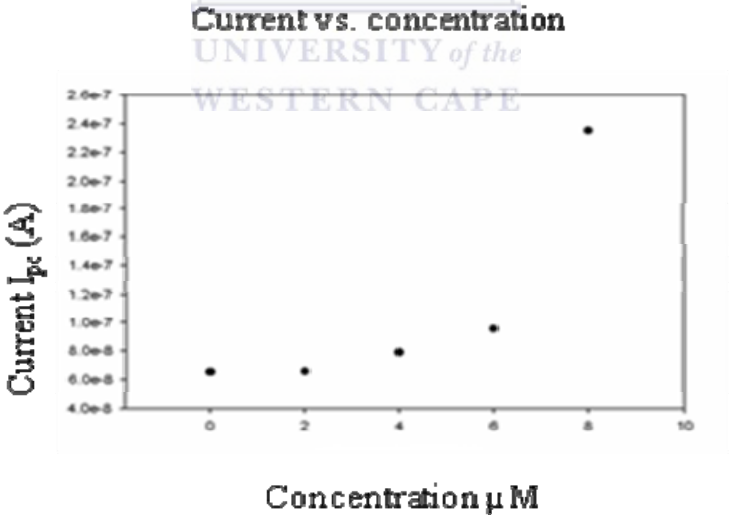

Figure 28: Calibration curve for CV of biosensor in 0.1 M PBS pH =7 at different concentration of Prussian blue (0, 2, 4, 6, and 8 µM)

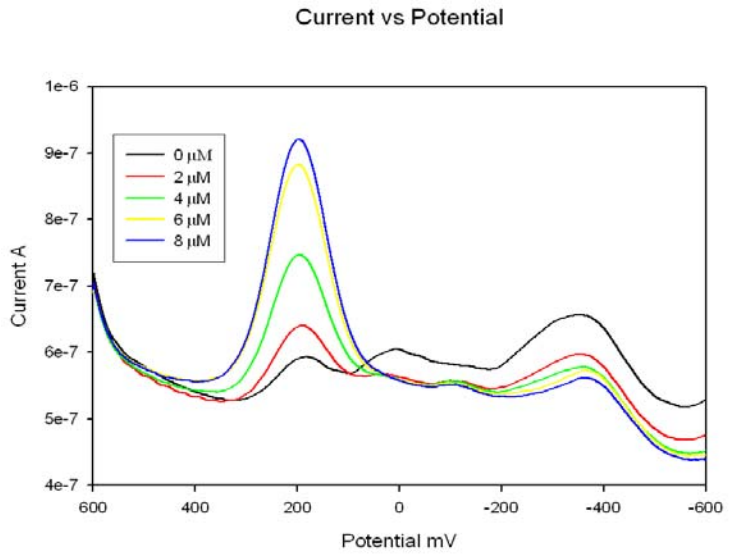

Figure 29: SWV of biosensor in 0.1 M PBS pH = 7 with Prussian blue (0, 2, 4, 6 and 8 µM)

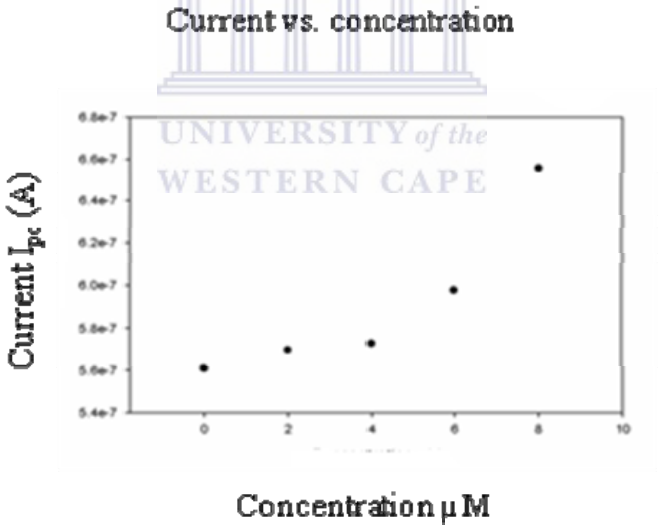

Figure 30: Calibration curve for SWV of biosensor in 0.1 M PBS pH= 7 at different concentrations of Prussian blue (0, 2, 4, 6 and 8 µM)

Figure 23, 25, 27 and 29 shows the biosensor response to increasing concentration of ferricyanide and Prussian blue, whilst figure 24, 26, 28 and 30 were not used to determine the concentration but to show binding of the respective analytes to the protein and this also account for their non-linearity. The formal potential at +198 mV was assigned to Fe^{3+}/Fe^{2+} and the reduction peak potential at -240 mV which shifts to more negative potentials with increasing scan rates is due to protein cyt c. The binding of CN^- was observed as a decrease in current at reduction peak potential of -240 mV while the catalytic oxidation reduction of Fe^{3+}/Fe^{2+} from ferricyanide and Prussian blue was observed as an increase in peak current at formal potential of +198 mV. The two peaks were very clearly resolved. Tables 12 and 13 show values of peak current against concentration measured at -240 mV. Cyanide ion binds to the protein thus blocking the electron transfer of the protein resulting in a decrease in current with each addition of ferricyanide and Prussian blue, respectively. The experiment also confirmed that the heme site of the protein was unaffected by cyanide binding to the immobilized protein. This is a significant result since it confirms a completely different interaction between CN^- and cytochrome c as opposed to $CN^-$and cytochrome c oxidase. Binding to the heme group is the mechanism responsible for most biosensors which are based on cytochrome c oxidase.

4.4 Electrochemical Impedance Spectroscopy (EIS)

Electrochemical impedance spectroscopy (EIS) can provide information on impedance changes of the electrode surface after each modification step. In EIS, the semicircle diameter of impedance equals the electron transfer resistance. This resistance reflects the electron transfer kinetics of the redox probe at the electrode interface. Figure 23 shows complex Nyquist plots of

the bare BDD electrode and the modified BDD electrode. The frequency used was 1 kHz to 100 mHz.

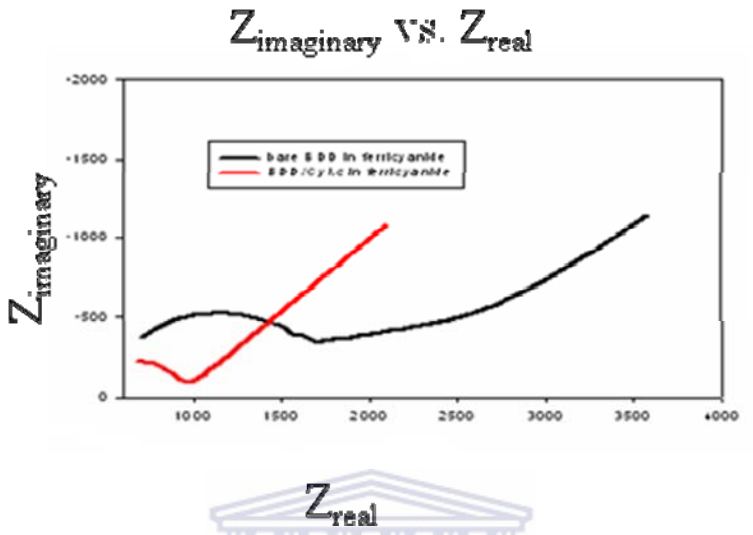

Figure 31: Nyquist plots of impedance for the bare BDD and biosensor in 5mM ferricyanide

From ω_{max} (frequency at maximum imaginary impedance of the semicircle in Hz) useful kinetic parameters such as capacitance (C in Farad), exchange current i_0 and heterogeneous rate constant *k*et were calculated using $\omega_{max} = 2\ \pi\ f$

where $\omega_{max} = 2\ \pi\ f$, R_s is the solution resistance, R_{ct} is the charge transfer resistance, C capacitance (Farad), R is the gas constant (8.314 J K^{-1} mol^{-1}), F is the Faradays constant (96 486 C mol^{-1}), n is the number of electrons, C_0 is the concentration (mol cm^{-3}) and k_{et} is the heterogeneous rate constant (cm^2/s).

The *i*o was calculated using the equation below

*i*o (modified) = RT/nFR_{ct}……(10)

From this value of exchange current (io) we were able to calculate the electron transfer kinetics (k_{et}) as shown below

k_{et} (modified) = io / nFAC$_o$……(10)

where $k$et electron transfer kinetics (cm^2/s), C$_o$ is the concentration of the solution (mol cm^{-3}), A is the area of the electrode (cm^2). The capacitance and surface coverage was calculated from the obtained value of $k$et as is shown by the equation below.

C and θ = 1- R_{ct} (modified)/R_{ct}

Table 13: Calculated impedance parameters

	k_{et}	io	ω	C	Θ
Modified BDD electrode	1.897×10^{-4}	5.189×10^{-5}	89	3.3×10^{-5}	0.4169
Bare BDD electrode	1.111×10^{-5}	3.026×10^{-5}	28	6.6×10^{-5}	

Both the modified and the bare electrode show that the impedance semi-circle and the electron transfer resistance of the modified electrode were smaller than that of the bare electrode. The R_{ct} values were obtained from equivalent electrical circuit fitting using Zplot software. The R_{ct} for modified electrode was found to be 413.6 Ω and the one for bare electrode was found to be 848.7 Ω suggesting that the modified electrode is a better catalytic system than the bare electrode and this also tells us that the protein on the electrode is facilitating the electrons hence the faster electrochemical transduction. The electron transfer rate constant k_{et} was calculated using k_{et}

(modified) = io / nFAC$_o$ and it was found to be higher (1.897×10^{-4}) for modified electrode and compared to bare electrode (1.111×10^{-5}). Other parameters were calculated as shown by table 13.

Different parameters (diffusion coefficients and surface coverage) were calculated from cyclic voltammetry and square wave voltammetry parameters. The diffusion coefficients were found to be of the same order of magnitudes and they were comparable with other work. The effect of ferricyanide and Prussian blue on the protein was observed by the decrease in peak currents of the protein with an increasing concentration of the analytes (Figure 24, 26, 28, and30). The calibration curves (Figure 25, 27, 29 and 31) confirm the decrease in peak currents of the protein, hence it was concluded that both analytes do show an effect on the protein. The impedance analysis of a bare BDD and modified electrode confirmed a smaller R_{ct} for the biosensor compared to the bare electrode showing good electron transfer kinetics was maintained in biosensor (Figure 23).

Chapter 5

Results and discussion

5.1 Application of biosensor to Potassium cyanide and Arsenic trioxide

A number of studies have been carried out using KCN to show inhibition of cytochrome c oxidase [99]. In these biosensor systems, the binding of CN^- is to the heme site of the cytochrome c oxidase. In a study by Su et al., where characterization of cyanide binding to cytochrome c oxidase immobilized in electrode-supported lipid bilayer membranes was carried out [98]. Bovine cytochrome *c* oxidase was successfully immobilized in electrode-supported lipid bilayer membrane to investigate the effect of cyanide binding on the oxidation of ferrocytochrome *c* and the electro-reduction of dioxygen. Cyanide binding to oxidase was found to be reversible and exhibited 1:1 stoichiometry. Binding constants (K_i) were also determined for binding of cyanide to the reduced and oxidized forms of the oxidase. The cytochrome *c* oxidase-modified electrodes described could potentially be used as an amperometric biosensor for the detection of cyanide (L. Su et al.,) [98]. A study in the interaction of cyanide and nitric oxide with cytochrome c oxidase was carried out as an implication for acute cyanide toxicity by Heather B et al [100]. In their work the interaction of cyanide with the oxidised and reduced forms of cytochrome c oxidase was investigated by kinetic and equilibrium measurements at 20^oC and pH 7.4 [101]. A study of the inhibition by cyanide to cytochrome c oxidase in the oxidised form under different conditions, showed that when the oxidised form of cytochrome oxidase was mixed with cyanide, the heme-absorption bands were changed extremely slowly in a process whose rate was independent of the concentrations of cyanide and protein. The stability constant for the complex was found to be 1.8×10^3 M^{-1} and the rate constant for its formation

1.3×10^2 m^{-1} sec^{-1} (E. Antonini et al.,). Inhibition of an aa_3-Type Two-Subunit Cytochrome *c* Oxidase from Nitrobacter agilis by N,N′- dicyclohexylcarbodiimide was also carried out by Fukumori Y et al., [102].

Cytochrome c is the precursor to cytochrome c oxidase and transports electrons between Complex III and Complex IV in the electron transport chain typically occurring in the mitochondria of cell walls. Cyt c has a simple chemical structure consisting mainly of a polypeptide chain attached to a heme group. The cationic side chains of several lysine and arginine residues are clustered at the surface on one face of the molecule (cyt c) and are thought to provide a binding site for anionic groups whereas anionic groups such as glutamic and aspartic acids may provide binding sites for cationic groups.

Cytochrome c is thought to carry a net positive charge since the positive amino acids predominate [84]. In the construction of the biosensor in the current research cyt c was used for the efficient quantitative measurement of some well known asphyxiants such as CN^-, As_2O_3 and $Fe_2K(CN)_{12}.16H_2O$, through irreversible binding to the positive side chains on the protein surface.

Biosensor response to potassium cyanide, KCN

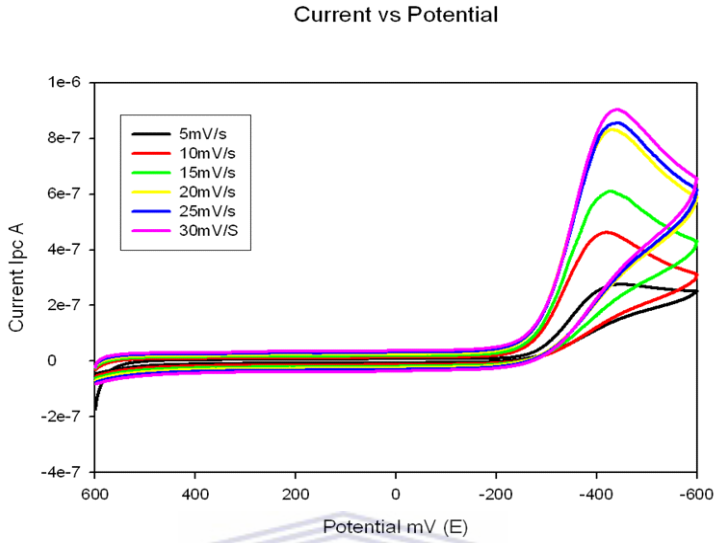

Figure 32: CV for biosensor in 1mg/ml potassium cyanide at different scan rates

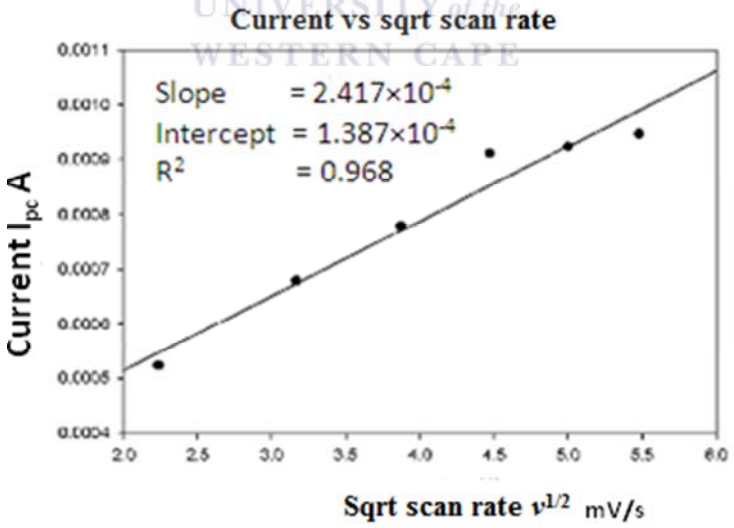

Figure 33: Peak current vs. square root of scan rate of biosensor in 1 mg/ml of potassium cyanide

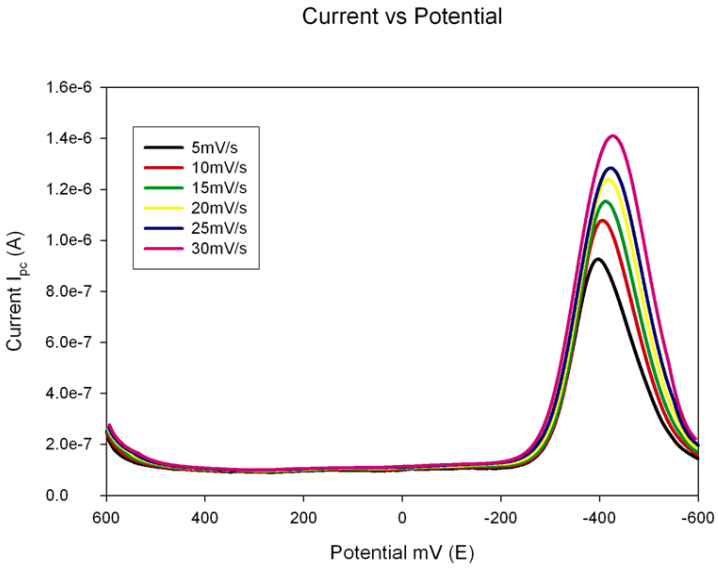

Figure 34: SWV for biosensor in 1 mg/ml potassium cyanide at different scan rates

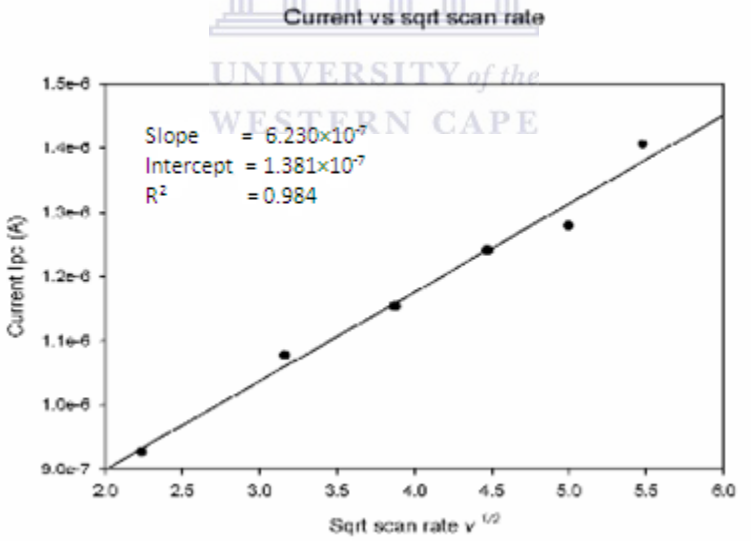

Figure 35: Peak current vs. square root of scan rate of biosensor in 1 mg/ml of potassium cyanide

Table 14: Calculated values of Dimensionless peak currents (ψ_p) for SWV and obtained values of peak currents and scan rates

Scan rate = Es ×*f*	Dimensionless peak current $\Delta\psi_p$	Change in peak current ΔI (A)
5	0.7451	9.266×10^{-7}
10	0.7467	1.077×10^{-6}
15	0.7485	1.154×10^{-6}
20	0.7499	1.241×10^{-6}
25	0.7519	1.279×10^{-6}
30	0.7533	1.406×10^{-6}

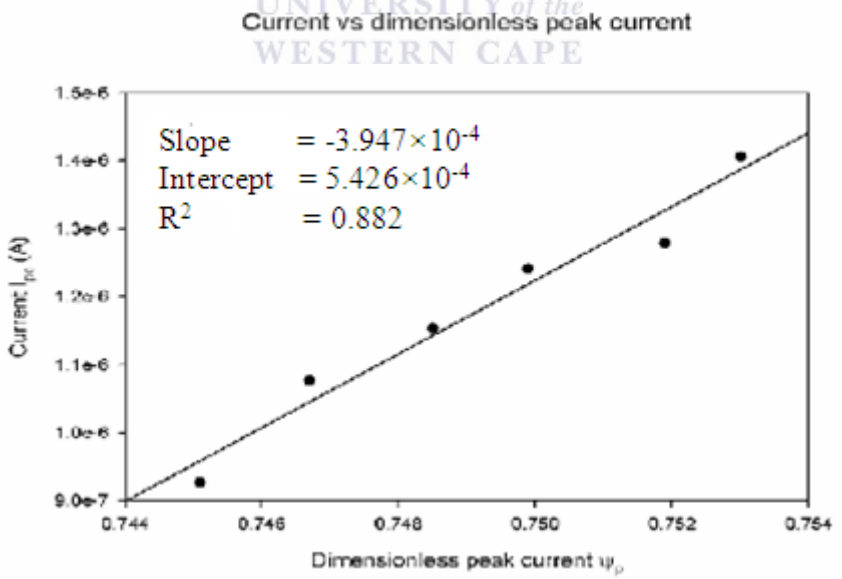

Figure 36: **SWV peak currents vs. dimensionless peak currents**

CV and SWV analysis of biosensor in 1 mg/ml of Arsenic trioxide were observed at low scan rates (Figure 32 and 34) and an increase in reduction peak current with increasing scan rate was observed. The plots of peak current vs. square root of scan rate were observed to remain linear with regression coefficient (R^2) equal to 0.990 (Figure 33) and 0.945 (Figure 35), though some of the points are not on the line, this can be due to an instrument error. The diffusion coefficients were calculated using the irreversible equation **(2)** for CV and equation **(5)** for SWV and were found to be in good agreement i.e. 1.05×10^{-9} cm^2/s for CV and 1.15 10^{-9} cm^2/s for SWV Table 14 reports the full range of dimensionless peak currents obtained from literature and experiment. A plot of dimensionless peak currents vs. current was used to calculate the diffusion coefficient for SWV (Figure 36). The rate constant was calculated using $K\ (E_p) = 2.18\ [\ D\ \alpha\ n\ Fv/RT]^{1/2}$ and found to be 4.804×10^{-2} s^{-1} for CV and 6.139×10^{-3} s^{-1} for SWV. Compared to literature values from similar systems our rate constant values are one order of magnitude smaller i.e. 2.4 s^{-1} and 1.39 s^{-1} Koh et al.,(using a Cyt c/poly-TTCA).

Arsenic trioxide, As_2O_3

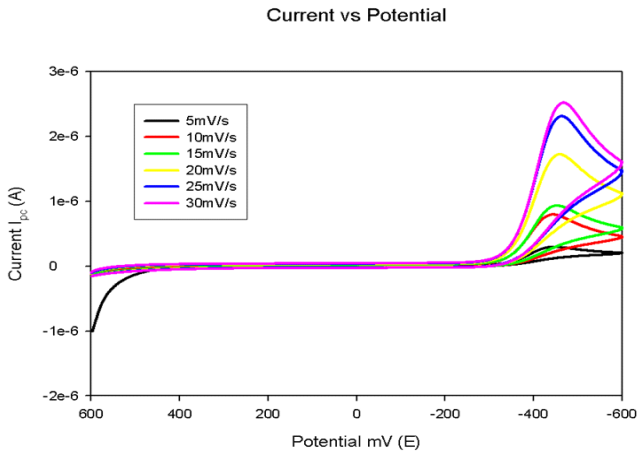

Figure 37: CV for biosensor in 1 mg/ml arsenic trioxide at different scan rates

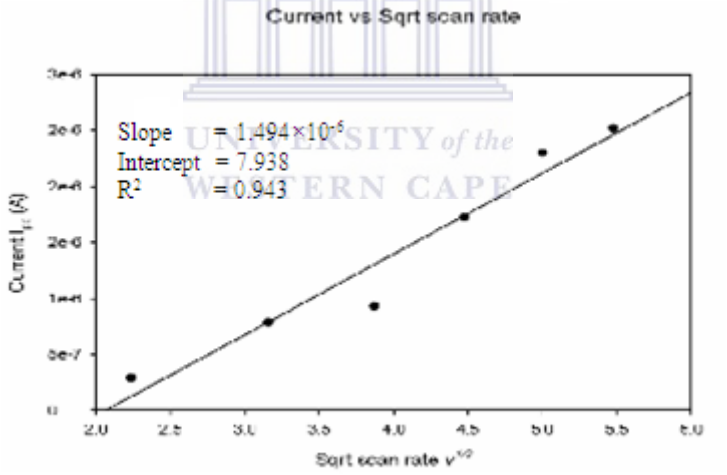

Figure 38: CV calibration curve for biosensor in 1 mg/ml arsenic trioxide at different scan rates

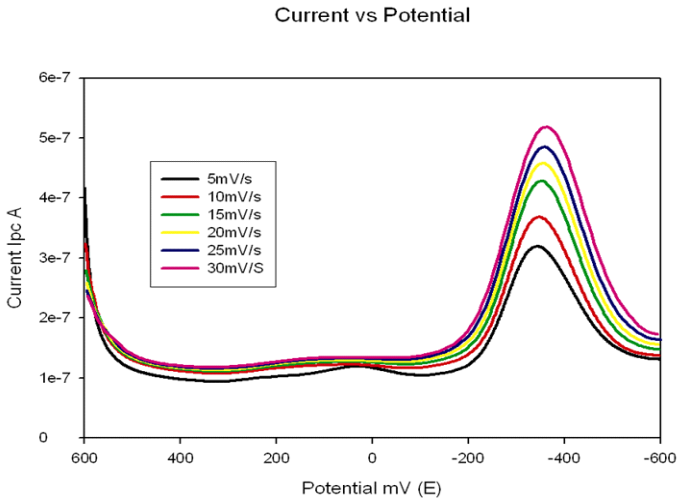

Figure 39: SWV for biosensor in 1mg/ml arsenic trioxide at different scan rates

Table 15: Calculated values for dimensionless peak currents and peak currents values obtained from SWV

Scan rate = Es ×*f*	Dimensionless peak current $\Delta\psi_p$	Change in peak current ΔIp (A)
5	0.7451	3.195×10^{-7}
10	0.7467	3.690×10^{-7}
15	0.7485	4.274×10^{-7}
20	0.7499	4.576×10^{-7}
25	0.7519	4.862×10^{-7}
30	0.7533	5.170×10^{-7}

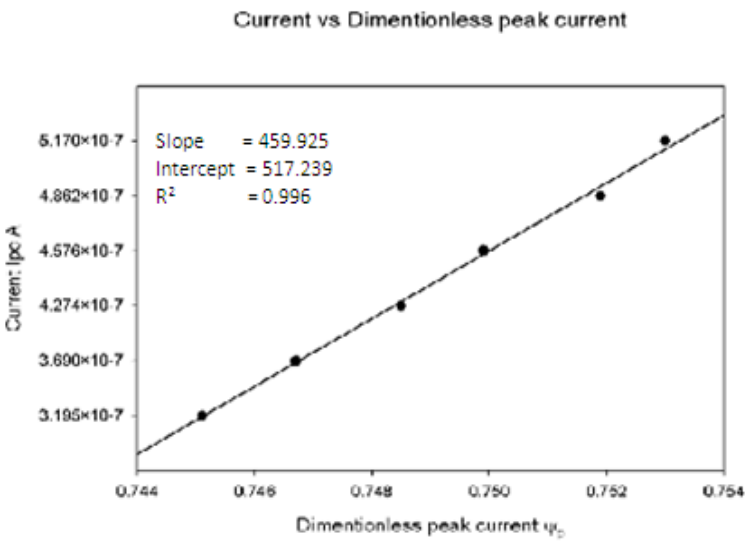

Figure 40: SWV peak currents vs. dimensionless peak currents

The influence of the scan rate was investigated to determine whether the system was diffusion controlled or adsorption process. Figure 37 and 39 shows CV and SWV for biosensor 1 mg/ml of As_2O_3 at different scan rates respectively. The reduction peak for each analyte linearly increased with the square root of the scan rate ($v^{1/2}$) from 5 to 30 mV/s at peak potential of -240 mV. In other words the current function ($i_p/ v^{1/2}$) had a constant value at different scan rates, indicating that the biosensor reaction was controlled by diffusional process. Peak current vs. square root of scan rates were plotted to quantify the diffusion control process (Figure 38), even though the plot does not show the best fit, which can be due to system error. The diffusion coefficient obtained from CV was 2×10^{-9} cm^2/s for arsenic trioxide. The surface coverage was calculated using Laviron's equation was found to be 3.066×10^{-12} mol/cm^2 and that of potassium cyanide was calculated to be 1.431×10^{-11} mol/cm^2. Geng et al., (using a system of A sandwich structured SiO_2/cyt c/SiO_2 on a boron-doped diamond film electrode as an electrochemical nitrite biosensor) [44] found the surface coverage of 2.22×10^{-9} mol/cm^2 which is three orders of

magnitude higher than what we found. This suggest that the calculated value found in literature is higher than our value but the theoretical value found by Chen et al.,(using a L-cysteine/Au system) was found to have same order of magnitude as ours 1.4×10^{-12} mol/cm^2. Using slopes of dimensionless current plots the diffusion coefficients from SWV for arsenic trioxide was found to be 9×10^{-9} cm^2/s figure 40. The rate constants k_s were calculated as 1.067×10^{-4} s^{-1} (CV) and 1.229×10^{-9} s^{-1} (SWV).

5.1.2 Biosensor response as a function of increasing concentration of potassium cyanide and arsenic trioxide.

The biosensor response to As_2O_3 and KCN concentration was evaluated (Figure 41a,b, 42a,b, 43a,b and 44a,b).

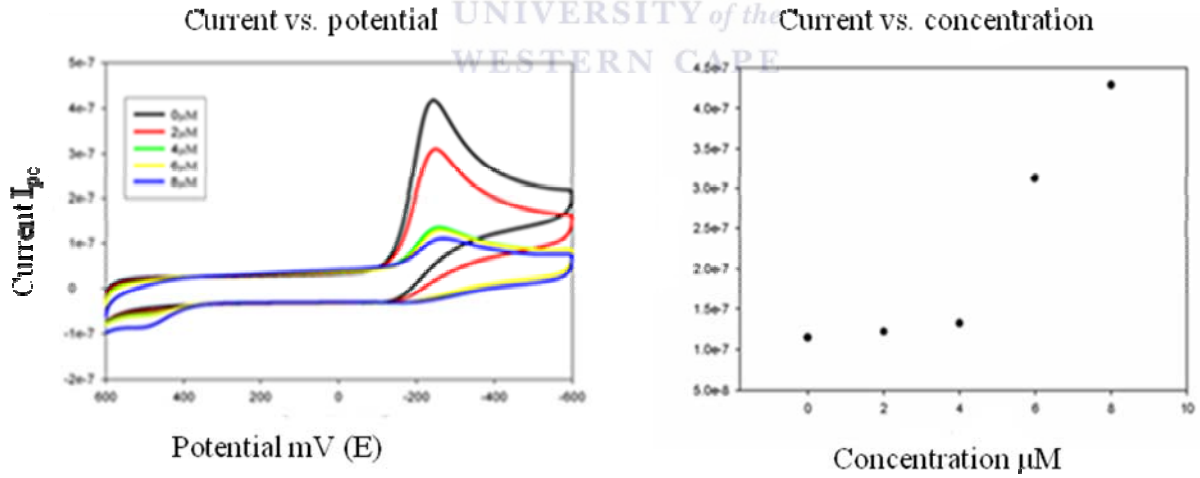

(a) **(b)**

Figure 41: (a) CV of biosensor 0.1 M PBS (pH = 7) at different concentrations of potassium cyanide (0, 2, 4, 6 and 8 µM) (b) Calibration curve for KCN

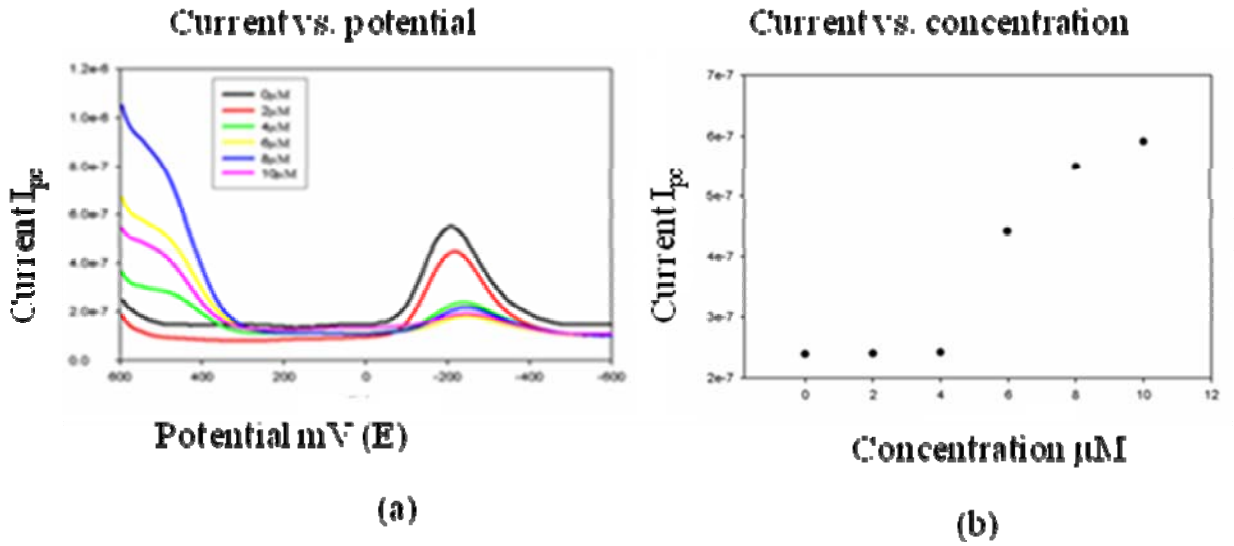

Figure 42: (a) SWV of biosensor 0.1 M PBS (pH = 7) at different concentrations of potassium cyanide (0, 2, 4, 6 and 8 µM) (b) Calibration curve for KCN

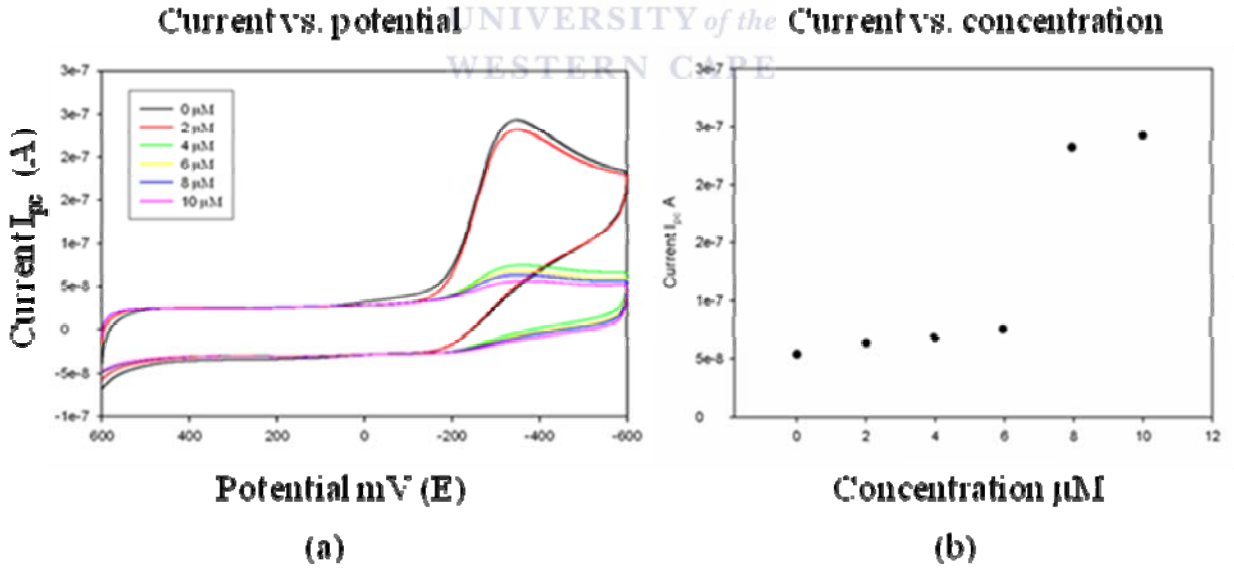

Figure 43: (a) CV of biosensor in 0.1 M PBS (pH =7) at different concentrations of arsenic trioxide (0, 2, 4, 6, 8 and 10 µM) (b) Calibration curve for As_2O_3

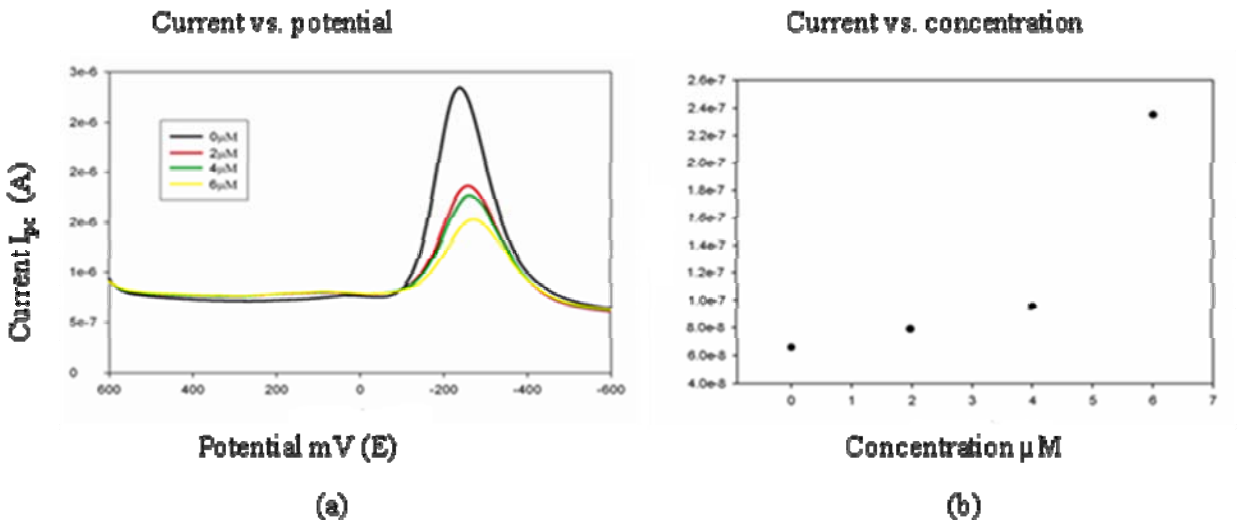

Figure 44: (a) SWV of biosensor in 0.1M PBS pH =7 at different concentrations of arsenic trioxide (0, 2, 4, 6 and 8µM) (b) Calibration curve for As_2O_3

5.1.3 Detection limits and sensitivity for KCN and As_2O_3

Table 16: Calculated Detection limit and Sensitivity from CV and SWV for the analytes

	Sensitivity (A/µM)	Detection Limit (µM)	Regression analysis (r^2)
CV (KCN)	3.9715×10^{-8}	4.22	0.940
CV (As)	2.07894×10^{-8}	8.076	0.951
CV (PB)	1.8479×10^{-8}	9.086	0.882
SWV (KCN)	4.4880×10^{-8}	9.082	0.975
SWV (As)	1.8509×10^{-8}	22.020	0.854
SWV (PB)	1.0870×10^{-8}	37.496	0.884

Table 17: **Allowable limits of detection for cyanides and arsenic compounds by EPA and WHO**

	Allowable limit of detection by EPA and WHO in drinking water (µg/L)	Limit of detection from literature (µg/L)
Arsenics	10	0.5
Cyanides	200	-

The detection limits calculated for the biosensor in table 16 were calculated by determining the standard deviation (SD) from plots and multiplying the SD by 3 and then divided by the sensitivity which was obtained by ploting a calibration curve of concentration vs. current there by drawing a straight line through the origin and the slope of the calibration curve was taken to be equal to the sensitivity (SD × 3/ Sensitivity). The results show a decrease in current with an increase in concentration of both arsenic trioxide and potassium cyanide. The results show binding of potassium cyanide and arsenic trioxide to the protein cyt c by inhibiting the electron transfer therein (Figure 41a, 42a, 43a and 44a). It was also observed by Su et al. where the effect of KCN to the protein was carried out and the magnitude of the reductive peak after addition of cyanide become smaller [98]. Figure (41b, 43b for CV and 42b, 44b for SWV) shows the response of the biosensor before and after different additions of cyanide and arsenic compounds. These calibration curves also confirm the decrease in current with increasing concentrations.

In the construction of the biosensor in the current research, cytochrome c was used rather than cytochrome c oxidase for the efficient quantitative measurement of some well known

asphyxiates such as CN^-, As_2O_3 and Prussian blue, through irreversible binding to the positive side chains on the protein surface. This binding was attained for cyanide and arsenic compounds (Figure 41a,b, 43a,b for CV and 42a,b, 44a,b for SWV) for different analytes cyanide and arsenic compound. These plots showed how a toxic compound can bind to the protein and inhibit the electron transport process. The results obtained were meaningful since the biosensor was able to measure far below the EPA and WHO guidelines.

The controlled adsorption of functional proteins on bare electrode metal electrodes can be very critical. They may denature or adopt an orientation or change in structure [103]. An irreversible reduction peak was observed in our analysis and was due to adsorption. The reduction peak showed no denaturation of the protein since the current increased with increasing scan rates but decreased as we spiked different concentrations of toxic compounds, showing a change in the environment of the protein. Similar work for determine the behaviour/the redox reaction of the protein cyt c has been carried out to determine the behaviour/the redox reaction of the protein cyt c by Lie Wang [56] but in their case a gold electrode was coated with denatured cyt c horse heart. The analysis was carried out to determine the behaviour of denatured protein. There were no redox peaks observed in their analysis. In this another study of GCE/cyt c in 0.1 M PBS was carried out in which an irreversible reduction peak potential of -240 mV was observed [104]. Thus based on these findings it is concluded that the irreversible reduction peak reported by us is due to the protein but it changes its structure as we add higher concentrations of the toxic compounds.

Chapter 6

Impedance and spectroscopic analysis

6.1 UV/vis spectroscopy

From cyclic voltammetry and square wave voltammetry it was seen that the peak potential of the protein observed -240 mV decreased with increasing concentrations of potassium cyanide, Prussian blue and arsenic trioxide, which showed a binding of the cyanides and arsenic to the protein. The UV/vis analysis was carried out to investigate the binding of the analytes to the protein in solution and to show that the protein is not denature but is infact intact. UV/vis analysis of a 0.1 M solution of cytochrome c prepared in phosphate buffer (pH=7) was recorded for observation of cytochrome c before and after successive additions of the respective analyte. Cytochrome c displayed two characteristic UV/vis absorption bands i.e. the soret band at 409 nm and the Q band at 550 nm (Figure 45).

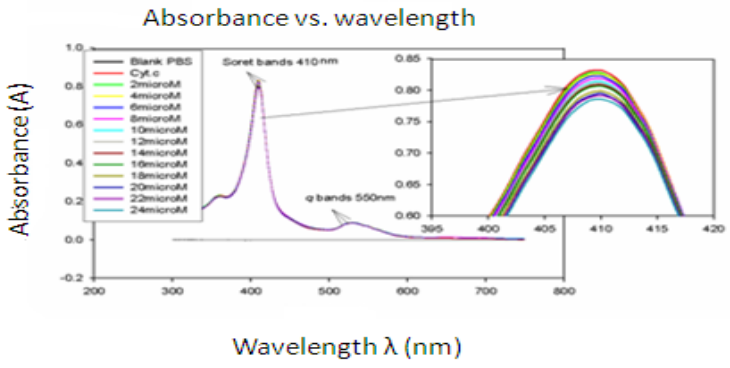

Figure 45: UV/vis absorption spectra for cytochrome c solution (pH = 7) with As_2O_3 concentration 2, 4, 6, 8, 10, 12, 14, 16, 18, 20, 22 and 24 µM

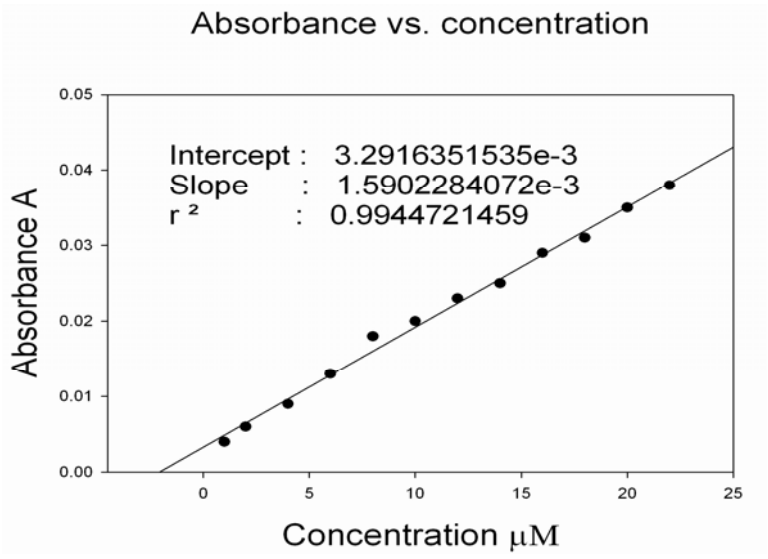

Figure 46: Calibration curve for biosensor response to As_2O_3 concentration.

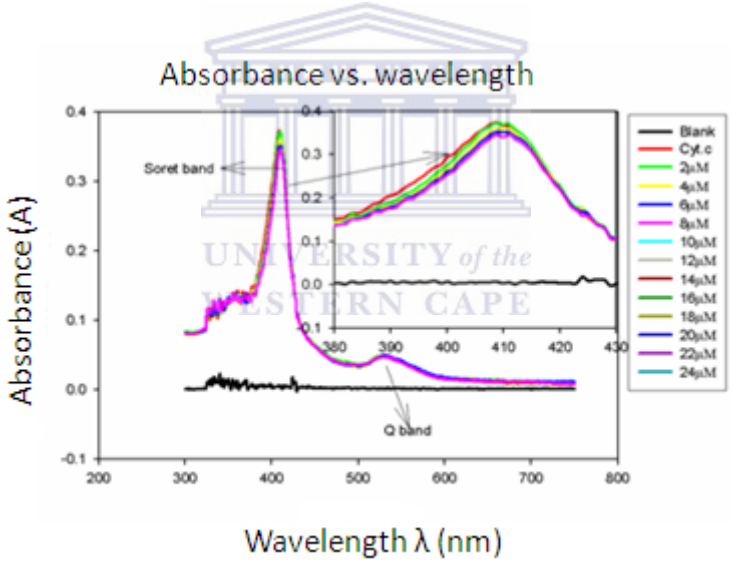

Figure 47: **UV/vis absorption spectra for cytochrome c solution (pH = 7) with KCN concentration 2, 4, 6, 8, 10, 12, 14, 16, 18, 20, 22 and 24 µM**

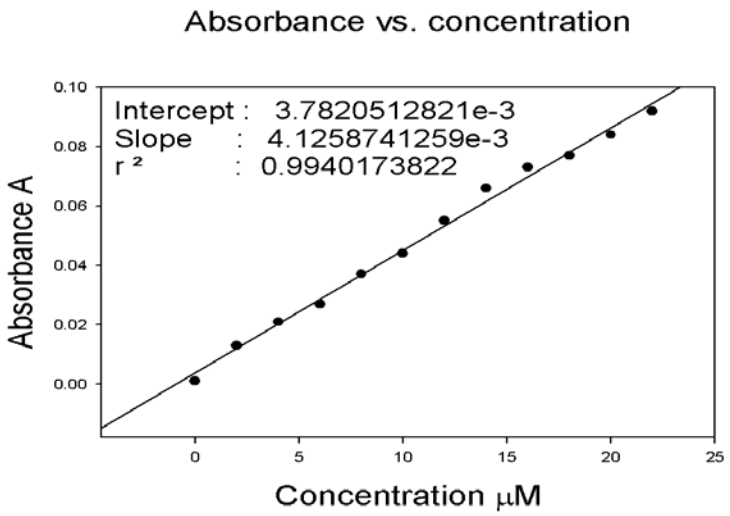

Figure 48: Calibration curve for biosensor response to KCN concentration.

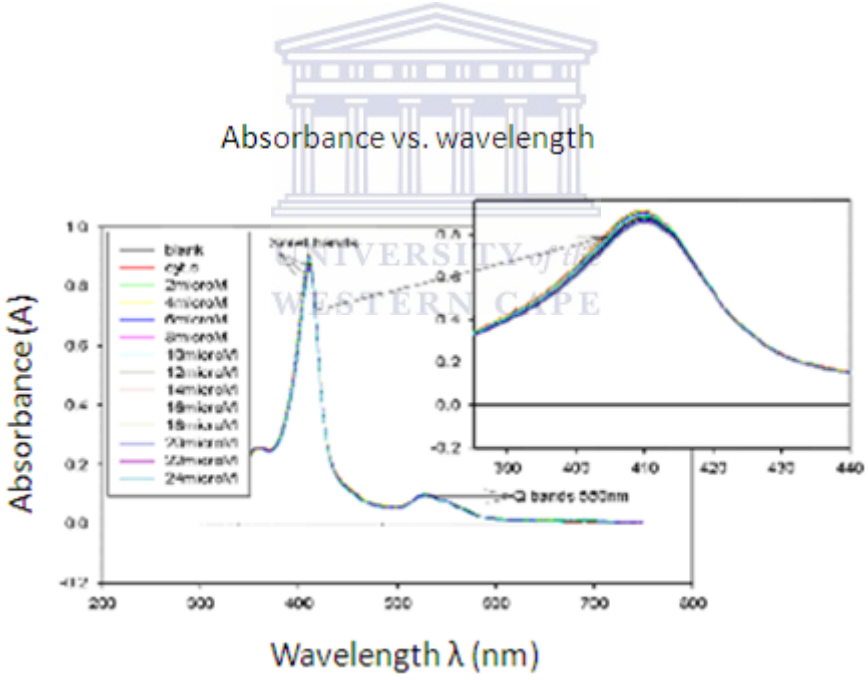

Figure 49: UV/vis absorption spectra for cytochrome c solution (pH = 7) with Prussian blue concentration 2, 4, 6, 8, 10, 12, 14, 16, 18, 20, 22 and 24 µM

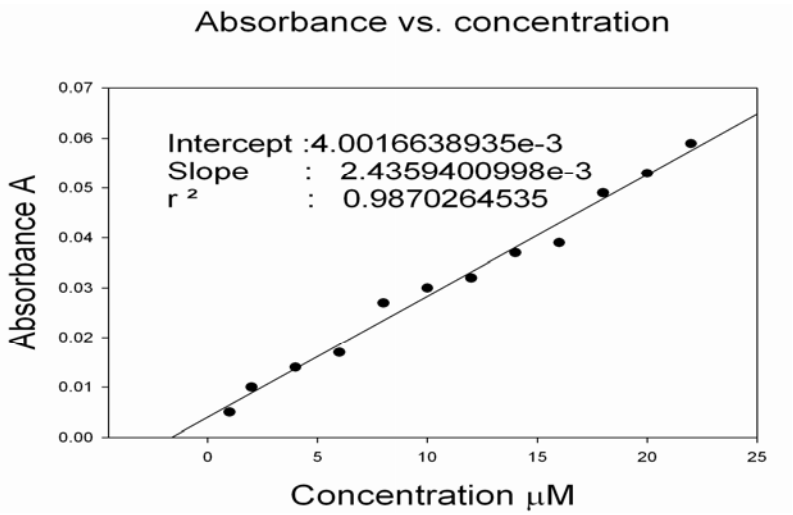

Figure 50: Calibration curve for biosensor response to Prussian blue concentration.

Cytochrome c aqueous solution of 4.06×10^{-4} M displayed absorption bands at 409 nm and 550 nm in 0.1 M PBS (pH= 7). The band at 409 nm is the soret band and the one at 550 nm is the Q-band. According to literature [105] these bands are essentially π–π^* band associated with the porphyrin ring which is present in protein cyt c. The electronic absorption spectrum of a typical porphyrin ring consists of a strong transition to the second excited state (S0→S2) at about 410 nm (the Soret or B band) and a weak transition to the first excited state (S0→S1) at about 550 nm (the Q band). The Soret band is allowed and therefore intense. The Q band is forbidden, it is observed because of vibronic coupling with the Soret band. Upon addition of different concentrations of arsenic trioxide, potassium cyanide and Prussian blue, respectively, a small decrease in the absorption intensity of the Soret band and Q bands were observed, indicating that the environment of the protein had changed. A slight shift at 409 nm to 410 nm was observed also suggesting a change in the protein's structure. This was interpreted as evidence of analyte binding to the native cytochrome c in solution. A plot of absorbance vs. concentration showed a

strong linear relationship for the binding event over the concentration range used and this linearity was confirmed by correlation coefficient of 0.99 in each case (Figure 46, 48 and 50). The molar absorption coefficient (ε) for cytochrome c obtained from slope of the calibration curve was found to be 4.05 $cm^{-1}mM^{-1}$ for Potassium cyanide at 409 nm, 1.59 $cm^{-1}mM^{-1}$ for arsenic trioxide 409nm and 2.43 $cm^{-1}mM^{-1}$ for Prussian blue at 409 nm. The values calculated for molar absorption coefficients are found to be lower compared to the ones obtained in literature which are 11.2 cm/mM at 528 nm and 21 cm/mM at 600 nm [106].

Therefore UV/vis absorbance analysis was able to confirm the binding of the analyte to the cytochrome c in solution, since the Soret bands and Q bands are associated are considered to be purely electronic transitions involving the porphyrin ring of the heme [105]. This observation served to confirm the CV and SW data which indicated that the main interaction between the analyte and the cytochrome c was in fact not at the heme site but rather at the amino acids attached to the protein sites.

6.2 Electrochemical Impedance Spectroscopy (EIS)

The potential controlled impedance behaviour of a bare BDD electrode and the biosensor were measured separately in KCN and As_2O_3 at potentials starting at -250 mV and stepped by 50 mV increments. The smallest R_{ct} value for As_2O_3 was observed at -300 mV as 1.267×10^5 Ω (Figure 52). The potential at which the smallest R_{ct} value was observed was then chosen to monitor the biosensor response to the analyte. The frequency range used was 1 kHz to 100 mHz.

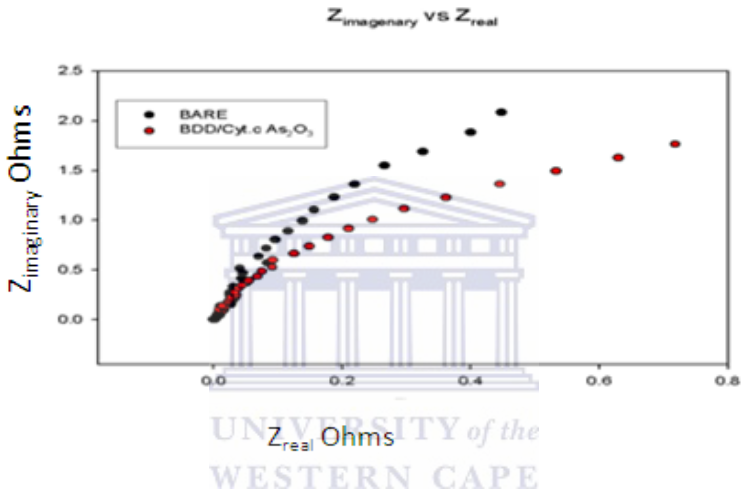

Figure 51: Nyquist plots of impedance for bare BDD in and biosensor in 1 mg/ml As_2O_3 at -300 mV (vs. Ag/AgCl).

A simple Randles circuit was used to model the biosensor response and the equivalent circuit fitting results for the bare electrode and the biosensor was compared for a quantitative assessment of the electrochemical transduction.

Table 18: Impedance parameters obtained from electrical circuit fitting of Randles Sevick for biosensor response to As_2O_3.

	R_{ct} (Ω)	R_s (Ω)	C (F)
Biosensor	1.267×10^5	741	4.220×10^{-7}
Bare electrode	2.467×10^5	798	7.064×10^{-7}

Nyquist plots of bare BDD electrode and biosensor in 1 mg/ml of KCN is shown by figure 52. The EIS experimental parameters were kept the same as for the previous experiment with As_2O_3.

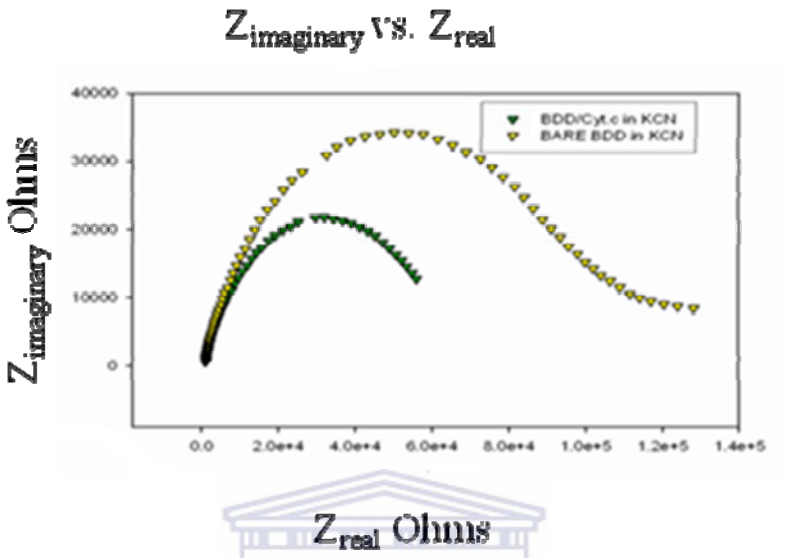

Figure 52: Nyquist plots of impedance for bare BDD in and biosensor in 1 mg/ml KCN at -300 mV (vs. Ag/AgCl).

Electrical equivalent circuit fitting data for the KCN experiment are reported in Table 19.

Table 19: Impedance parameters obtained from electrical circuit fitting of Randles Sevick for biosensor response to KCN.

	R_{ct} (Ω)	Rs (Ω)	C (F)
BDD/cyt c electrode	1.0789×10^{6}	860	8.207×10^{-7}
Bare electrode	5.9568×10^{5}	880	9.008×10^{-7}

The modified electrode showed faster electrochemical transduction in the presence of both analytes compared to the bare electrode as evidenced by the smaller value of R_{ct} and also due the protein facilitating the electron transport. Hence the biosensor is a more favourable transducer compared to bare electrode.

6.2.2 Biosensor response to analytes as measured by EIS

Electrochemical impedance spectroscopy (EIS) can provide useful information on the impedance changes of the electrode surface during the fabrication process. The plots of the EIS include a semicircular part and a linear part. The semicircle at higher frequencies corresponds to the electron-transfer-limited process and its diameter is equal to the electron transfer resistance (R_{et}), which controls the electron transfer kinetics of the redox probe at the electrode interface, while the linear region at lower frequencies corresponds to the diffusion process [90]. Figure 53, 56 and 59 shows the impedance plots of biosensor response to different concentration of KCN, As_2O_3 and $Fe_2(CN)_{12}.16H_2O$, respectively in 0.1 M PBS (pH=7). A fixed potential of -300 mV was used for analysis of analyte binding.

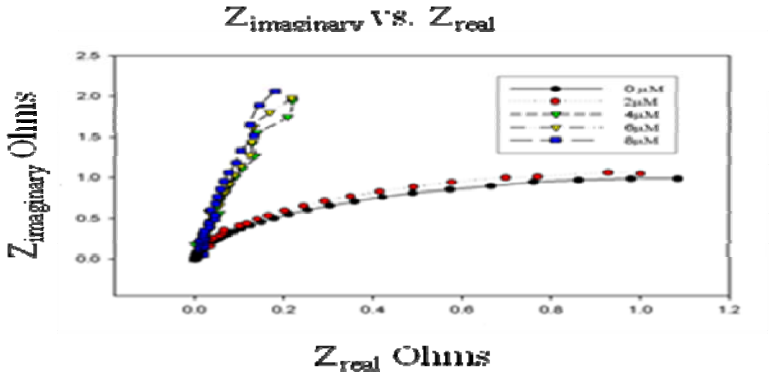

Figure 53: Nyquist plots of impedance for biosensor at different As_2O_3 concentration, at potential of -300 mV (vs. Ag/AgCl)

Table 20: Impedance parameters obtained from electrical equivalent circuit fitting EIS data for biosensor response to As_2O_3.

Concentration (μM)	Capacitance (F)	R_{ct} (Ω)
0	8.091×10-7	1.9424×10^{6}
2	8.207×10^{-7}	1.921×10^{6}
4	8.768×10^{-7}	3.2597×10^{6}
6	8.922×10^{-7}	$6..949\times10^{6}$

It is evident from the complex plot of the biosensor response to As_2O_3 that there is a marked difference in the interfacial electrokinetics after the addition of more than 2 μM As_2O_3 as the impedance becomes more diffusional. This is in good agreement with the detection limit for the biosensor towards As_2O_3 as determined by CV i.e. 8.1 μM. The EIS method may not lend itself as easily towards field measurements as CV or SWV, but could be a useful laboratory monitoring tool for fast and highly sensitive measurement of As_2O_3.

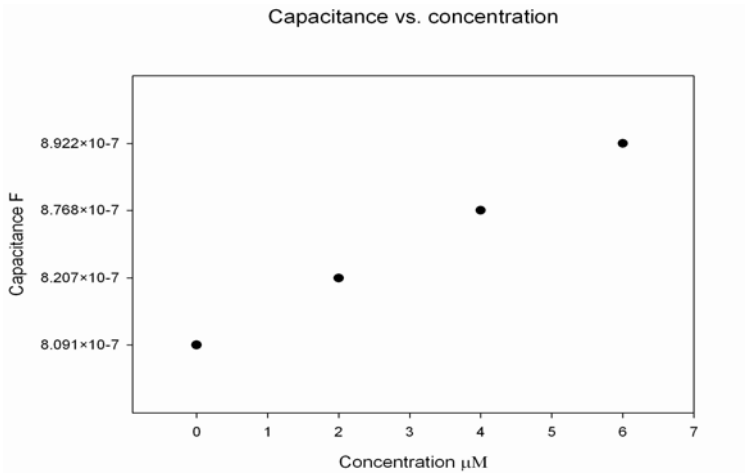

Figure 54: Calibration curve based on interfacial capacitance of biosensor response to As_2O_3.

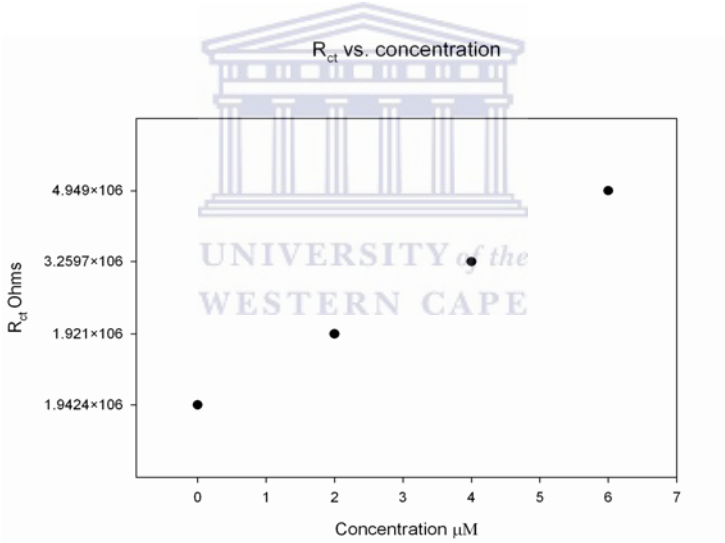

Figure 55: Calibration curve based on interfacial charge transfer resistance biosensor response to As_2O_3.

Table 20 shows the R_{ct} values, R_s values and Capacitance values for arsenic trioxide. These values are plotted against different concentrations of analytes (Figure 54 and 55). All the parameters increase with increasing concentrations.

Potassium cyanide, KCN

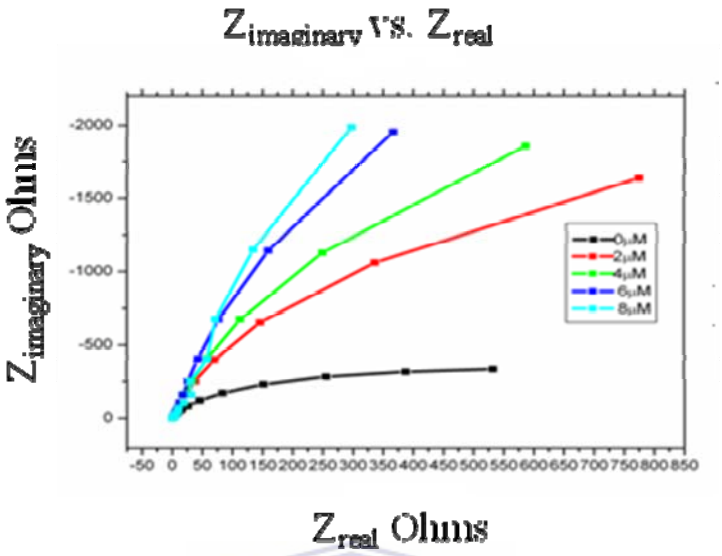

Figure 56: Nyquist plots of impedance for biosensor at different KCN concentration, at potential of -300 mV (vs. Ag/AgCl)

The binding of CN^- to the biosensor yields a marked change in the interfacial electrokinetics towards a system dominated by a capacitive interface. This is characteristic of irreversible binding events, which facilitates the attachment of the analyte to the available biosensor surface. The extent of binding is governed by the availability of biomolecule and the size of the analyte molecule. Equivalent circuit fitting analysis supports the detection limits obtained by SWV analysis.

Table 21: Impedance parameters obtained from electrical equivalent circuit fitting EIS data for biosensor response to KCN.

Concentration	Capacitance F	R_{ct} Mohms
0	67.7×10^{-7}	8.88
2	59.5×10^{-7}	10.03
4	49.5×10^{-7}	11.25
6	48.9×10^{-7}	11.81
8	48.0×10^{-7}	12.498

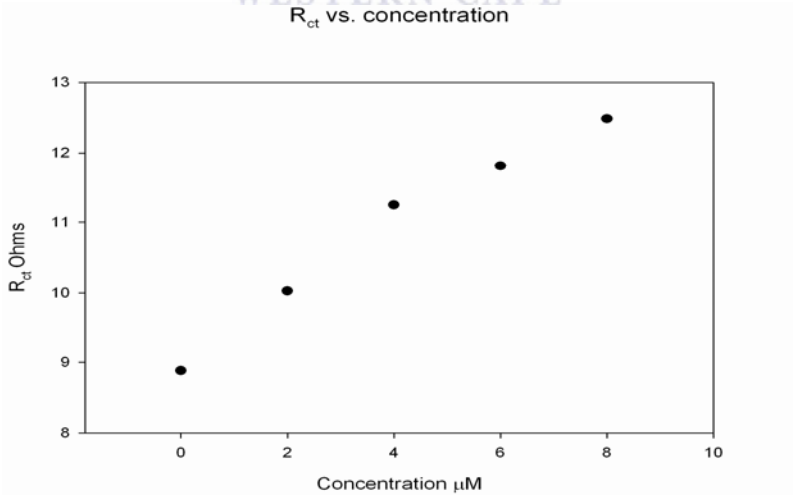

Figure 57: Calibration curve based on interfacial charge transfer resistance biosensor response to KCN.

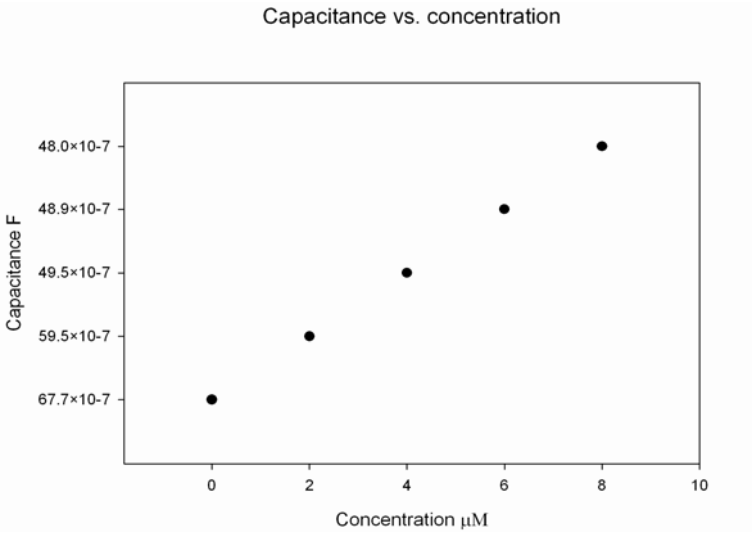

Figure 58: Calibration curve based on interfacial capacitance of biosensor response to KCN.

Table 21 shows the impedance parameters obtained and the concentration used for potassium cyanide. This data obtained was used to plot a calibration curve of R_{ct} vs. concentration and capacitance vs. concentration (Figure 57 and 58) and the R_{ct} value was observed to increase with increasing concentrations, showing slower electron transfer kinetic as the analyte binds to the biosensor interface.

Prussian blue, $Fe_2K(CN)_{12}.16H_2O$

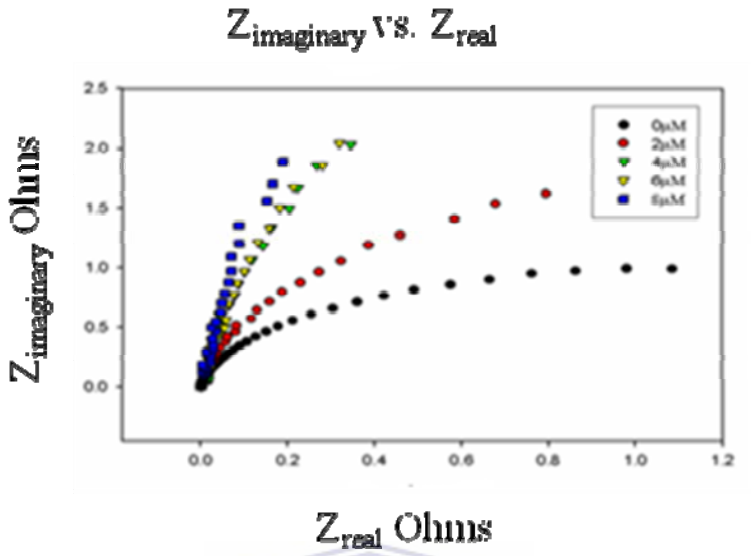

Figure 59: Nyquist plots of impedance for biosensor at different Prussian blue concentration, at potential of -300 mV (vs. Ag/AgCl)

The impedance response of the biosensor to Prussian blue shows a gradual change in interfacial electrochemistry as a function of changing concentration (Figure 59). It is evident that the binding event takes place at concentrations higher than 2 μM, this was shown by parameters such as charge transfer resistance (Rct) and Capacitance (C) were charge transfer resistance (R_{ct}) increases with increasing concentrations of the analyte and also the capacitance, hence the electron transfer is sluggish at higher concentrations than 2 μM and the impedance becomes more diffusional showing binding. Modeling the data as an equivalent electrical circuit (Randles circuit; Figure 62) and plotting the interfacial capacitance as a function of concentration, provided numerical data that agrees well with the detection limit obtained by CV i.e. 9.1 μM . However, since the Prussian blue contains a redox couple which influences the overall electron transfer process at the interface, the quantitative data should be interpreted with care. Table 22

below shows the calculated parameters values obtained for modified electrode and these values are plotted against concentration (Figure 60 and 61).

Table 22: Impedance parameters obtained from electrical equivalent circuit fitting EIS data for biosensor response to Prussian blue

Concentration (μM)	R_{ct} (Ω)	Capacitance (F)
0	1.4941×10^{7}	1.805×10^{-6}
2	1.5193×10^{7}	2.731×10^{-6}
4	2.449×10^{7}	7.065×10^{-7}
6	3.1942×10^{7}	7.881×10^{-7}
8	4.146×10^{6}	8.181×10^{-7}

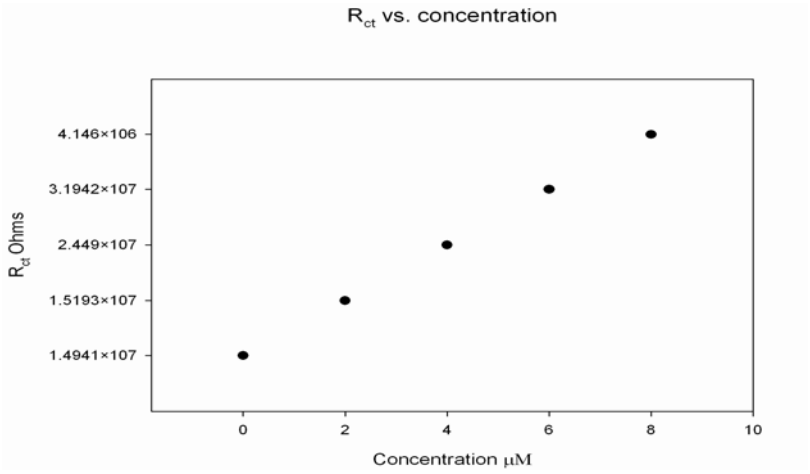

Figure 60: Calibration curve based on interfacial capacitance of biosensor response to Prussian blue.

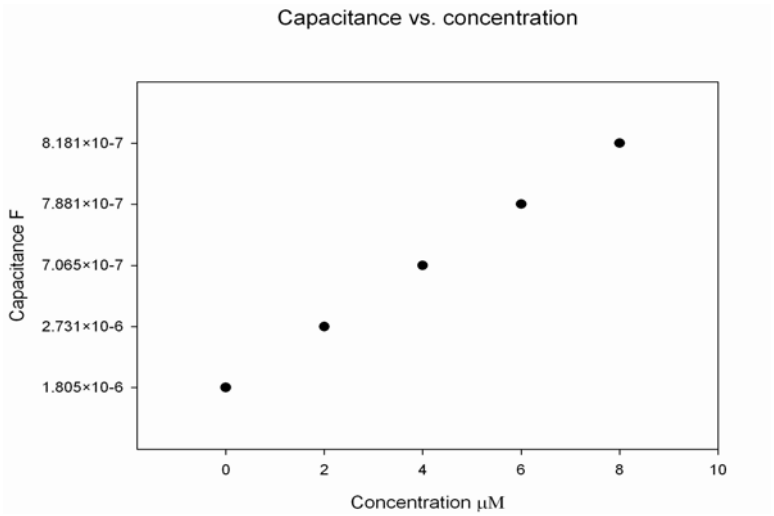

Figure 61: Calibration curve based on interfacial charge transfer resistance of biosensor response to Prussian blue.

Table 23: **Calculated Detection limit and Sensitivity from EIS for the analytes**

	Sensitivity Ω/µM	Detection Limit µM
KCN	0.451	9.971
As	0.5	8.989
PB	0.5	9.001

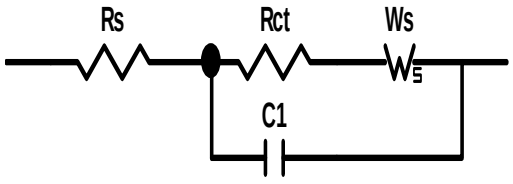

Figure 62: Circuit used for all impedance Analysis

As the concentration of analyte is increased the typical semi-circle nature of the system, which tells us about the electron transfer kinetics of the system, changed towards a more capacitive representation. This trend is due to a decrease in the charge transfer resistance (R_{ct}) of the system as a function of increasing concentration. The electrochemical system becomes diffusion controlled at higher concentration. The electron transfer process at the interface is slowed down due to the increasing capacitive layer developing at the interface, when opposite charges bind due to electrostatic attraction. A plot of R_{ct} vs. concentration is shown by figure 60, at concentrations of 4 µM the R_{ct} shows a sharp increase due to increasing concentration.

6.3 FTIR spectroscopy

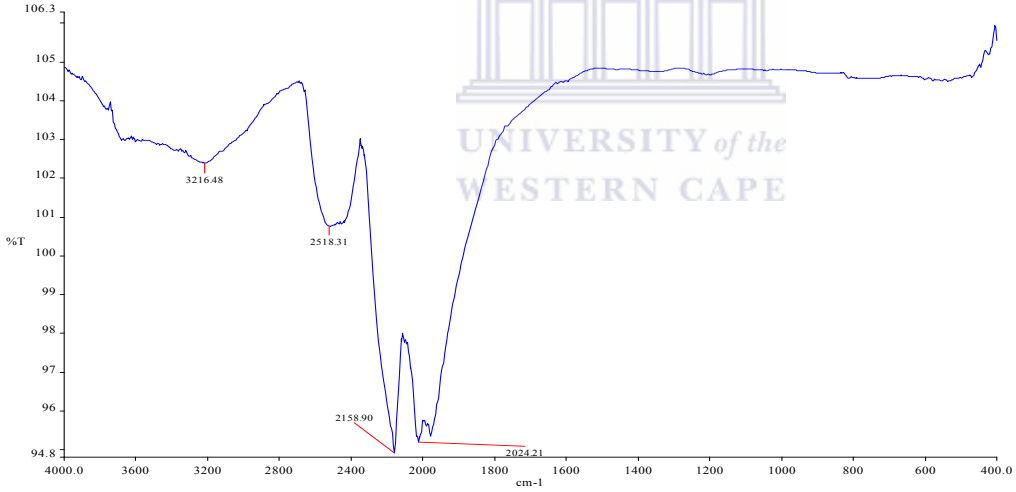

Figure 63: FTIR spectrum for cyt c immobilised at the BDD electrode

Table 24: FTIR Spectra assignment of functional groups

Wavelength, cm^{-1}	Assignment	Intensity	Functional class
2514	C-H, O-H, S-H	Medium, strong	Alkanes, acids
2024	C ≡ C, C≡ N	Vary, medium	Alkynes
3217	N-H, OH(H-bonded)	weak	amines

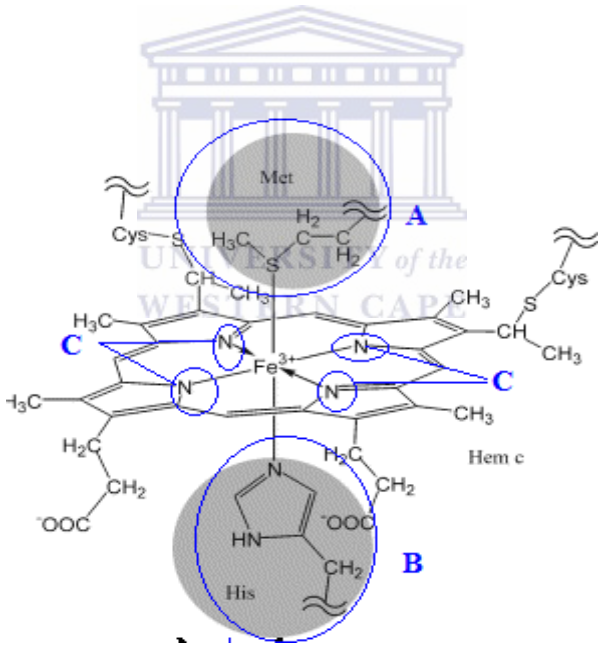

Figure 64: Cytochrome c structure of heme c

Table 24 shows the functional groups obtained from FTIR spectra as shown in figure 63. According to figure 64 above four C-N functional groups at frequencies of 3217 cm^{-1} are attached to the metal center (Fe^{3+}) of the protein as denoted by symbol (C). S-H functional

groups which is found at the Methionine 80 (A) and cystein of the protein appears at frequencies of 2514 cm^{-1} and the C=N is found at the Histidine of the protein and it appears at frequencies of 2024 cm^{-1} as shown in (B). Histidine and the Methionine 80 are also linked to the metal center as shown in A and B. FTIR spectra confirms the existence of the functional groups mentioned and this is also observed from figure 64.

The FTIR spectrum of the immobilised cyt c, obtained here is in good agreement with literature references for immobilised cyt c and confirmed the efficient adsorption of the protein onto the BDD electrode, in the biosensor assembly [107].

6.4 SNIFTIR results:

Cytochrome c was drop coated onto a Pt disk electrode of diameter of 70 mm and interferograms were recorded using Ag/AgCl reference electrode and Pt wire counter electrode. Spectra were obtained at potentials from 0 mV to -700 mV at 100 mV intervals. Spectra were also recorded in the reverse direction. Spectra were obtained by Fourier transformation after averaging 300 interferograms acquired at each potential. The CaF_2 window was used in order to limit the influence of solvent on the spectra. Infrared spectra have been normalized with respect to the reference spectrum collected at -500 mV and are displayed as $\Delta R/R$ [(Rs-Rr)/Rr] difference spectra. SNIFTIRS spectra obtained in this way therefore, contain only information of the molecular changes occurring from modification of the protein. Potentials of -200 mV, -300 mV and -400 mV were closely analysed, since our reductive peak potential in CV and SWV was observed in this region (Figure 64, 65 and 66).

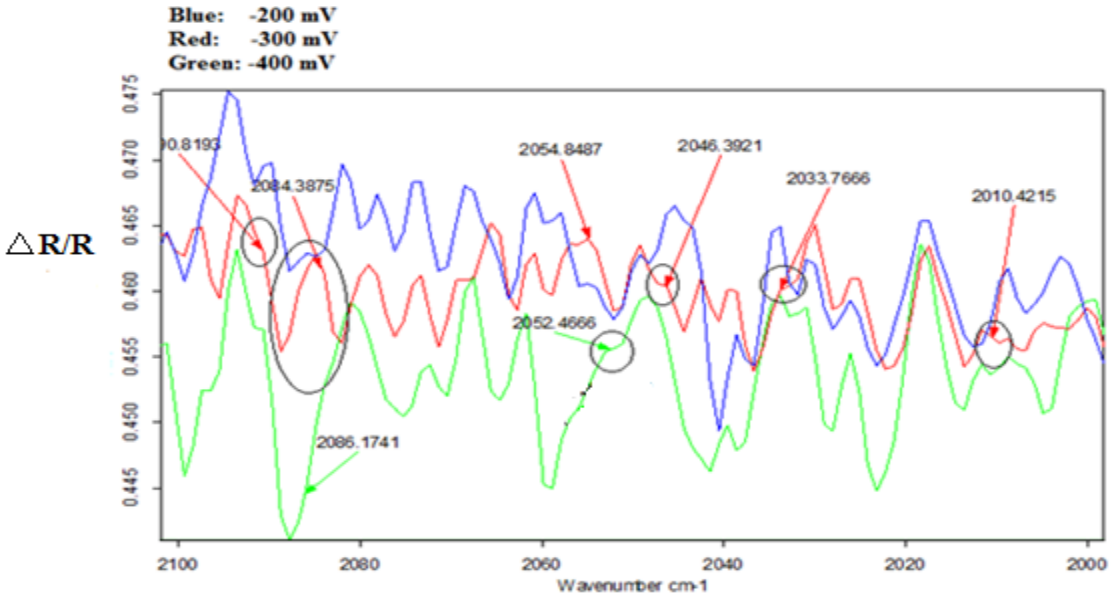

Figure 65: SNIFTIRS spectra of Pt/cyt c showing the enlargement of the finger print region.

The upward spectra show a decrease in absorption and downward show an increase in absorption spectra. The peak at 2081 cm^{-1} decreases in absorption intensity and develops a shoulder as the potential was stepped from -200 to at -400 mV. 2081 cm^{-1}. A small doublet was observed at 2084cm^{-1} which merged into a single peak and became more intense as we stepped through the reduction potentials. These vibrations were interpreted as evidence of the C-C and C=C resonance structures within the prophyrin rings which may develop potential induced alkyne resonance structures. The small peak observed at 2046 cm^{-1}, due to C-N stretching, was associated with an intermediate reduction state and disappeared at -400 mV. A doublet appears in SNFTIR spectra because of Fermi resonance, which may be observed in S-H and N-H functional group stretching. The shift in peak position and reduction of peak intensity as a function of stepped potential, was observed at 2010 cm^{-1} and was assigned to the C=N and C=C stretches,

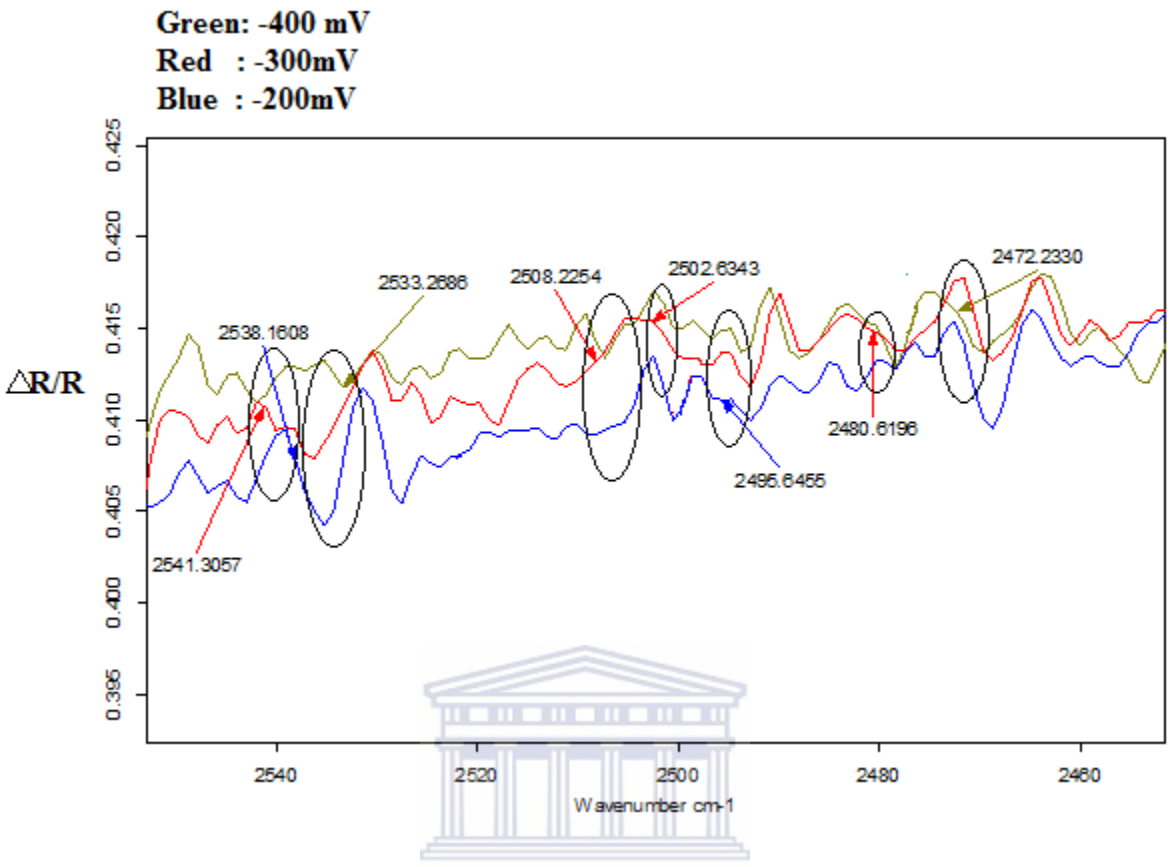

Figure 66: **SNIFTIRS spectra of Pt/cyt c showing the enlargement of the finger print region**.

There are changes in peak intensity and shift to lower wavenumber at 2541 and 2533 $cm^{-1}$and eventual decrease in the peak at 2538 cm^{-1} when we reach -400 mV was assigned to S-H and N-H stretches. At 2538 cm^{-1} the S-H stretch is a weak stretch, hence the slight shift in peak position as we step the potential. A sharp peak at 2508 cm^{-1} was observed which broadened and disappeared as we stepped the potential. This is due to S-H and N-H stretching vibrations

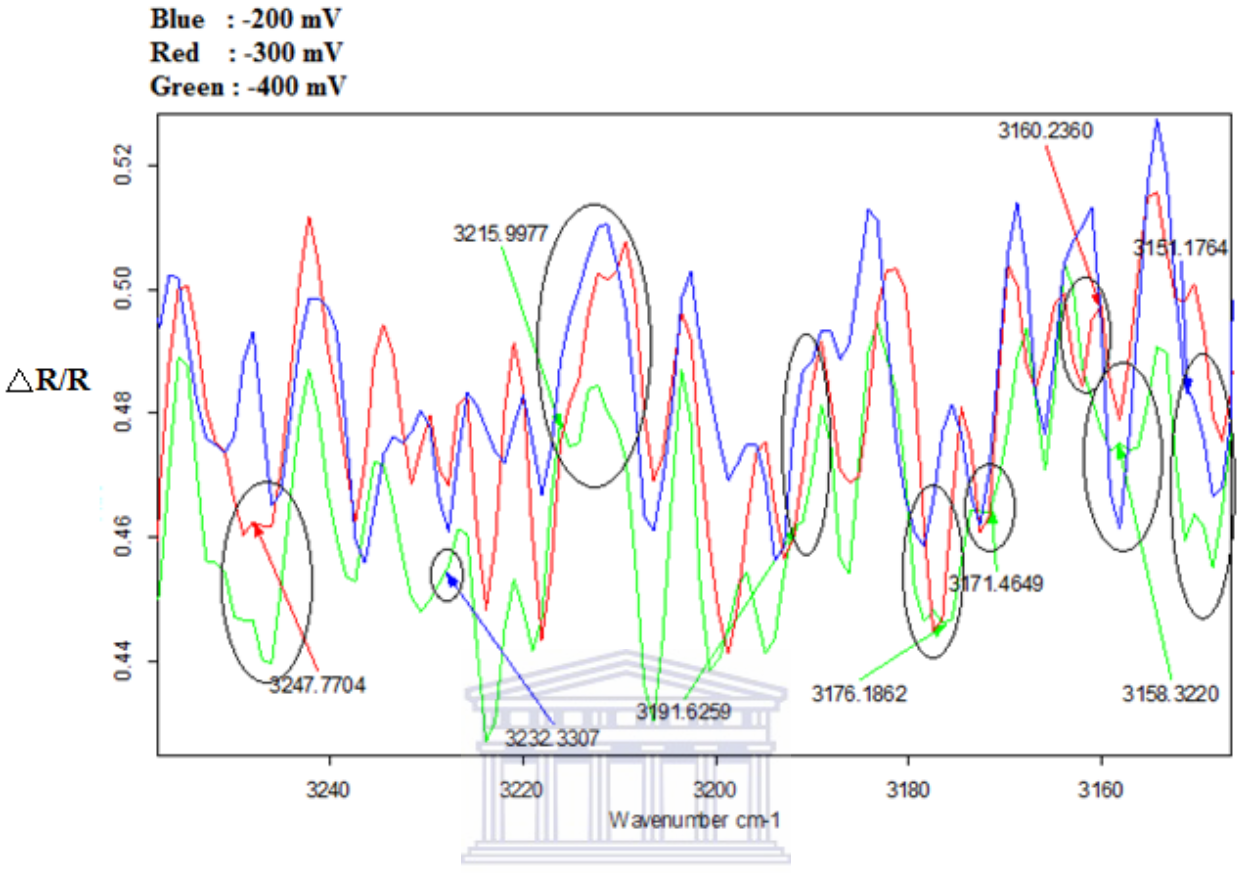

Figure 67: **SNIFTIRS spectra of Pt/cyt c showing the enlargement of the finger print region.**

A very strong positive band at 3247 cm^{-1} which decreases drastically in intensity as we move towards more reducing potentials, was observed. The peak grew in intensity and the disappeared at -400 mV. At 3176 cm^{-1} and 3158 cm^{-1} an intense downward peak was observed, which split at -400mV. This splitting was cause by coupled resonance of another functional group that was very weak at preceding potentials. The stretching behaviour is assigned to the N-H and S-H functional group.

Cytochrome *c* (MW 12, 400) consists of a single polypeptide chain of 104 amino acid residues and covalently attached to a heme group. They are roughly spherical with a diameter of 34Å [39]. The heme is surrounded by many tightly packed hydrophobic side chains. Therefore we concluded that, the behavior observed in SNIFTIR correlates well with infrared spectra of cytochrome c. SNFTIR results confirm that the functional groups within the protein, undergoes many resonance vibrations. Resonance vibrations were associated with the porphyrin ring and amino acid side chains and did not indicate any permanently ruptured bonds, therefore supporting evidence from UV/vis spectroscopy, that the protein was not denatured in the immobilised state.

6.5 Scanning electrode microscopy (SEM) for cyt c

A scanning electron microscope (**SEM**) is a type of electron microscope that images a sample by scanning it with a high-energy beam of electrons in a raster scan pattern. The electrons interact with the atoms that make up the sample producing signals that contain information about the sample's surface topography, composition, and other properties such as electrical conductivity. Cyt c structural morphology has been studied using this technique (SEM). Figure 68a shows SEM images of gold foils with dimensions of 12 cm^2 modified with HA (Humic Acid)–Cyt c [108] and figure 68b shows SEM images for cyt c on gold screen printed electrode at 10 μm.

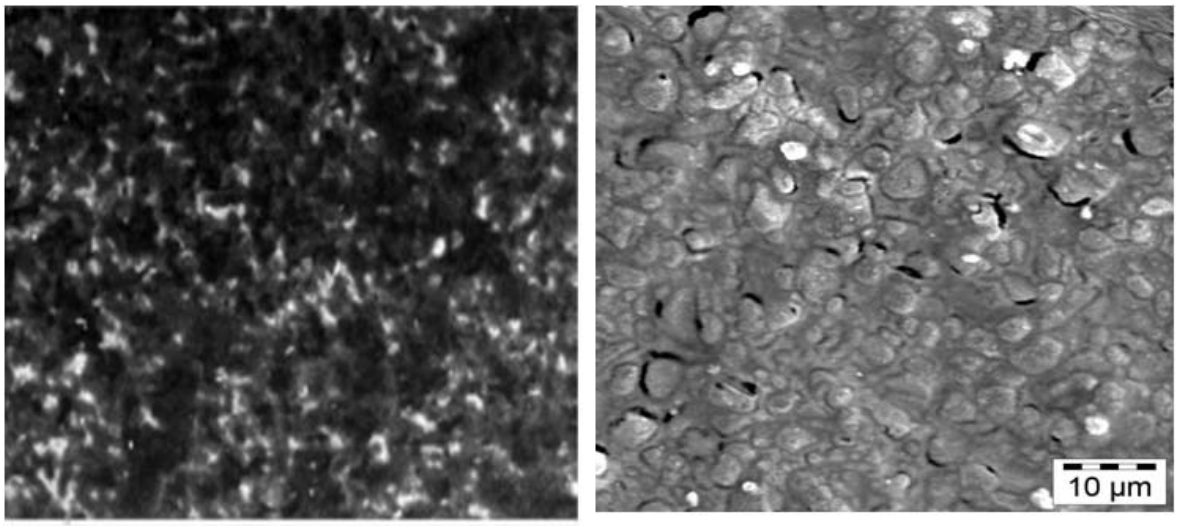

(a) SEM images of gold foils with dimensions of 12 cm^2 modified with HA–Cyt c.

(b) SEM images on gold screen printed electrode modified with Cyt c

Figure 68: **(a) SEM images for HA-cyt c (b) SEM images for cyt c**

Electron transport is assured in part by a class of proteins, the cytochromes, which act as electron carriers. Cyt c belongs to this class of electron shuttling. Cyt *c* (MW 12, 400) consists of a single polypeptide chain of 104 amino acid residues and covalently attached to a heme group [7, 11]. They are roughly spherical with a diameter of 34Å [109]. From our preparation we were able to observe dense spherical-shaped particles, distributed uniformly on the surface of the gold screen printed electrode. SEM images gave the direct visual evidence that cyt c is attached on the electrode surface. The spherical-shapes show native nature of the protein and shows that the protein still retains its stability and it is not denatured, whereas the almost fading cycles shows the protein's denaturation. The results are in good agreement with the spherical shape of the protein from literature (gold electrode modified with HA–cyt c.) (Figure 68a). This result has also been confirmed by UV/vis analysis where the stable peak of the protein was observed at 408 (Soret bands). The protein peak slightly changed its shape upon addition of different concentrations of the analyte into the solution.

Chapter 7

7.1 Interference studies of analytes (KCN, $Fe_2K(CN)_{12}.16H_2O$ and As_2O_3)

The effects of various possible interferences on the electrode response were evaluated by recording cyclic voltammogram of the modified electrode in phosphate buffer solution (pH=7) with constant additions (volumes) of 2 µl cyanide and arsenic analytes and 2, 20, 100 and 200 µl of interferences. These species include inorganic substances in various concentrations i.e. Na_2S 1.2×10^{-8} mol/L (S^{2-}), $Na_2S_2O_3$ $6.\times10^{-8}$ mol/L ($S_2O_3^{2-}$), $NaNO_2$ 1.4×10^{-8} mol/L (NO_2^-) and NaCl 1.7×10^{-8} mol/L (Cl^-) [110]. Stock-Solutions of 5.05×10^{-9} mol/L for arsenic trioxide, 0.15×10^{-9}mol/L for potassium cyanide and 1.33×10^{-9} mol/L Prussian blue were prepared for each compound. The biosensor response to 2 µM of analyte was measured in the presence of interfering species , in 0.1 M PBS [110-111].

7.1.1 Potassium cyanide, KCN with interference of $Na_2S_2O_3$

Sodiumthiosulfate's cation was found to interfere with KCN, hence CV measurements were carried out to investigate this interference from our biosensor. Figure 69 shows a plot of KCN with interferent at one ration whereas the other ratios are reported in the appendices.

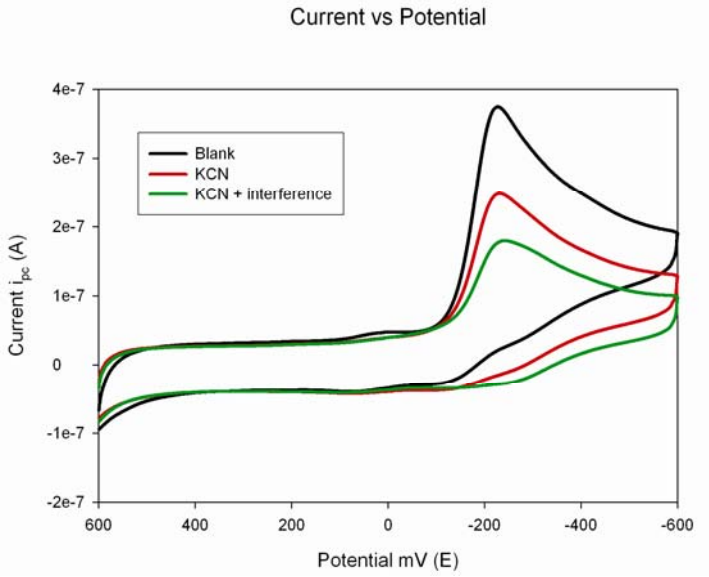

Figure 69: CV of biosensor response to KCN in the presence of $Na_2S_2O_3$ (1:1)

Figure 69 shows a decrease in peak current as we added interference and there was no other peak shown rather than the protein peak decreasing. The percentage interference obtained was 27.5% this showed little interferences to the analyte, this result is shown by table 25. The percentage interference for other interferences are shown by table 25.

7.1.2 Potassium cyanide, KCN with interference of NaCl

NaCl was also suspected to interfere with KCN. CV analysis of this interference was carried out in the ratios of (1: 340; 1: 3400; 1: 17000 and 1: 34000) in moles [110].

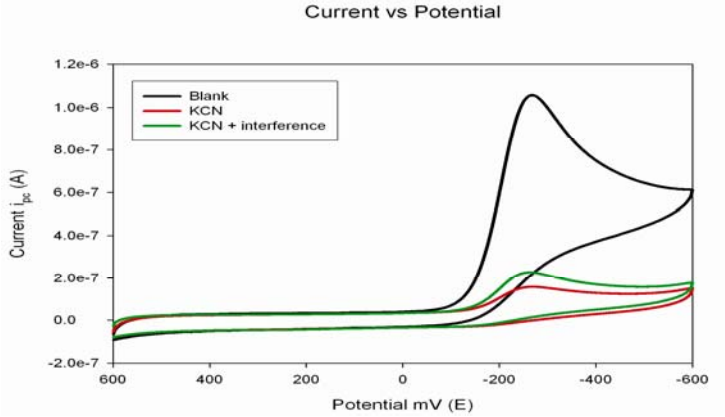

Figure 70: CV of biosensor response to KCN in the presence of NaCl (1:1)

7.1.3 Potassium cyanide, KCN with interference of $NaNO_2$

In addition of the analyte the peak current decrease but as we add the interference the peak current shows a slight increase (Figure70). The percentage interference obtained was calculated to be 44.7% as shown by table 25. Percentage interference for other interferences are reported in table 25.

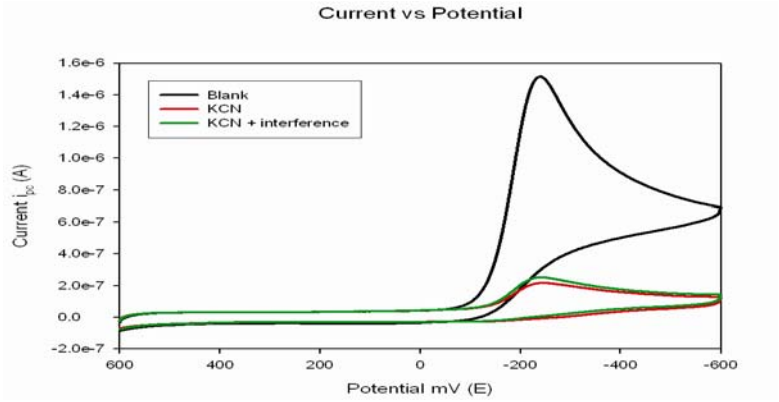

Figure 71: CV of biosensor response to KCN in the presence of $NaNO_2$ (1:1)

7.1.4 Potassium cyanide, KCN with interference of Na_2S

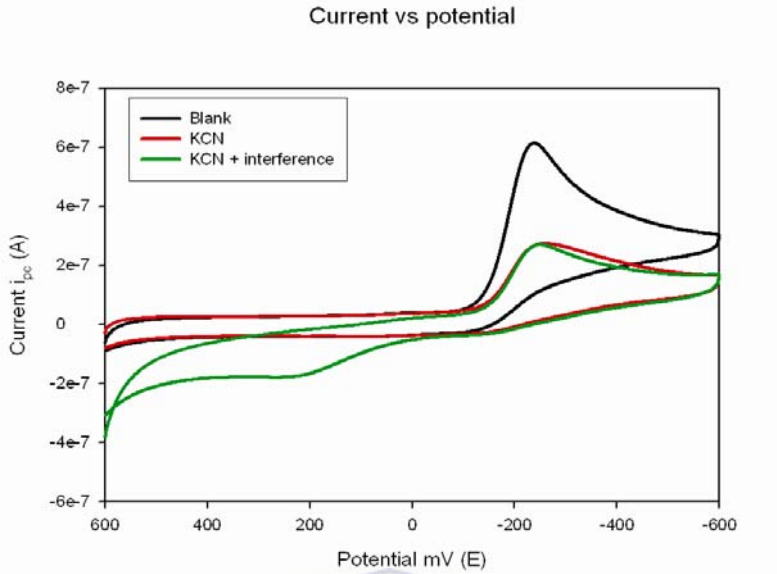

Figure 72: CV of biosensor response to KCN in the presence of Na_2S (1: 100)

The interference of $NaNO_2$ and Na_2S were also carried out in the ratios of 1:1. The peak current of the $NaNO_2$ showed a slight increase in peak current and the percentage interference obtained was calculated to be 25% (Figure 71 and 72) and table 25 reports other percentage interference at different ratios of. The peak current of Na_2S did not show any decrease/increase in current hence there was no percentage interference reported, this interference showed a reverse peak at potentials of +200 mV figure 72.

Table 25: Calculated interferences as percentage interference to the analyte KCN

% interference $Na_2S_2O_3$ mole ratios: (1:1200; 1:12000; 1:60000; 1: 120000)	% interference $NaNO_2$ mole ratios: (1: 280; 1: 2800; 1: 14000; 1: 28000)	% interference NaCl mole ratios: (1: 340; 1: 3400; 1: 17000; 1: 34000)	% interference Na_2S
27.5	25	44.7	-
22.4	20.6	3.8	-
20.9	31.96	5.9	-
39.7	34.65	51.9	-

7.1.5 Arsenic trioxide, As_2O_3 with $Na_2S_2O_3$ interference

The interference studies for As_2O_3 were carried out. The following interferences were investigated ($Na_2S_2O_3$, NaCl, $NaNO_2$ and Na_2S) and were carried out using cyclic voltammetry. This was carried out at different ratios for each interferent. Only data for one of the ratios will be used for convenience and others are reported in table 26.

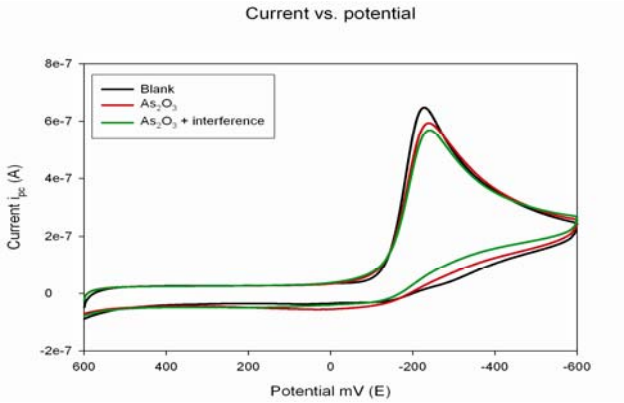

Figure 73: CV of biosensor response to As_2O_3 in the presence of $Na_2S_2O_3$ (1:1)

The peak current of the interference + analyte shows a decrease in peak current figure 73. The percentage interference was calculated to be 45% and that of (1:1200; 1:12000; 1:60000; 1: 120000) were found to be (24%, 28.7%, 57.9%) respectively as shown by table 25.

7.1.6 Arsenic trioxide, As_2O_3 with $NaNO_2$ interference

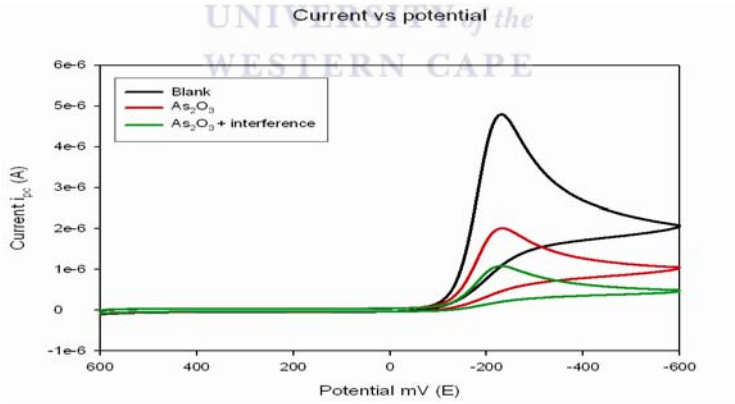

Figure 74: CV of biosensor response to As_2O_3 in the presence of $NaNO_2$ (1:1)

A peak of biosensor decreased as we added the analyte KCN showing binding. The peak of analyte+ interference also showed a decrease in peak current as shown by figure 73 and the percentage interference obtained was calculated to be 32.92% for a 1:1 ratio. Other percentage

interferences are reported in table 26 and the plots of these interferences are show in the appendixes

7.1.7 Arsenic trioxide, As_2O_3 with NaCl interference

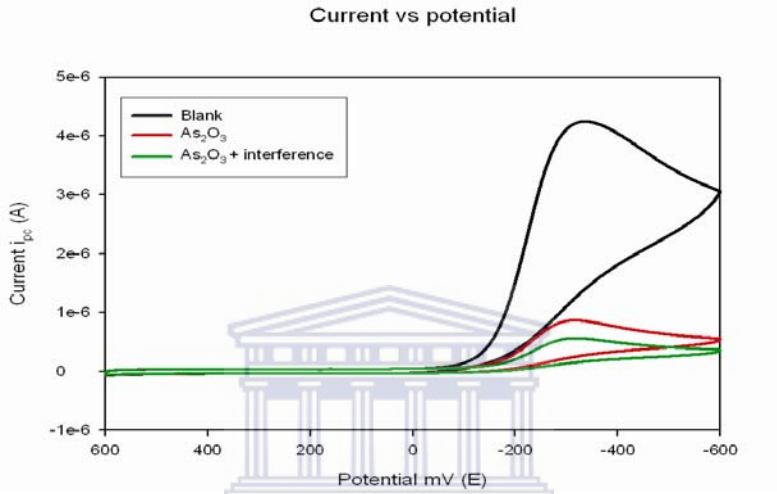

Figure 75: CV of biosensor response to As_2O_3 in the presence of NaCl (1:1)

7.1.8 Arsenic trioxide, As_2O_3 with Na_2S interference

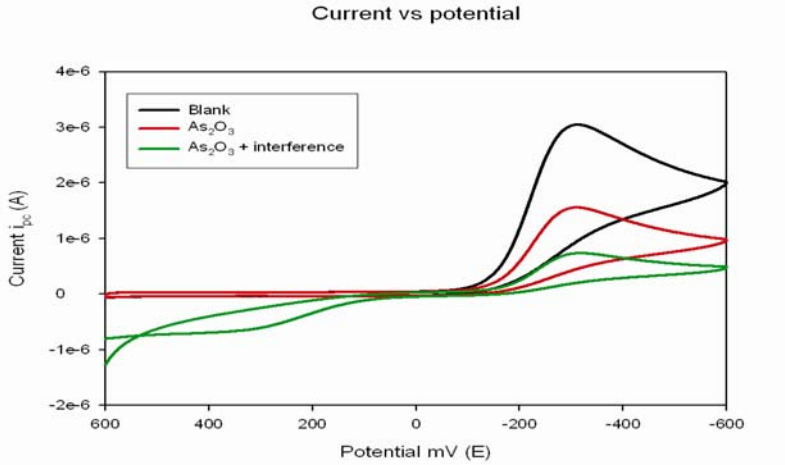

Figure 76: CV of biosensor response to As_2O_3 in the presence of Na_2S (1:1)

KCN+ Na_2S interference showed a decrease in peak current and it also shows a reversible peak at potentials of +300 mV (Figure 75), the calculated percentage interference was found to be 43%. Figure 76 shows a plot of analyte (As_2O_3) and analyte (As_2O_3) + interference in the ratio of 1:1 and both peak currents decreases. The percentage interference was found to be 34.99%. The percentage interference for other interference are reported by table 26.

Table 26: Calculated interferences as percentage interference to the analyte As_2O_3

% interference $Na_2S_2O_3$ mole ratios: (1:12; 1:120; 1:600; 1: 1200)	% interference $NaNO_2$ mole ratios: (1: 3; 1: 28; 1: 140; 1: 280)	% interference NaCl mole ratios: (1: 3; 1: 34; 1: 120; 1: 340)	% interference Na_2S mole ratios : (1: 240)
45	32.97	34.99	43
24	39	52.6	
28.7	22.6	20.2	
57.9	43.5	41.97	

7.1.9 Prussian blue, with interference of $Na_2S_2O_3$

A biosensor in 0.1 M PBS was run before any additions of the analyte and interferences. As we added the analyte the peak current decreased (Figure 77) and there is a reversible peak of iron observed at potentials of +200 mV. The interference ($Na_2S_2O_3$) was also added and a decrease in peak current was also observed (Figure 77).

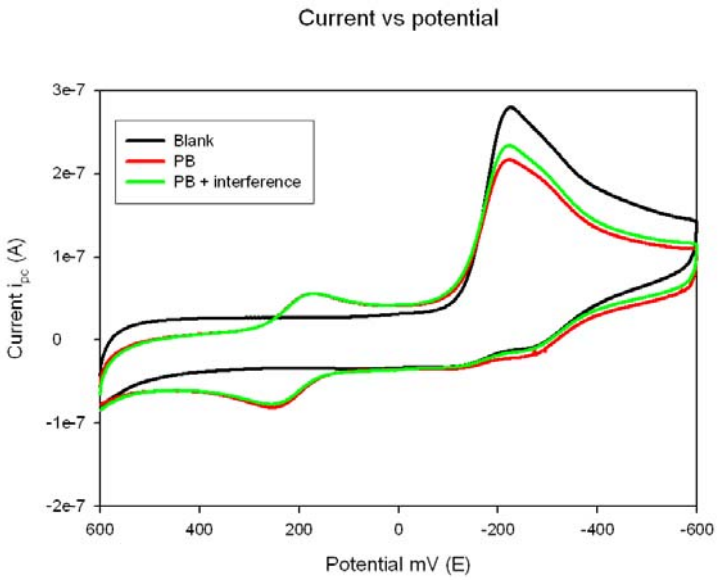

Figure 77: CV of biosensor response to Prussian blue in the presence of $Na_2S_2O_3$ (1:1)

The percentage interference for analyte: analyte interference was calculated to be +6.8%. This interferent did not interfere with the iron peak. Percentage interference for i.e. 1:45; 1:451; 1:2255; 1: 4511 are reported by table 27

7.1.9 Prussian blue, with interference of $NaNO_2$

$NaNO_2$ was also one of the investigated interference for our biosensor. The CV analysis were carried out in the ratios in molar ratios of (1: 10; 1: 105; 1: 526; 1: 1052) and only data for one ratio is shown here while other results are reported in the appendixes.

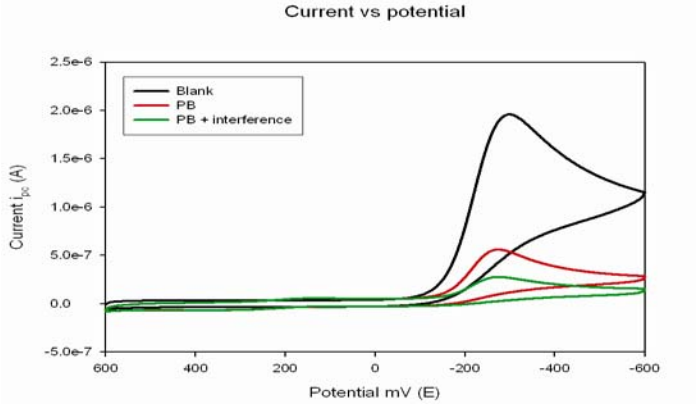

Figure 78: CV of biosensor response to Prussian blue in the presence of $NaNO_2$ (1:1)

Figure 78 show a plot of biosensor in 0.1 M PBS (pH =7) in the presence of PB and $NaNO_2$ (1:10 ratio). The percentage interference calculated was found to be 42% for a 1:10 ratio. The peak of analyte + interference showed a decrease in peak current. Table 27 shows calculated percentage interference of other interferences.

7.1.10 Prussian blue, with interference of NaCl

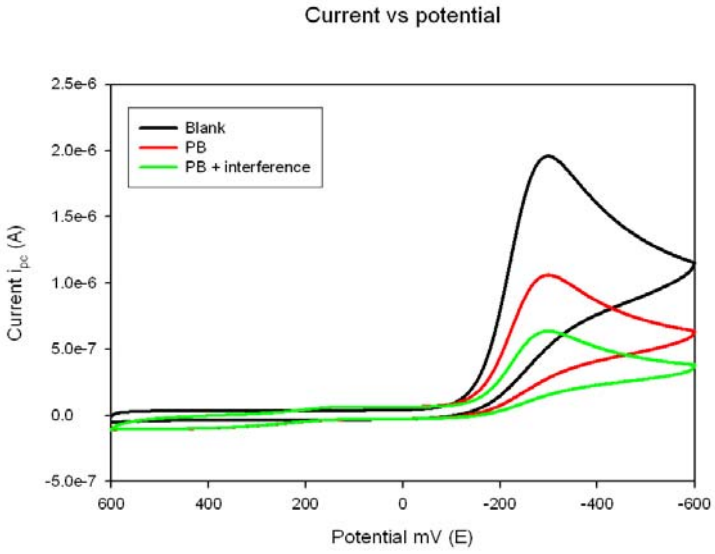

Figure 79: CV of biosensor response to Prussian blue in the presence of NaCl (1:1)

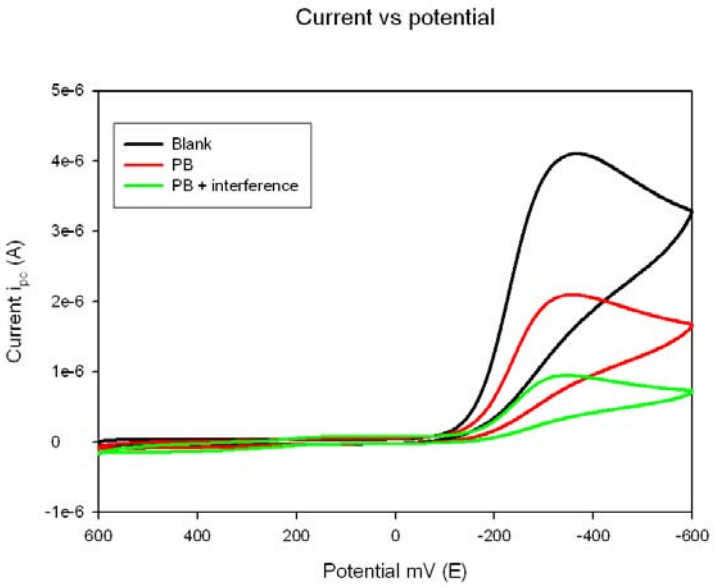

Figure 80: CV of biosensor response to Prussian blue in the presence of Na_2S (1:1)

The peak current of the biosensor decreases as the analyte is added and also a decrease in analyte + interference was observed (Figure 79 and 80). The percentage interference obtained for NaCl interference was 40% and that of Na_2S was calculated to be 66%. Other percentage interferences are reported in table 27

Table 27: Calculated interferences as percentage interference to the analyte $Fe_2K(CN)_{12}.16H_2O$

% interference $Na_2S_2O_3$ mole ratios: (1:45; 1:451; 1:2255; 1: 4511)	% interference $NaNO_2$ mole ratios: (1: 10; 1: 105; 1: 526; 1: 1052)	% interference NaCl mole ratios: (1: 12; 1: 128; 1: 639; 1: 1278)	% interference Na_2S mole ratios: (1: 962)
6.8	42	40	66
60	59	55	-
76	50	57	-
69	67	59	-

The selected interference compound (Na_2S, NaCl, $NaNO_2$, $Na_2S_2O_3$) which were found to interfere with the analytes cyanide and arsenic compounds did not interfere with the analytes from 20 to 100 folds. The peak potentials -240 mV increased or decreased when we introduced or spiked different interference. Sodium sulphide shows an extra peak at peak potentials of 400mV.

Chapter 8

8.1 Conclusion

A biosensor, developed on an activated BDD platform by immobilization of cytochrome c, was prepared in a simple and quick manner. CV and SWV confirmed the presence of an irreversible reduction peak at -240 mV which was used for monitoring the binding between the analytes and the biosensor. As it is shown in literature cytochrome c exhibits voltammetric response from reversible to irreversible peaks at various electrodes [55]. In this work the reduction peak observed between -200 mV and -400 mV was an irreversible peak and was due to the protein (cytochrome c). Similar findings were also reported by Langmuir et al., were an investigation of redox reacting mechanism of cytochrome c at modified gold electrodes was carried out and Zhao et al.,. They reported that the potential of the adsorbed cytochrome c is 440 mV more negative than the potential of native cytochrome c which is 60 V (vs. Ag/AgCl in saturated KCl). Based on these findings it is concluded that the irreversible reduction peak at negative potentials is not denatured but showed a change in protein structure.

Interfacial kinetic parameters such as charge transfer resistance and capacitance, as measured by EIS, were quantitatively related to the concentration dependent binding of analyte to the biosensor. The biosensor was shown to have low detection limit and sensitivity for the analytes KCN, prussian blue and As_2O_3. The sensitivity and the detection limits of the biosensor were quantified using voltammetry (CV and SWV) as well as electrochemical impedance spectroscopy (EIS).

The sensitivity and limit of detection calculated for the biosensor by different electrochemical methods are summarized in the table below.

Table 28: Summary of biosensor performance parameters

	Sensitivity A/μM	Detection Limit μM	EIS Sensitivity Ω/μM	EIS Detection limit μM
CV (KCN)	3.9715×10^{-8}	4.22	0.451	9.971
CV (As)	2.07894×10^{-8}	8.076	0.5	8.99
CV (PB)	1.8479×10^{-8}	9.086	0.5	9.00
SWV (KCN)	4.4880×10^{-8}	9.082μM		
SWV (As)	1.8509×10^{-8}	22.020 μM		
SWV (PB)	1.0870×10^{-8}	37.496 μM		

The diffusion coefficients calculated for the biosensor in 0.1M PBS was found to be 5.093×10^{-10}cm^2/s (CV) and 10×10^{-10} cm^2/s (SWV). The surface coverage for the BDD electrode was calculated to be 1.746×10^{-11} mol/cm^2. The diffusion coefficients calculated for the biosensor in the presence of migrating analyte was fund to be one order of magnitude bigger, with the fastest diffusion coefficient measured for As_2O_3.

The diffusion coefficients obtained when compared to the ones obtained in literature seems to be in agreement with other cytochrome c biosensor systems [24, [97-98]

The sensitivity and detection limit of the biosensor for these selected analytes (established to be in the micro molar range) were much lower than sensitivity and detection limit of other

analytical methods such as titrimetric, colorimetric (spectrophotometry), and cyanide ion selective electrodes (ISEs) chromatography, spectrophotofluorometry and indirect atomic absorption spectrometry currently employed (reported in literature as being in the molar range) Groom and Luong (1991).

UV/vis absorption spectroscopy was used to confirm the binding of the individual analyte compounds to the native protein in solution, by measuring the response of the Soret band at 409 nm as a function of concentration. The molar absorptivity coefficient for the protein binding was determined as 2.43 cm/mM (PB) 4.05 cm/mM (KCN) and 1.59 cm/mM (As_2O_3). Spectroscopic techniques (SNFTIR, and FTIR) were used to confirm the native state of the immobilized cytochrome c on BDD, Au and Pt electrodes. FTIR confirmed the bond vibrations of the surface functional groups associated with the protein amino acid backbone and SNFTIR showed the resonance coupling of these functional group as the protein is electrochemically reduced.

Therefore the work presented shows a new approach in the detection of toxic compounds by a BDD electrode, by the construction of a simple, cheap, less time Consuming, sensitive and environmentally friendly and lower detection limits biosensor.

8.2 Future work

As a continuation of the research technology developed as part of this thesis, we would like to apply the biosensor to the detection of CN^- and As^{3+} in environmental samples such as water and even air samples. We would also proceed with the analytical measurement of other cyanide and arsenic containing compounds. However the method of detection established in this work, indicated that the electrochemical signal for both CN- and As^{3+} were observed at the same potential in phosphate buffer systems. Therefore our first efforts would be to separate the analytical signals for quantitative measurement of cyanide and arsenic compounds in the same sample. One possibility would involve selective complexation of these analytes and separation using High Performance Liquid Chromatography (HPLC). The biosensor may then be applied as an end column detector for the two analytes. Also the effects of interfering species will be more closely analysed.

Another aspect related to the sensing protocol developed in this thesis is the transfer of biosensor technology to screen printed glassy carbon electrode (SPGCE). This would facilitate the portability of the technology and on site measurement for monitoring and early detection of environmental threats.

However the results obtained in this work holds great promise for the development of a fast and efficient methodology for determining cyanide and arsenic compounds.

References

1. Shireesh, P., Apte, R.S., *cellular respiration and Carcinogenesis*. Alcon Laboratories ed. 2009, USA: Human press p. 73-91.

2. Comninellis, C., *Electrocatalysis in the electrochemical conversion/combustion of organic pollutants for waste water treatment.* Electrochimica Acta, 1994. **39**(11-12): p. 1857-1862.

3. Holt, K.B., Del Campo, J., Foord, J.S, Compton, R.G, *Catalytic Effect of Gold Nanoparticles Self-Assembled in Multilayered Polyelectrolyte Films.* electroanal. Chem, 2001. 513: p. 94.

4. Comninellis, C., Plattner, E., *Characterization of DSA-type electrodes for oxygen evolution I. Titanium/iridium dioxide-tantalum pentoxide electrode.* Chimica Acta, 1988. 42: p. 2-250.

5. Terashima, C.R., Sarada, B. V.; Tryk, D.A.; Fujishima, A., *Electrochemical Oxidation of Chlorophenols at a Boron-Doped Diamond Electrode and Their Determination by High-Performance Liquid Chromatography with Amperometric Detection.* Anal Chem, 2002. 74: p. 895.

6. Crosby, D.G., *Environmental Toxicology and chemistry*, ed. U.o.C. John W.Birks. 1998: Oxford University Press p. 28.

7. Gribble, G.W., *The natural production of chlorinated compounds.* Environ. Sci. Technol., 1994. p. 28.

8. http://en.wikipedia.org/wiki/Cellular_respiration.

9. Apte, S., *Cellular Respiration and Carcinogenesis*, ed. F.W. T.X. 2009, USA: Human Press p.1.

10. Crosby, D.G., *Environmental Toxicology and chemistry*, ed. J.W. Birks. 1998, New York: Oxford University p. 30.

11. Abedon, S.T., et al., *Respiration*, in *Encyclopedia of Ecology*, J. Sven Erik and F. Brian, Editors. 2008, Academic Press: Oxford. p. 3010-3020.

12. Heinemeyer, B., Egbert J. Boekema, H.P., and Kouril, R., *A Structural Model of the Cytochrome c Reductase/Oxidase Supercomplex from Yeast Mitochondria.* Biological chemistry, 2007. **22**(16): p. 12240-12248.

13. Hossain Khan, F., et al., *Inhibition of rat brain mitochondrial electron transport chain activity by dopamine oxidation products during extended in vitro incubation: Implications for Parkinson's disease.* Biochimica et Biophysica Acta (BBA) - Molecular Basis of Disease, 2005. **1741**(1-2): p. 65-74.

14. Knowles, C.J. and A.W. Bunch, *Microbial Cyanide Metabolism*, in *Advances in Microbial Physiology*, A.H. Rose and D.W. Tempest, Editors. 1986, Academic Press. p. 73-111.

15. Denton, W.D., *Evolution: A Theory in Crisis*. 1985: Adler & Adler p. 277-8.

16. Kim, J., et al., *Oxidative modification of cytochrome c by singlet oxygen.* Free Radical Biology and Medicine, 2008. **44**(9): p. 1700-1711.

17. Isom, A.L., et al., *Modification of Cytochrome c by 4-hydroxy- 2-nonenal: evidence for histidine, lysine, and arginine-aldehyde adducts.* Journal of the American Society for Mass Spectrometry, 2004. **15**(8): p. 1136-1147.

18. http://arsenic-trioxide.co.tv.

19. Gosselin, R.E., Smith, R.P. and Hodge, H.C, *Clinical toxicology of commercial products*. 5th ed. 1984, Baltimore: Williams and Wilkins: p. 178

20. Mak, K., Yanase, H., and Renneberg, R., *Cyanide fishing and cyanide detection in coral reef fish using chemical tests and biosensors.* Biosensors and Bioelectronics, 2005. **20**(12): p. 2581-2593.

21. Skoog, A., West, M., Holler, F., Crouch, R., *Fundamentals of Analytical Chemistry*. 2004, David Harris: USA p. 785.

22. Szolar, O.H.J., *Environmental and pharmaceutical analysis of dithiocarbamates.* Analytica Chimica Acta, 2007. **582**(2): p. 191-200.

23. Wang, J., *Analytical electrochemistry*. 2nd ed. 2000, New York. p. 32-34.

24. Rodriguez-Mozaz, S., et al., *Biosensors for environmental monitoring: A global perspective.* Talanta, 2005. **65**(2): p. 291-297.

25. Arnold, M.A.M., *Recent Advances in the Development and Analytical Applications of Biosensing Probes.* Anal. Chem, 1988. **20**: p. 149-196.

26. Dorothee, G., R.M., Janos, V., and Erik, R., *Electrochemical Biosensors - Sensor Principles and Architectures.* Sensors, 2008. **8**: p. 1400-1458.

27. Löffler, U., Wiemhöfer, H.D. and Göpel,W., *Amperometric biosensors: characterization of dispersed mediator systems.* Biosensors and Bioelectronics, 1991. **6**(4): p. 343-352.

28. Kissinger, P.W et al., *Laboratory Techniques in Electroanalytical Chemistry*. 2ed ed. 1996 p. 01-23.

29. Pastorino, L., et al., *Development of a piezoelectric immunosensor for the measurement of paclitaxel.* Journal of Immunological Methods, 2006. **313**(1-2): p. 191-198.

30. Mosbach, K., *Thermal biosensors.* Biosensors and Bioelectronics, 1991. **6**(3): p. 179-182.

31. Rodriguez-Mozaz, M.-P.M., Maria J., Lopez, D.A., Damià B., *Analytical and Bioanalytical Chemistry*. Vol. 378. 2003: Chemistry and Material Science p. 588-598.

32. Woodcock, J.M., Bagley, C.J., and Lopez, A.F., *5 Receptors of the cytokine superfamily: mechanisms of activation and involvement in disease.* Baillière's Clinical Haematology, 1997. **10**(3): p. 507-524.

33. Batzias, F. and C.G. Siontorou, *A novel system for environmental monitoring through a cooperative/synergistic scheme between bioindicators and biosensors.* Journal of Environmental Management, 2007. **82**(2): p. 221-239.

34. Kandimalla, V.B., V.S. Tripathi, and H. Ju, *Biosensors based on immobilization of biomolecules in sol-gel matrices*, in *Electrochemical Sensors, Biosensors and their Biomedical Applications*. 2008, Academic Press: San Diego. p. 503-529.

35. Amine, A., et al., *Enzyme inhibition-based biosensors for food safety and environmental monitoring.* Biosensors and Bioelectronics, 2006. **21**(8): p. 1405-1423.

36. Nayak, M., et al., *Detection of microorganisms using biosensors--A smarter way towards detection techniques.* Biosensors and Bioelectronics, 2009. **25**(4): p. 661-667.

37. Reynolds J.A., and Donald, T.C., *Nature's Robots: A History of Proteins* 2003, New York: Oxford University Press p. 15.

38. Delaney, B., et al., *Evaluation of protein safety in the context of agricultural biotechnology.* Food and Chemical Toxicology, 2008. **46**(Supplement 2): p. S71-S97.

39. Zhao, J., Pridgeon, W., James, J., Gary, G., *Cytochrome c Gene and Protein Expression: Developmental Regulation, Environmental Response, and Pesticide Sensitivity in Aedes aegypti.* Journal of Medical Entomology, 2008. **45**: p. 401-408.

40. Wallace, B.A., *The oxidation-state-dependent ATP-binding site of cytochrome c A possible physiological significance.* Biochem, 1986 **236**: p. 359-364.

41. Goodsell, D.S., *The Molecular Perspective: Cytochrome c and Apoptosis.* TheOncologist, 2004. **9**: p. 226-227

42. Denton, D.W., et al., *Evolution: A Theory in Crisis*. 1985: Adler & Adler p. 8-277.

43. Villani, G.A., et al., *In Vivo Control of Respiration by Cytochrome C Oxidase in Human Cells.* Biol. Med, 2000. **29**: p. 202–210.

44. Geng, R., et al., *A sandwich structured SiO_2/cytochrome c/SiO_2 on a boron-doped diamond film electrode as an electrochemical nitrite biosensor.* Biomaterials, 2008. **29**(18): p. 2794-2801.

45. Yin, H., et al., *Amperometric nitrite biosensor based on a gold electrode modified with cytochrome c on Nafion and Cu-Mg-Al layered double hydroxi.* Springer-Verlag, 2010. **171(3-4)**: p. 385–392.

46. http://www.sigmaaldrich.com/life-science/metabolomics/enzyme-explorer/learning-center/cytochrome-c.html.

47. Kuwana T, N.D., *Bcl-2 family proteins and the role of mitochondria in apoptosis.* Curr Opin Cell Biol, 2003. **15**: p. 691-699.

48. Borgia, A., et al., *Fast folding kinetics and stabilization of apo-cytochrome c.* FEBS Letters, 2008. **582**(6): p. 1003-1007.

49. Checinska, A., et al., *Comparative proteomics analysis of caspase-9-protein complexes in untreated and cytochrome c/dATP stimulated lysates of NSCLC cells.* Journal of Proteomics, 2009. **72**(4): p. 575-585.

50. Diwan, J.J., *Biochemistry of metabolism*. 3rd ed. 1998-2007: Voet & Voet p. 571-574 and 802-820.

51. Shireesh P., Apte, R.S., *Cellular respiration and Carcinogenesis*. 2009, USA: Human press p. 45-19.

52. Tielens, A.G.M. and J.J. Van Hellemond, *The electron transport chain in anaerobically functioning eukaryotes.* Biochimica et Biophysica Acta (BBA) - Bioenergetics, 1998. **1365**(1-2): p. 71-78.

53. Lodish H, B.A., Zipursky. S.L., *Molecular Cell Biology*. 4th ed. 2000, New York: p. 89-103

54. Watabe, M., and T. Nakaki., *ATP depletion does not account for apoptosis induced by inhibition of mitochondrial electron transport chain in human dopaminergic cells.* Neuropharmacology, 2007. **52**(2): p. 536-541.

55. Sagara, T.N.K., Sone, A., Hinnen, C., and NikiK., *Redox Reaction Mechanism of Cytochrome c at Modified Gold Electrodes.* American Chemical Society, 1990. **6**: p. 254-262.

56. Liu, Y.C., et al., *Direct electrochemical behavior of cytochrome c on DNA modified glassy carbon electrode and its application to nitric oxide biosensor.* Electrochimica Acta, 2007. **52**(14): p. 4848-4852.

57. Crosby, D.G., *Envoronmental toxicology and chemistry*, 2nd ed. John. W.Birks. 1998, New York: Oxford University 122-123.

58. Crosby, D.G., *Environmental Toxicology and Chemistry*, 2nd ed. John W.Birks. 1998: Oxford University press p. 127.

59. Marken, F., Salter C, Compton R.G, Foord J.S,, *Electron induction modification of the surface electrochemical properties of diamond electrodes.* Chem Commun, 1999: p. 1697.

60. Wang H.S., and Chen H.Y., *Adsorption stripping voltammetry detection of sinle-stranded electrodes.* 2002. **14**: p. 1615.

61. Boonsong, K., et al., *Electroanalysis of lincomycin using boron-doped diamond thin film electrode applied to flow injection system.* Sensors and Actuators B: Chemical, 2005. **108**(1-2): p. 627-632.

62. Zhou, Y., and Zhi, J., *The application of boron-doped diamond electrodes in amperometric biosensors.* Talanta, 2009. **79**(5): p. 1189-1196.

63. Girotti, S., et al., *Monitoring of environmental pollutants by bioluminescent bacteria.* Analytica Chimica Acta, 2008. **608**(1): p. 2-29.

64. Skoog, A., West, M., Holler, F., Crouch, R., *Fundamentals of Analytical Chemistry.* 8th ed. 2004. p. 521-260

65. Angus J.C, M.H.B., Candau U, Evstefeera Y.E, Miller B, *New diamond and Fronteir Carbon Technology.* 1999. **9**: p. 175.

66. Lee, J., *Fundamentals of corrosion Compilation of ASTM Standard Definitions*. 4th ed. 1979 152, p. 759.

67. Marken F.A., Asogan, D., *Direct cytochrome c electrochemistry at boron-doped diamond electrodes*. Electrochemistry Communications, 2002. **4**: p. 62-66.

68. Del Campo, F., et al., *Voltammetry at boron-doped diamond electrodes in liquid ammonia: solvent window effects and diamond surface modification.* Electrochem. Solid State Letters, 2000. **3**: p. 224-227.

69. Dash, R.R., Balomajumder, C., and Kumar, A., *Removal of cyanide from water and wastewater using granular activated carbon.* Chemical Engineering Journal, 2009. **146**(3): p. 408-413.

70. Lindsay, A.E., Greenbaum, A.R., and O'Hare, D.., *Analytical techniques for cyanide in blood and published blood cyanide concentrations from healthy subjects and fire victims.* Analytica Chimica Acta, 2004. **511**(2): p. 185-195.

71. Kirk-Othmer., *encyclopedia of chemical technology*. 3rd ed. Vol. 7. (1979), New York, NY: John Wiley & Sons p. 308.

72. Ballantyne B, M.T., *Clinical and experimental toxicology of cyanides*. 3ed ed. Vol. 78. 1987, England: Bristol: IOP Publishing p. 217-247.

73. Eisler, R., *Cyanide Hazards to Fish, Wildlife, and Invertebrates*. U.S. Fish Wildl. Serv., Biol., 1991. 85(1.23) p. 246.

74. Bhattacharya, R., et al., *Acute toxicity of some synthetic cyanogens in rats and their response to oral treatment with alpha-ketoglutarate.* Food and Chemical Toxicology, 2009. **47**(9): p. 2314-2320.

75. Aitken, W.D., Smith F, *Cyanide toxicity following nitroprusside-induced hypotension.* Can Anaesth Soc J, 1977. **24**: p. 651-660.

76. Fargette, C.F., *African Cassava Mosaic Virus:Etiology, Epidemiology, and Control.* Tha Amerlurn Phytopthdoglml SoeIety, 1990. **74**: p. 404-411.

77. Liu, Z., et al., *Arsenic trioxide uptake by human and rat aquaglyceroporins.* Biochemical and Biophysical Research Communications, 2004. **316**(4): p. 1178-1185.

78. Giacomino, O.A., Marco, L., Mery, M., Edoardo, M., *Determination of As(III) by anodic stripping voltammetry using a lateral goldelectrode: Experimental conditions, electron transfer and monitoring of electrode surface.* Elsevier, 2010. **83**: p. 1428-1435.

79. Asghar-Ensafi, A.C.R., Ingrid F., *Highly Sensitive Voltammetric Speciation and Determination of Inorganic Arsenic in Water and Alloy Samples Using Ammonium 2-Amino-1-Cyclopentene-1-Dithiocarboxylate.* Wiley-VCH Verlag GmbH&Co, 2010. **11**: p. 1175-1185.

80. Sykes, A.G., *subject index, in advances in inorganic chemistry*. 2nd ed. 1999, USA: Academic press. p. 340.

81. D'Sousa.S.F., *Microbial biosensors.* Biosensors & Bioelectronics, 2001. **16**: p. 337–353.

82. Kazunori, A.M., Seung, J.C., Yoko N., Sang, M and Y.Y. Chang, Yasushi H., Uchiyamab S., Karube I., *Microbial cyanide sensor for monitoring river water.* Biotechnology 1996. **48**: p. 73-80.

83. Wang Y., *Amperometric Flow-Biosensor for Cyanide Based on an Inhibitory Effect upon Bioelectrocatalytic Reduction of Oxygen by Peroxidase-Modified Carbon-Felt.* Electroanalysis, 2010. **22**: p. 1-7.

84. Ge, B. and Lisdat, F., *Superoxide sensor based on cytochrome c immobilized on mixed-thiol SAM with a new calibration method.* Analytica Chimica Acta, 2002. **454**(1): p. 53-64.

85. Oh, S.Y., et al., *Electrochemical properties of self-assembled cytochrome c on gold substrate patterned with a photosensitive polyimide film.* Optical Materials, 2003. **21**(1-3): p. 265-269.

86. Xiang, C., et al., *Direct electron transfer of cytochrome c and its biosensor based on gold nanoparticles/room temperature ionic liquid/carbon nanotubes composite film.* Electrochemistry Communications, 2008. **10**(1): p. 38-41.

87. Skoog A., West M., Holler F., Crouch R., *Fundamentals of Analytical Chemistry*. 8th ed. 2004, New York: p. 771-772.

88. Holler F., Skoog A.,West M., *Fundamentals of Analytical chemistry*. 5th ed. 2004, USA: Chemistry: David Harris p.710-784.

89. Skoog A., West M., Holler F., Crouch R., *Fundametals of Analytical Chemistry*. 8th ed. 2004, New: David Harris p. 691-693.

90. Bard, A and Faulkner J., *Electrochemical Methods: Fundamentals and Applications* 2ed ed. 2000 p. 12-18.

91. Kounaves, S.P., *Voltammetric Techniques: Handbook of Instrumental Techniques for Analytical Chemistry*. 2007 p. 709-725.

92. Skoog, E.A., *Principles of Instrumental analysis*. 6th ed. 2007: Thomson Brooks/Cole p. 169-173.

93. Kang, X.M., Zou Z., Cai X., Mo P., Jinyuan, *A novel glucose biosensor based on immobilization of glucose oxidase in chitosan on a glassy carbon electrode modified with gold-platinum alloy nanoparticles/multiwall carbon nanotubes.* Analytical Biochemistry, 2007. **369(1)**: p. 71-79.

94. Suzuki, E., *High-resolution scanning electron microscopy of immunogold-labelled cells by the use of thin plasma coating of osmium.* Journal of Microscopy 2002. **3**(208): p. 153–157.

95. Hall, J.L.H., Dean C. R., *Electron Microscopy of Plant Cells*. 2002, London: Academic Press p. 313–413.

96. ODea. J.J, Osteryoung.J., *Dimensionless square wave voltammograms.* Electroanal. Chem, 1986. **14**(209) p. 89.

97. Chen, Q., et al., *A nitrite biosensor based on the immobilization of Cytochrome c on multi-walled carbon nanotubes-PAMAM-chitosan nanocomposite modified glass carbon electrode.* Biosensors and Bioelectronics, 2009. **24**(10): p. 2991-2996.

98. Su, L., et al., *Characterization of cyanide binding to cytochrome c oxidase immobilized in electrode-supported lipid bilayer membranes.* Journal of Electroanalytical Chemistry, 2005. **581**(2): p. 241-248.

99. Zhao, G.C., et al., *Direct electrochemistry of cytochrome c on a multi-walled carbon nanotubes modified electrode and its electrocatalytic activity for the reduction of H_2O_2.* Electrochemistry Communications, 2005. **7**(3): p. 256-260.

100. Nůsková, H., M.V., Drahota, Z., Houštěk, J., *Cyanide inhibition and pyruvate-induced recovery of cytochrome c oxidase.* Bioenerg Biomembr, 2010. **42**(7): p. 395–403.

101. Antonini A., Colin M.B., Bo, G., Malmstrong, G., Giacomo C., Rotilio., *The Interaction of Cyanide with Cytochroine Oxidase.* Biochemical and Biophysical Research Communications, 1971. **23**(1) p. 396-400.

102. Fukumori, Y., *Inhibition of an aa3-Type Two-Subunit Cytochrome c Oxidase from Nitrobacter agilis by N,N'-Dicyclohexylcarbodiimide* 1985 **26** (3): p. 961-965.

103. Beatrice, D.A., Bizzarri, A.R., and Cannistraro, S., *Topological and Electron-Transfer Properties of Yeast Cytochrome c Adsorbed on Bare Gold Electrodes.* Wiley-VCH, 2003. **4** (9): p. 1183-1188.

104. Zhao, Q.K.Z., *Direct Electrochemistry of Cytochrome C on the Glassy Carbon Electrode Modified with 1-Pyrenebutyric Acid/MWNTs.* Chinese Chemical Letters, 2005. **16**(10): p. 1237-1240.

105. Franzen, S.E., and Andrew P. S., *Heme Charge-Transfer Band III Is Vibronically Coupled to the Soret Band.* American Chemical Society, 2002. **124**(2): p. 7148.

106. Battistuzzi, G., Borsari, M., Cowan, J. A., Ranieri, A., Sola, M, *Spectroelectrochemical Determination of the Redox Potential of Cytochrome c via Multiple Regression.* Chem. Soc, 2002. **83**(2): p. 5315-5324.

107. Denton, D.W., et al., *Absorption Spectra and Some Other Properties of Cytochrome c and of Its Compounds with Ligands.* Royal Society 1962. **156**(1): p. 429-458

108. Xu, J.J., et al., *Interfacing cytochrome c to Au electrodes with humic acid film.* Electrochemistry Communications, 2004. **6**(3): p. 278-283.

109. Senn, H. and Wüthrich, K., *Amino acid sequence, haem-iron co-ordination geometry and functional properties of mitochondrial and bacterial c-type cytochromes.* Quarterly Reviews of Biophysics, 1985. **18**(02): p. 111-134.

110. McCloskey, J., *Direct Amperometry of Cyanide at Extreme Dilution.* Anal.Chem, 1961. **33**(3): p. 1843.

111. Salimi, A., et al., *Electrochemical detection of trace amount of arsenic(III) at glassy carbon electrode modified with cobalt oxide nanoparticles.* Sensors and Actuators B: Chemical, 2008. **129**(1): p. 246-254.

Appendix:

Interference results in volume ratios

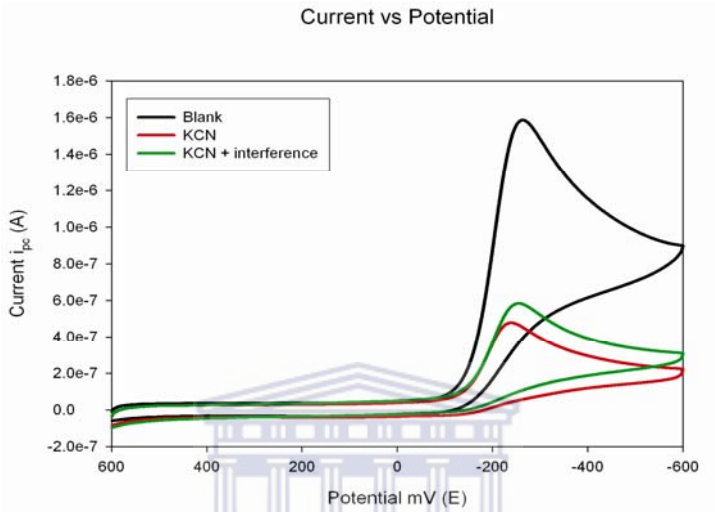

CV of biosensor response to KCN in the presence of $Na_2S_2O_3$ (1:20 ratio)

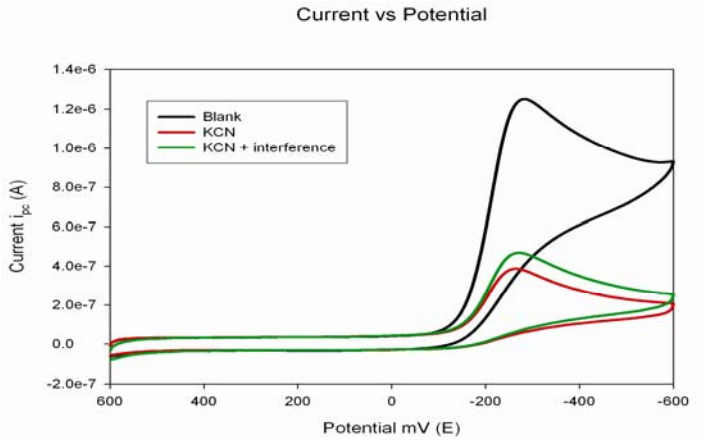

CV of biosensor response to KCN in the presence of $Na_2S_2O_3$ (1:100ratio)

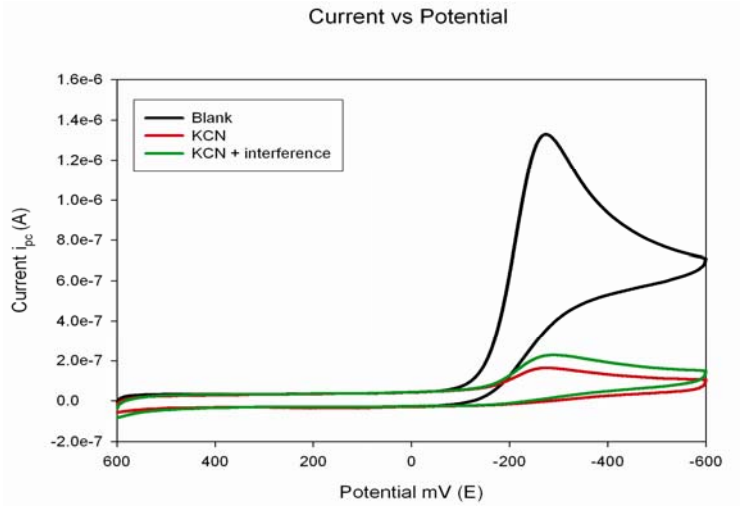

CV of biosensor response to KCN in the presence of $Na_2S_2O_3$ (1:200ratio)

7.1.2 Potassium cyanide, KCN with interference of NaCl

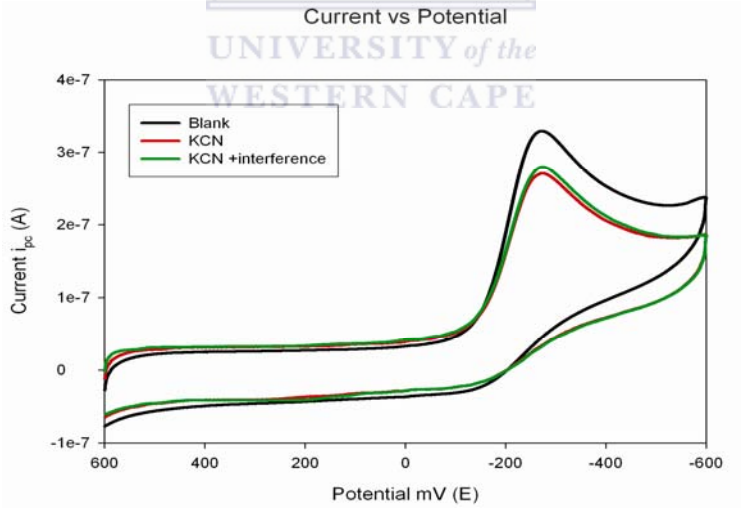

CV of biosensor response to KCN in the presence of NaCl (1:20ratio)

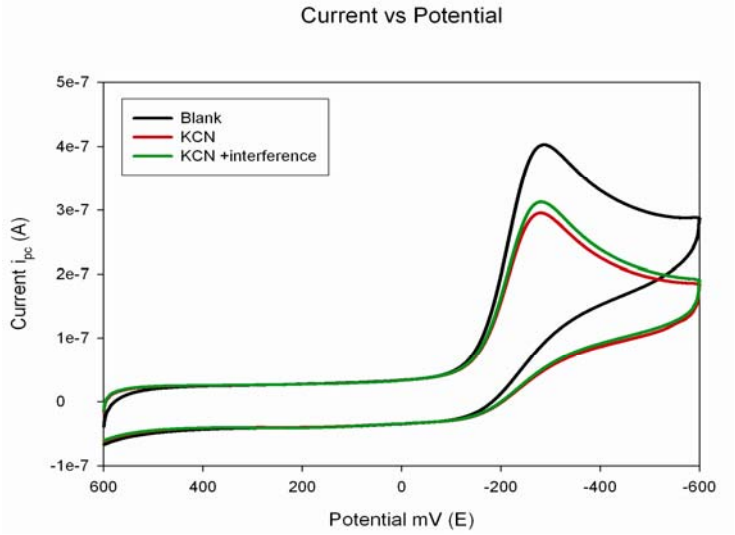

CV of biosensor response to KCN in the presence of NaCl (1:100ratio)

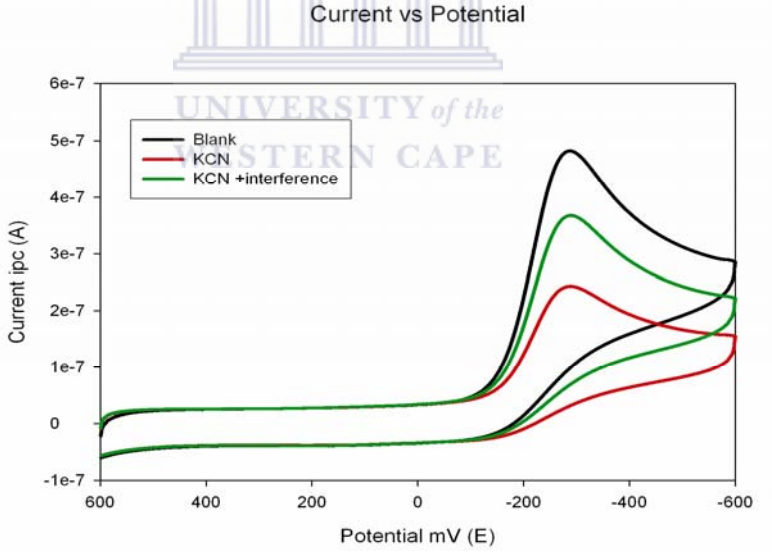

CV of biosensor response to KCN in the presence of NaCl (1: 200ratio)

Potassium cyanide, KCN with interference of $NaNO_2$

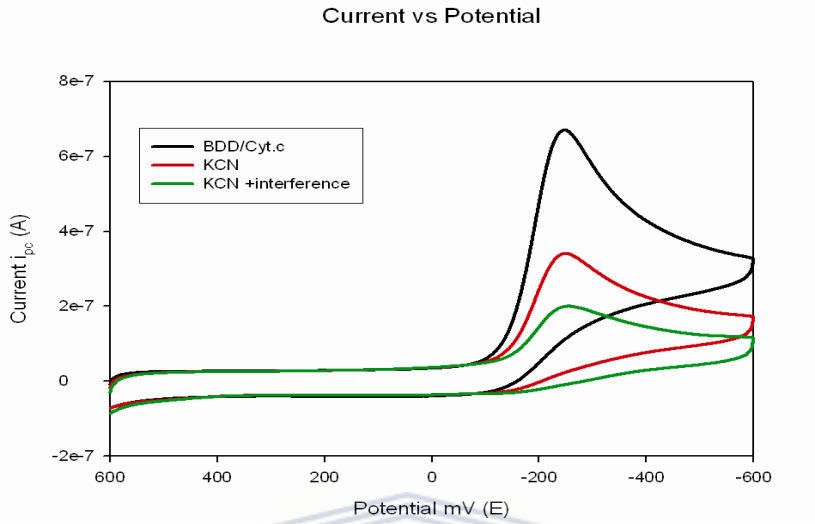

CV of biosensor response to KCN in the presence of $NaNO_2$ (1:20ratio)

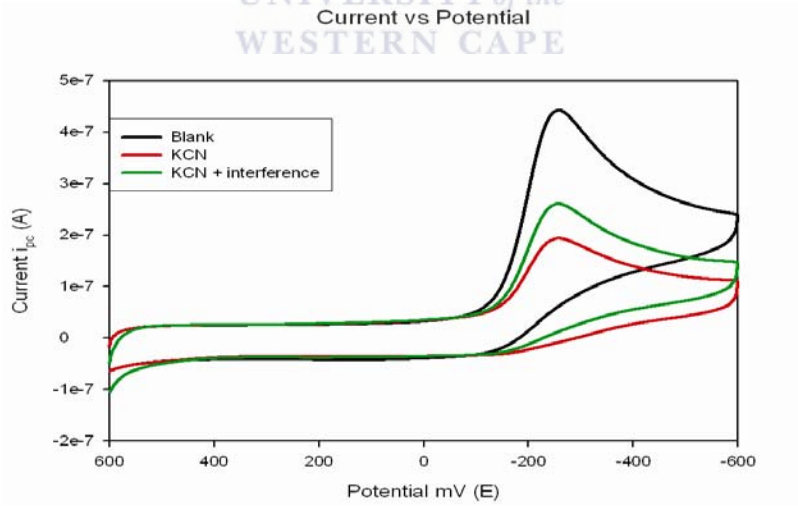

CV of biosensor response to KCN in the presence of $NaNO_2$ (1:100 ratio)

Potassium cyanide, KCN with interference of Na_2S

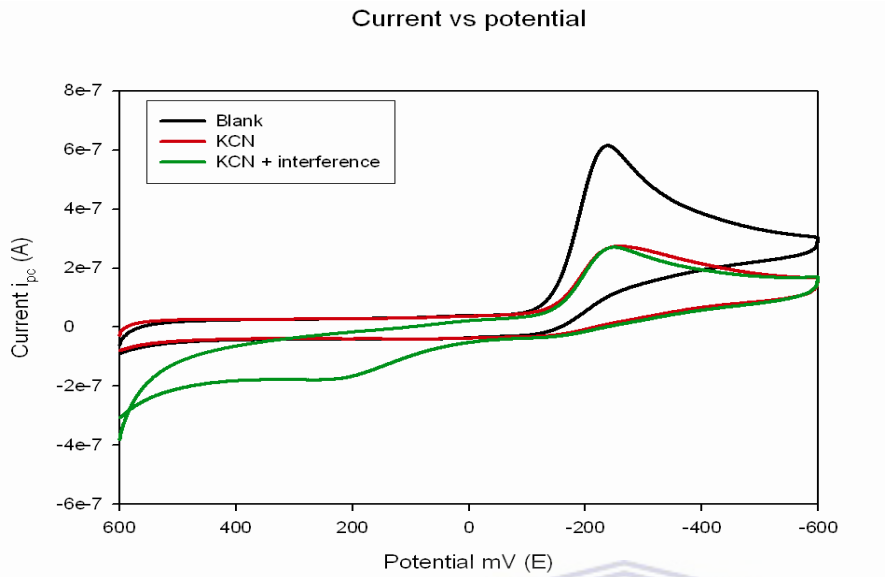

CV of biosensor response to KCN in the presence of Na_2S (1:200 ratio)

Arsenic trioxide, As_2O_3

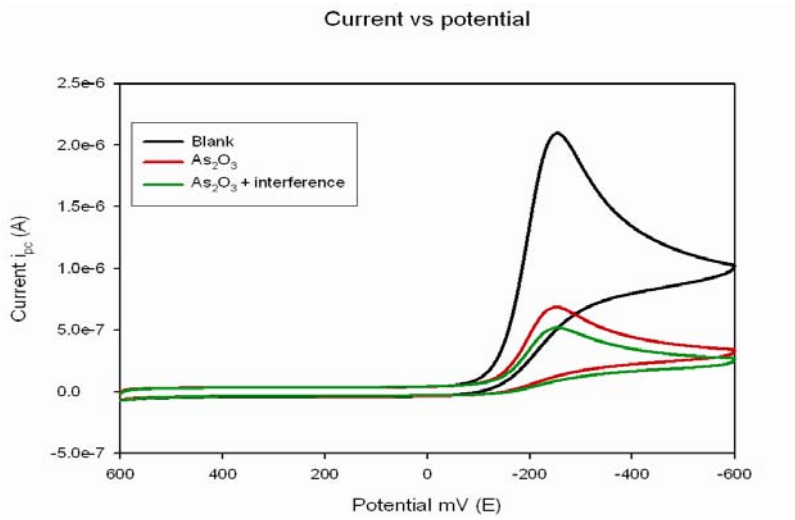

CV of biosensor response to As_2O_3 in the presence of $Na_2S_2O_3$ (1:20ratio)

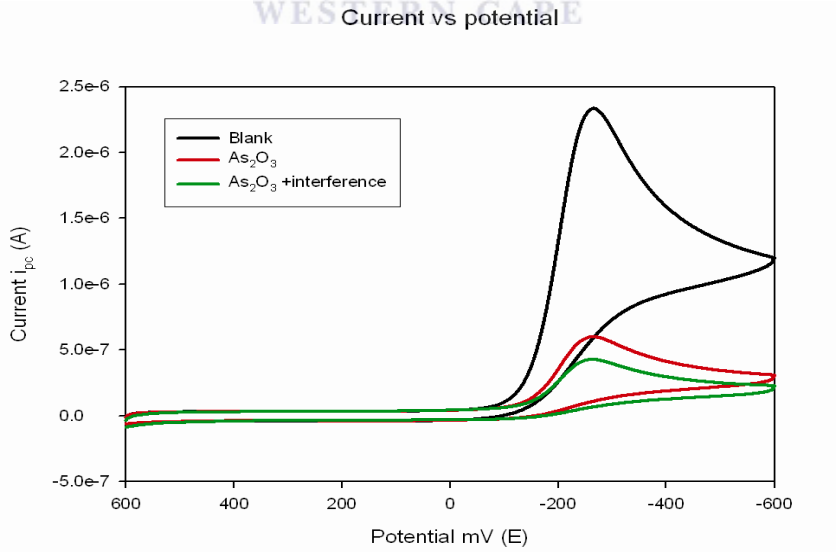

CV of biosensor response to As_2O_3 in the presence of $Na_2S_2O_3$ (1:100 ratio)

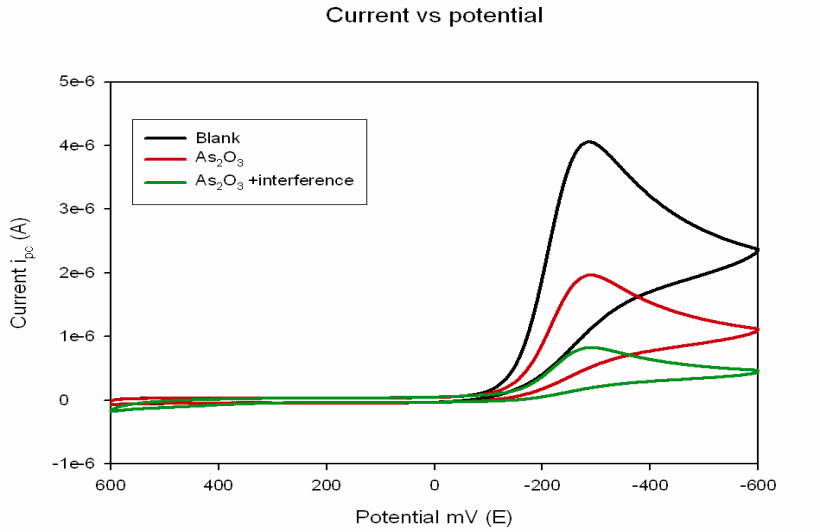

CV of biosensor response to As_2O_3 in the presence of $Na_2S_2O_3$ (1: 200ratio)

Arsenic trioxide, As_2O_3 with $NaNO_2$ interference

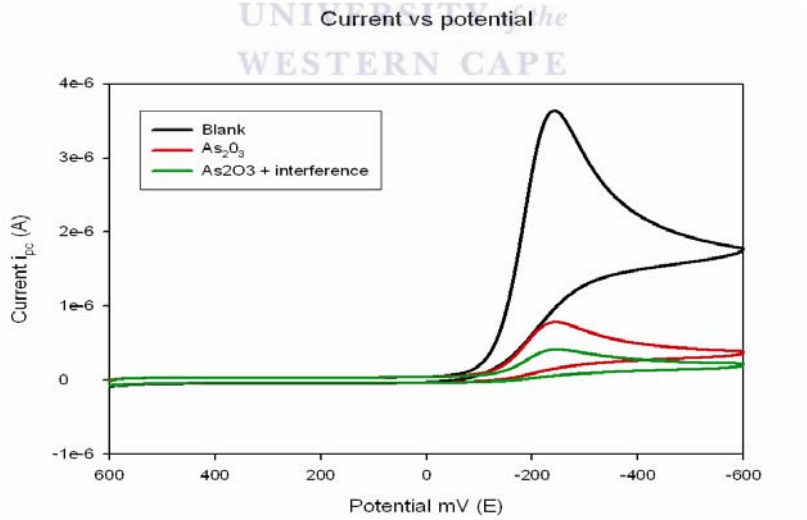

CV of biosensor response to As_2O_3 in the presence of $NaNO_2$ (1:20 ratio)

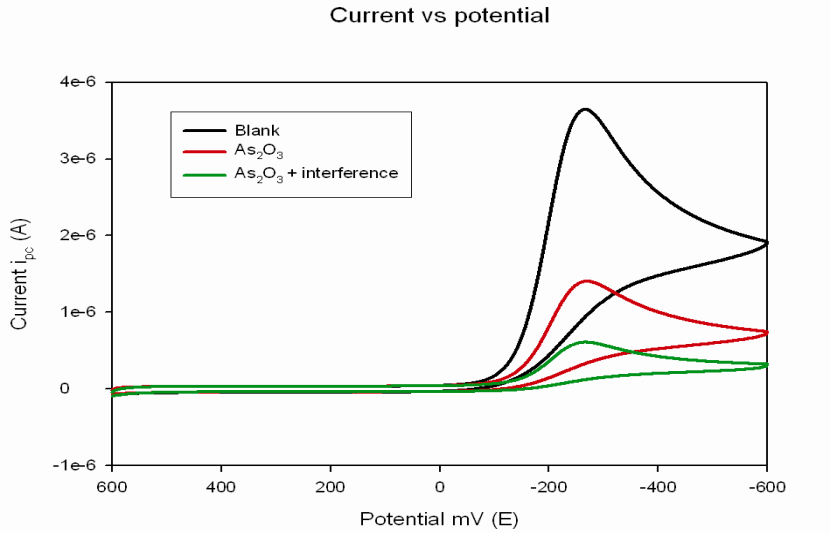

CV of biosensor response to As_2O_3 in the presence of $NaNO_2$ (1:100 ratio)

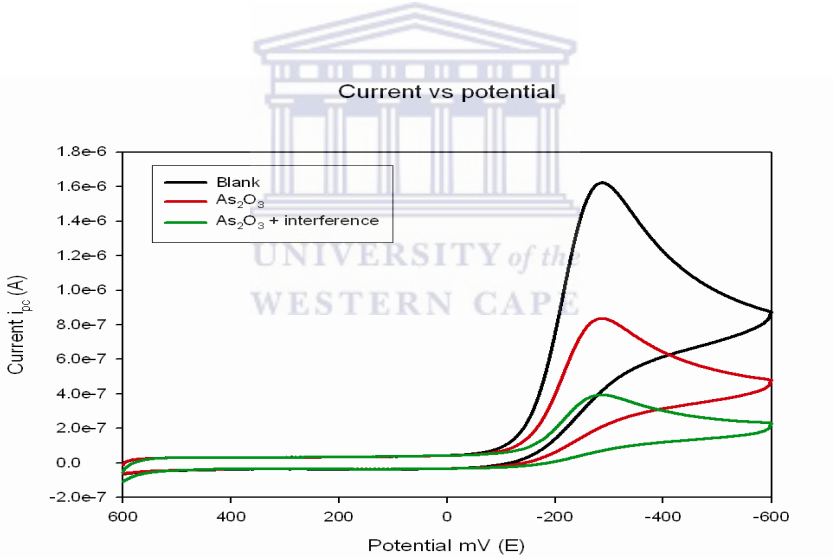

CV of biosensor response to As_2O_3 in the presence of $NaNO_2$ (1:200 ratio)

Arsenic trioxide, As_2O_3 with NaCl interference

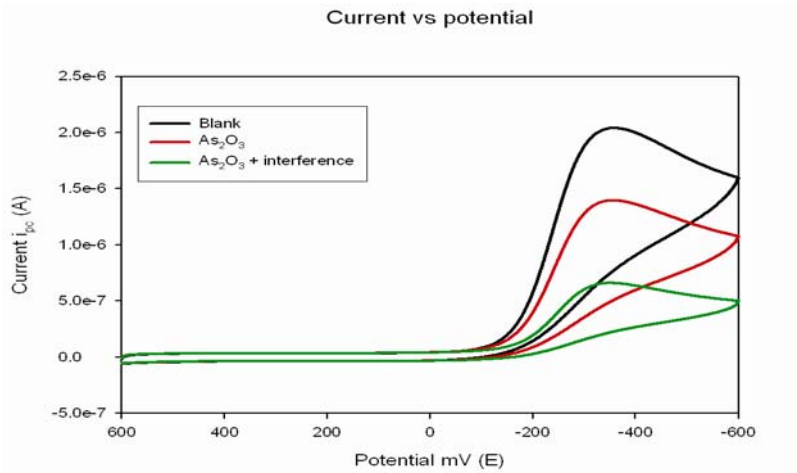

CV of biosensor response to As_2O_3 in the presence of NaCl (1:20 ratio)

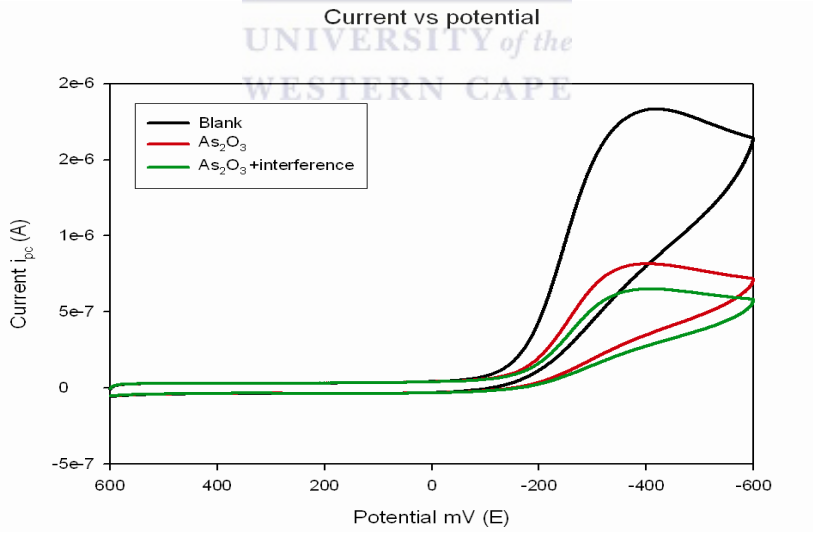

CV of biosensor response to As_2O_3 in the presence of NaCl (1:100 ratio)

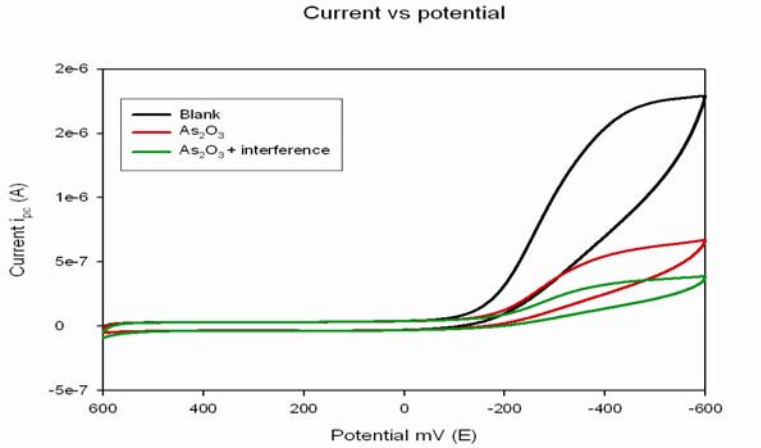

CV of biosensor response to As_2O_3 in the presence of NaCl (1:200 ratio)

Arsenic trioxide, As_2O_3 with NaS interference

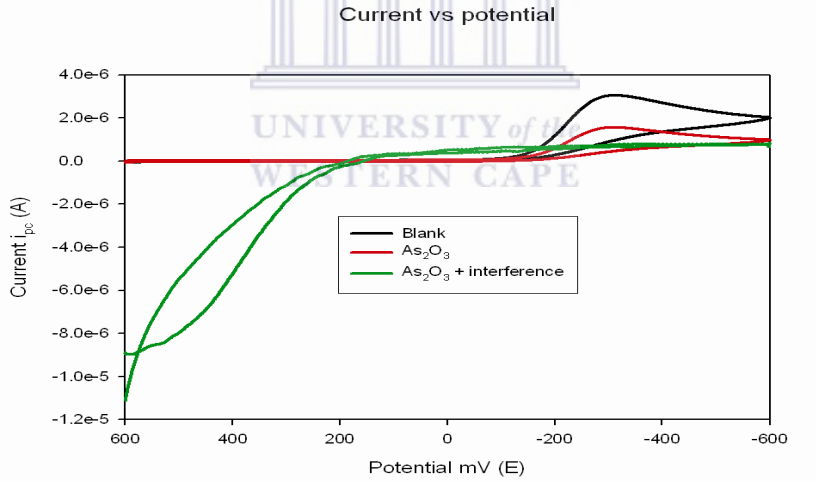

CV of biosensor response to As_2O_3 in the presence of Na_2S (1: 200 ratio)

UNIVERSITY of the
WESTERN CAPE